Czech Technical University in Prague
Faculty of Mechanical Engineering

Department of Mechanics, Biomechanics, and Mechatronics

Clinical Biomechanics of Upper Extremity

Dissertation

Ing. Adam Kratochvíl

Doctoral study programme: Mechanical Engineering

Field of study: Biomechanics

Supervisor: Prof. RNDr. Matej Daniel, Ph.D.

2024 Prague

Title: Clinical Biomechanics of Upper Extremity

Year: 2024

Author: Ing. Adam Kratochvíl

Supervisor: Prof. RNDr. Matej Daniel, Ph.D.
Department of Mechanics, Biomechanics and Mechatronics
Faculty of Mechanical Engineering
Czech Technical University in Prague

University: Czech Technical University in Prague

Faculty: Faculty of Mechanical Engineering

Department: Department of Mechanics, Biomechanics and Mechatronics

Address: Technická 4, 160 00, Prague, Czech Republic

Field of study: Biomechanics

Number of pages	108
Number of figures	107
Number of tables	10
Number of supplements	1

Keywords: biomechanics; shoulder; musculoskeletal model; Hill-type muscle model; reverse total shoulder arthroplasty; radiographical magnification; humerus prolongation; joint load

Annotation

This thesis introduces a comprehensive biomechanical analysis of reverse total shoulder arthroplasty (RTSA), incorporating both the shift of the center of rotation (COR) and humerus prolongation. The analysis is conducted using an innovative validated method based on widely available clinical data from preoperative and postoperative examinations of RTSA patients. We demonstrated that the magnification of plain radiographs in the shoulder region significantly varies among patients, with a mean value approaching 12%, which significantly differs from the commonly used 5%. Musculoskeletal geometry alterations are assessed through preoperative and postoperative X-rays, along with preoperative CT scans. An original method for evaluating COR shift in RTSA, based on postoperative X-rays, was introduced, and subsequently employed to determine the actual humerus prolongation. The findings unveiled an average actual humerus prolongation of 15.2 mm, that has not been previously reported. The influence of various musculoskeletal changes in RTSA was extensively examined and their impact on muscle forces and glenohumeral joint load was evaluated. Furthermore, a safe zone for humerus prolongation to prevent overloading the glenohumeral joint in RTSA was established, a crucial consideration for surgical procedures.

Anotace

Tato disertační práce představuje komplexní biomechanickou analýzu reverzní náhrady ramenního kloubu, zahrnující jak posun centra rotace, tak prodloužení humeru. Analýza je provedena pomocí vlastní validované metody založené na běžně dostupných klinických datech z předoperačních a pooperačních vyšetření pacientů s totální endoprotézou ramene. Jedním z cílů, bylo prokázat, že zvětšení rentgenu v oblasti ramene je větší než v klinické praxi běžně používaných 5 % a že se mezi pacienty významně liší. Tato hypotéza byla potvrzena naměřenou průměrnou hodnota zvětšení blížící se 12 % s rozsahem od 5 % do 20 %. Změny v muskuloskeletální geometrii byly vyhodnoceny pomocí předoperačních a pooperačních rentgenových snímků spolu s předoperačním CT. Na základě pooperačních rentgenových snímků byla také zavedena nová metoda pro hodnocení posunu centra rotace u pacientů s reverzní endoprotézou ramene. Toto posunutí centra rotace bylo následně použito ke stanovení skutečného prodloužení humeru, jehož průměrná hodnota byla vyhodnocena jako 15,2 mm. Jedná se o rozměr, který nebyl nikdy dříve publikován. Dále byly vyhodnoceny jednotlivé změny muskuloskeletální geometrie a jejich vliv na svalové síly a zatížení ramene. Na závěr byla stanovena bezpečná zóna pro prodloužení humeru tak, aby se zabránilo přetížení glenohumerálního kloubu, což je zásadním hlediskem pro chirurgické výkony.

Declaration

Herewith I declare that the thesis comprises only my original work except where indicated and due acknowledgement has been made in the text to all other material used. During the preparation of this thesis Writefull was used in order to check spelling and style. After using this tool/service, the author reviewed and edited the content as needed and take full responsibility for the content of the publication.

in Prague _____ _____

signature

Acknowledgement

I express my gratitude to my supervisor, prof. RNDr. Matej Daniel, Ph.D., for introducing me to the issue, providing invaluable assistance and guidance throughout my entire postgraduate study. Without his support, this work would not have come to fruition. Additionally, I extend my thanks to my colleagues at the Department of Biomechanics who played a role, directly or indirectly, in the development of this thesis. Finally, I extend my gratitude to my wife and son for their unwavering support and patience, not only throughout the completion of this thesis but in all aspects of my academic journey.

Poděkování

Rád bych poděkoval svému školiteli prof. RNDr. Mateji Danielovi, Ph.D., za uvedení do problematiky, za neocenitelnou pomoc a vedení po celou dobu mého postgraduálního studia. Bez jeho podpory by tato práce nemohla vzniknout. Dále děkuji všem kolegům z odboru biomechaniky, kteří se přímo či nepřímo podíleli na vzniku této práce. V neposlední řadě děkuji své ženě a synovi za jejich neochvějnou podporu a trpělivost, a to nejen po dobu psaní této práce, ale po celou dobu mého studia.

Contents

List of Figures

List of Tables

List of Symbols

2D	Two-dimensional
3D	Three-dimensional
A.K.	Adam Kratochvíl
ANOVA	Analysis of Variance
AP	Anterior-posterior
ASFE	Algorithm for Shoulder Force Estimation
BMI	Body mass index [$kg \cdot m^{-2}$]
CE	Contractile element
CI	Confidence interval
COR	Center of rotation
CSV	Comma-separated values, file format
CT	Computed tomography
CTA	Cuff tear arthropathy
DICOM	Digital Imaging and Communications in Medicine, file format
DOF	Degree of freedom
F	F-test value
HSD	Tukey's HSD Test for multiple comparisons
ICC	Intra-class correlation coefficient
ISB	International Society of Biomechanics
MTC	Muscle tendon complexes
OA	Omarthrosis
OCD	Osteochondrodysplasia
p	p-value
PA	Psoriatic arthritis
PCSA	Physiological cross-sectional area
PEE	Parallel elastic element
PTD	Post-traumatic deformity
R	Pearson correlation coefficient
RA	Rheumatoid arthritis
RTSA	Reverse total shoulder arthroplasty
SD	Standard deviation
SEE	Serial elastic element
STL	File format

t	T-test value
TSA	Total shoulder arthroplasty
W	Shapiro-Wilk normality test value
α	Alpha error
$\vec{d}_{COR}, d_{COR}$	COR shift vector and its length [mm]
$\vec{d}_{H}, d_{H}$	Humerus prolonging vector and its length [mm]
$\vec{d}_{T}, d_{T}$	Total change in musculoskeletal geometry vector and its length [mm]
F_{CE}	Contractile element force [N]
$\bar{F}_{CE}$	Normalized contractile element force [-]
F_{CE}^{min}	Minimum muscle force level [N]
F_{M}	Total muscle force [N]
F_{max}	Maximum isometrical force [N]
F_{PEE}	Parallel element force [N]
$\bar{F}_{PEE}$	Normalized parallel element force [-]
$\mathcal{F}_{PEE}$	Free muscle parameter [-]
F_{SEE}	Serial element force [N]
ΔF_{SEE}^{lin}	Tendon force increment in the linear part [N]
$\bar{F}_{SEE}^{toe}$	Normalized tendon force at toe section [N]
k_{PEE}	Stiffness parameter of parallel elastic element [N·m^{-1}]
k_{SEE}^{nll}	Stiffness parameter of serial elastic element (non-linear section) [N·m^{-1}]
k_{SEE}^{toe}	Stiffness parameter of serial elastic element (toe section) [N·m^{-1}]
k_{SEE}^{lin}	Stiffness parameter of serial elastic element (linear section) [N·m^{-1}]
l_{CE}	Contractile element length [mm]
$\bar{l}_{CE}$	Normalized muscle fiber length [-]
l_{CE}^{slack}	Muscle slack length [mm]
l_{MTC}	Total muscle tendon complex length [mm]
l_{PEE}	Parallel element length [mm]
l_{PEE}^{opt}	Optimal parallel element length [mm]
$\mathcal{L}_{PEE}$	Free muscle parameter [-]
l_{SEE}	Serial element length [mm]
l_{SEE}^{slack}	Tendon slack length [mm]
l_{SEE}^{nll}	Tendon length defining the non-linear–linear transition [mm]
M	Radiographic magnification [%]
r	Radius of a sphere

R_x	Reaction force in anterior-posterior direction [N]
R_y	Reaction force in inferior-superior direction [N]
R_z	Reaction force in medial-lateral direction [N]
ΔU_{SEE}^{lin}	Relative additional linear tendon stretch [-]
ΔU_{SEE}^{nll}	Relative stretch at non-linear–linear transition [-]
v_{PEE}	Free muscle parameter [-]
v_{SEE}	Tendon exponent [-]
w	Shape factor [-]
x, y, z	Coordinates [mm]
$x0, y0, z0$	Center point of a sphere
ϵ_{CE}	Passive muscle strain [-]
ϵ_{SEE}	Tendon strain [-]
ϵ_{SEE}^{toe}	Tendon strain defining non-linear behavior [-]
ϵ_{SEE}^{isom}	Tendon reference strain at maximal isometric force [–]
ϵ_{SEE}^{ref}	Tendon reference strain [-]
CoCrMo	Cobalt-Chrome-Molybdenum
H_2O	Water

1 Introduction

Nearly every human activity is intricately connected to shoulder movement. Whether the shoulder serves as the primary actor in an activity or contributes to stability, such as in walking [1], its role is crucial. Shoulder joint movements are also integral to sports activities, contributing to both physical fitness and mental well-being [2]. However, shoulder biomechanics are highly complex, involving 4 joints (glenohumeral, acromioclavicular, scapulothoracic, and sternoclavicular) and 18 muscles working in synergy. Any disbalances in the shoulder complex can be a source of potential future complications [3].

Shoulder anatomy isn't inherently suited for an active life beyond 80 years, leading to problems that increasingly emerge with age, connected with reduced mobility and significant pain [4]. With the increasing life expectancy, which has nearly doubled in the last century in developed countries [5], and as the population ages [6], there is a growing demand to address pathological conditions affecting the shoulder. While less severe shoulder conditions, particularly in younger patients, such as impingement syndrome or soft tissue inflammation, can often be managed through conservative treatments [7], more serious degenerative conditions such as omarthrosis or rheumatoid arthritis, rotator cuff ruptures, or post-traumatic issues in older individuals may necessitate total shoulder arthroplasty (TSA) for joint mobility restoration [8].

Reverse total shoulder arthroplasty (RTSA), a procedure reversing the joint's anatomical arrangement, has become increasingly prevalent in addressing shoulder issues [9]. This reversal creates more favourable biomechanical conditions by shifting the center of rotation (COR) of the glenohumeral joint medially and slightly inferiorly and thus increasing the moment arm of deltoid muscle, which is the main mobilizer of the arm [10; 11]. This arrangement not even enhance mobility but also increasing stability of the joint by prestressing the shoulder muscles, especially benefiting patients with insufficient rotator cuff muscles [12].

The utilization of shoulder arthroplasty has witnessed significant expansion over the last decade, a trend supported by data from US databases. These statistics can be attributed, at least in part, to an aging population that aspires to maintain an active lifestyle [13]. In 2012, a total of 22,835 primary RTSA procedures were conducted [9]. In 2017, this number experienced a significant surge, nearly tripling

to reach 62,705 RTSA procedures [9]. Over the same period, the count of anatomic total shoulder arthroplasty (TSA) procedures rose from 29,685 in 2012 to 40,665 in 2017 [9]. Conversely, the number of shoulder hemiarthroplasty procedures underwent a substantial decline, decreasing by almost half, from 11,695 in 2012 to 4,930 in 2017 [9].

To enhance the outcomes of RTSA, a thorough understanding of the biomechanical aspects of the resulting state is essential. While some characteristics can be measured from radiographs and other clinically available data of patients who have undergone RTSA [14], variables crucial to RTSA biomechanics, such as muscle forces, cannot be adequately assessed from these data alone. Hence, a comprehensive biomechanical analysis requires the utilization of mathematical musculoskeletal and muscle models.

Therefore, the presented thesis deals with clinical biomechanics of shoulder with emphasis on modifications of glenohumeral geometry induced by reverse shoulder arthroplasty. The structure of the thesis is as follows:

Chapter 2 provides description of basic anatomical and biomechanics terms. The kinematics and dynamics of the glenohumeral joint along with current approaches of shoulder arthroplasty are discussed. Systematic review of current biomechanical model is provided to highlight potential flaws in the current analysis.

Chapter 3 defines research problems identified based on a literature review. A critical point, not yet addressed in the biomechanical and orthopedics literature, is the issue of humeral prolongation during surgery and its impact on overall glenohumeral joint load.

Chapter 4 shows original research methods introduced in the study of shoulder biomechanics. First, a method for measurement of inherent magnification of plain radiographs is introduced and applied in a clinical study. Second, a mathematical model comparing various approaches to passive and active shoulder muscle force is adopted. Third, novel algorithm is proposed to estimate humeral prolongation from the preoperative and the postoperative radiograph though their alignment by CT scans.

Chapter 5 introduces results of clinical studies and mathematical simulations. The biomechanical analysis is accompanied with statistical method to estimate significance of measured parameters.

Chapter 6 compares the estimated values with the state of art in the literature and discuss potential limitations of the proposed methods and models. The future trends of biomechanical research in the field of shoulder arthroplasty are outlined.

Chapter 7 provides an overview of achieved results, clearly demonstrating the importance of humeral prolongation on overall joint biomechanics and summarizes the main accomplishments of the thesis.

2 State of the Art

2.1 Glenohumeral Joint

The glenohumeral joint is a part of shoulder complex (Fig. 1). It is the most mobile articulation within the human body [15]. The glenohumeral joint is synovial ball-and-socket joint, involving the coordinated action of 18 muscles and other structures such as the scapula and clavicle to provide full range motions with three rotational degrees of freedom (DOF) as well as three translational DOF [16]. In the specific context of the glenohumeral joint, the humeral head and the cavitas glenoidalis, forming the joint socket within the scapula, articulate with one another. Despite the partial widening of the fossa by the fibrous labrum glenoidale, it is important to note that the fossa's articular surface covers only a fraction, ranging from a quarter to a third of the humeral head's corresponding surface [17]. This anatomical feature permits a wide range of motion but, conversely, poses a potential source of dynamic instability [18].

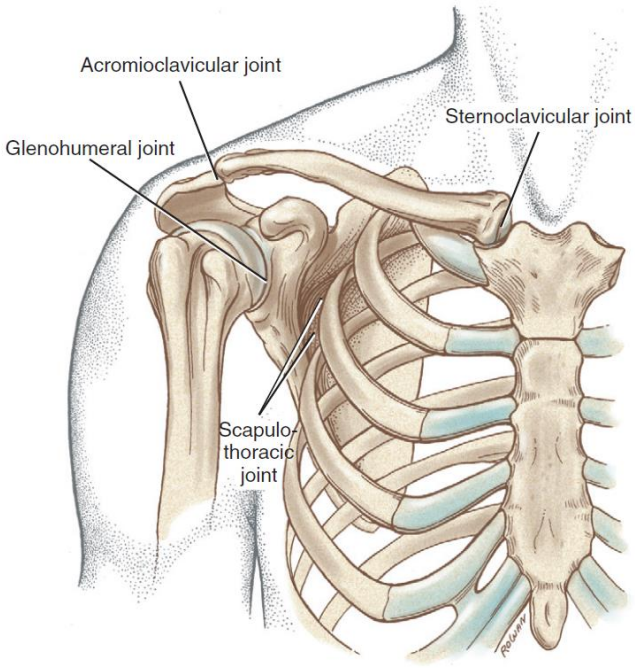

Fig. 1 Right shoulder complex [18]

2.1.1 Anatomy

2.1.1.1 Bones

The head of the humerus, constituting approximately half of a complete sphere, serves as the convex component within the glenohumeral joint [16]. The orientation of the head is predominantly medial, superior, and posterior relative to the humeral shaft. In a medial and superior direction, the head forms an inclination angle of approximately 135 degrees concerning the longitudinal axis of the humerus in frontal plane [18]. In the transversal plane, the head exhibits a posterior inclination of around 30 degrees, commonly referred to as the retroversion of the humerus (Fig. 2). This rotation positions the humeral head within the scapular plane to facilitate its articulation with the glenoid fossa [18].

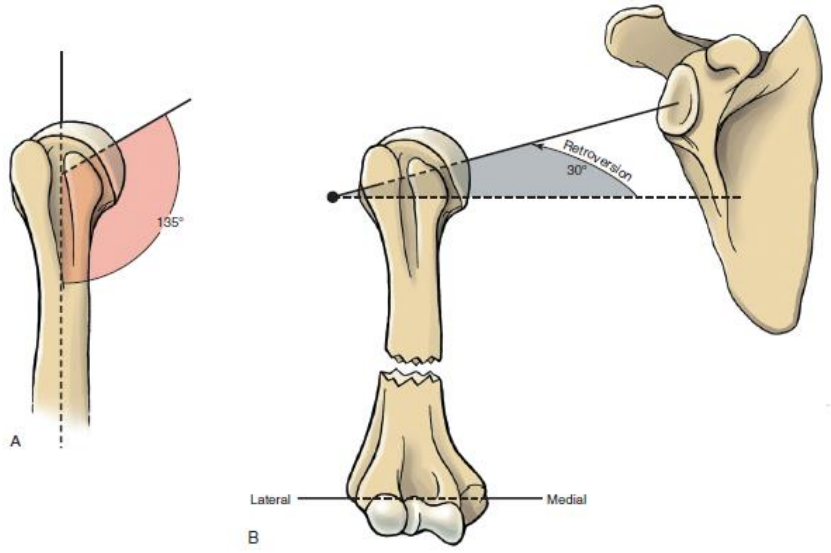

Fig. 2 The angle of inclination (A) and the retroversion of humerus (B) [18]

The glenoid fossa, situated on the scapula, serves as the concave articular surface for the joint. The orientation of this shallow concavity relative to the thorax can vary, depending on the resting position of the scapula on the thorax and movements at the sternoclavicular and acromioclavicular joints. Moreover, the orientation of the glenoid fossa can also be influenced by the specific morphology of the scapula itself. It may exhibit a slight upward or downward tilt, although most common representation is a slight upward tilt, around 5 degrees [19]. Additionally, the fossa may not always lie in a plane perpendicular to the scapula; it can be anteverted or retroverted up to 10 degrees, with 6 to 7 degrees of retroversion being the most typical as shown in Fig. 3 [19].

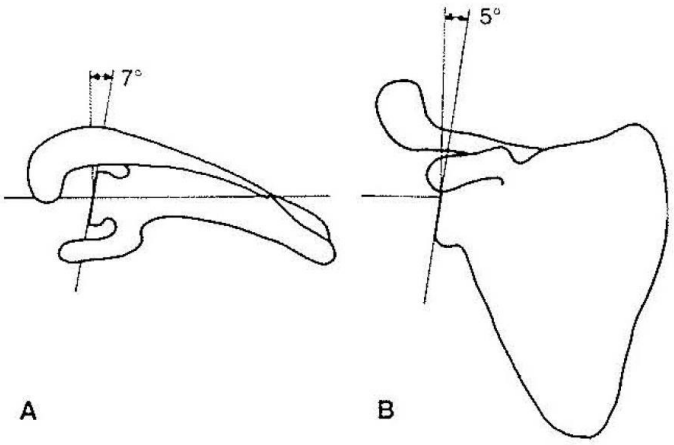

Fig. 3 Glenoid retroversion (A) and slight superior tilt (B) [20]

2.1.1.2 Ligaments

The fundamental structural element responsible for static stabilization is the combination of the joint capsule and the adjacent ligaments (Fig. 4). The fibrous capsule of the glenohumeral joint, although relatively thin, gains reinforcement from thicker external ligaments. While the majority of the ligament fibres attach to the humerus, a smaller number of circular fibres spiral around the joint and reattach within the capsule. The capsular ligaments of the glenohumeral joint are composed of intricate bands of interwoven collagen fibres, categorized into superior, middle, and inferior bands (Fig. 18) [21]. The stability of the joint capsule is further enhanced by the presence of the coracohumeral ligament [22].

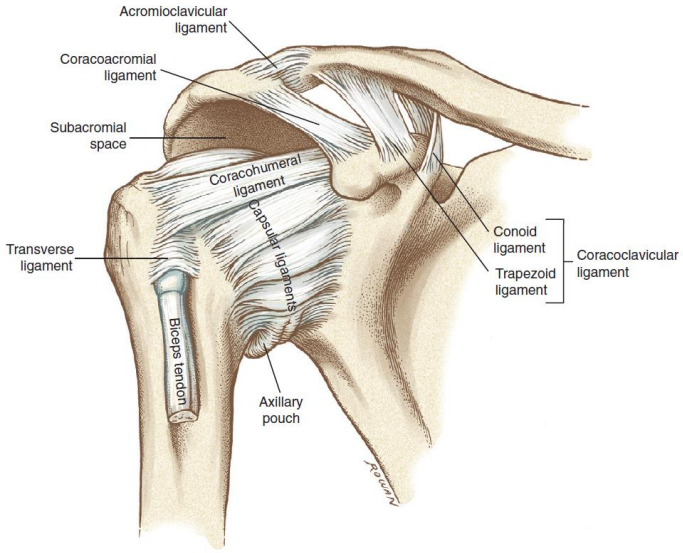

Fig. 4 Primary ligaments of the glenohumeral joint [18]

One of the important fibrous structures within the glenohumeral joint is the glenoid labrum (Fig. 5). It extends the glenoid fossa, augmenting its depth by

approximately 50% [23]. Additionally, the glenoid labrum serves as the attachment point for both the glenohumeral ligaments and the tendon of the long head of the biceps brachii [24].

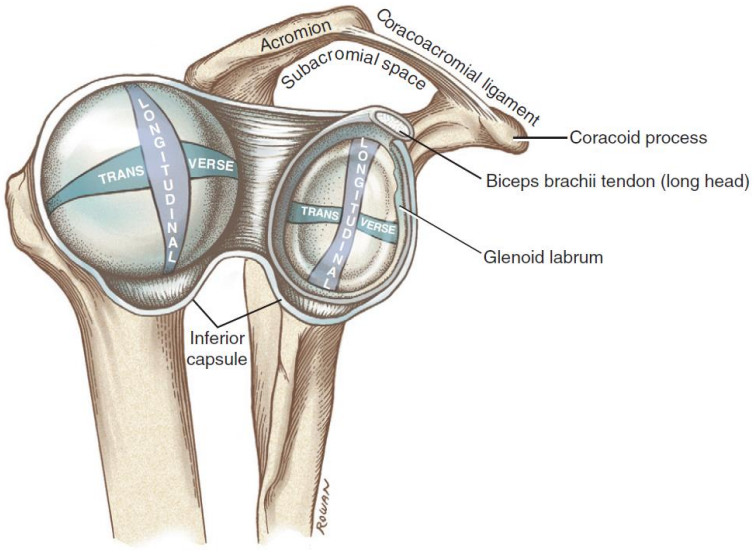

Fig. 5 Lateral perspective of an exposed glenohumeral joint [18]

2.1.1.3 Muscles

The majority of shoulder complex muscles can be categorized as either proximal stabilizers or distal mobilizers. Proximal stabilizers, such as the serratus anterior or trapezius, have origins on the spine, ribs, and cranium, and insert on the scapula and clavicle. Distal mobilizers, like the deltoid and biceps brachii, originate on the scapula and clavicle, inserting on the humerus or forearm. As explained later, the effective functioning of the shoulder complex necessitates coordinated interaction between these proximal stabilizers and distal mobilizers [18]. An overview of the primary shoulder muscles is provided in Tab. 1.

Tab. 1 Primary muscles (distal mobilizers) of the shoulder complex responsible for glenohumeral movements [15].

Muscle	Origin	Insertion	Function
Deltoideus (Anterior)	Outer third of clavicle, top of acromion, scapular spine	Deltoid tuberosity of humerus	Flexion, horizontal adduction, medial rotation
Deltoideus (Middle)			Abduction, horizontal abduction
Deltoideus (Posterior)			Extension, horizontal abduction, lateral rotation

Muscle	Origin	Insertion	Function
Supraspinatus	Supraspinous fossa	Greater tuberosity of humerus	Abduction, assists with lateral rotation
Infraspinatus	Infraspinous fossa	Greater tubercle of humerus	Lateral rotation, horizontal abduction
Teres major	Lower, lateral, dorsal scapula	Anterior humerus	Extension, adduction, medial rotation
Teres minor	Posterior, lateral border of scapula	Greater tubercle, adjacent shaft of humerus	Lateral rotation, horizontal abduction
Subscapularis	Entire anterior surface of scapula	Lesser tubercle of humerus	Medial rotation
Biceps brachii (Long head)	Upper rim of glenoid fossa	Radial tuberosity	Assists with abduction
Biceps brachii (Short head)	Coracoid process of scapula		Assists with flexion, adduction, medial rotation, horizontal adduction
Coracobrachialis	Coracoid process of scapula	Medial anterior humerus	Flexion, adduction, horizontal adduction
Triceps brachii (Long head)	Inferior to glenoid fossa	Olecranon process of ulna	Assists with extension, adduction
Pectoralis major (Clavicular)	Medial two-thirds of clavicle	Lateral aspect of humerus just below head	Flexion, horizontal adduction, medial rotation
Pectoralis major (Sternal)	Anterior sternum and cartilage of first six ribs		Extension, adduction, horizontal adduction, medial rotation
Latisimus dorsi	Lower six thoracic and all lumbar vertebrae, posterior sacrum, iliac crest, lower three ribs	Anterior humerus	Extension, adduction, medial rotation, horizontal abduction

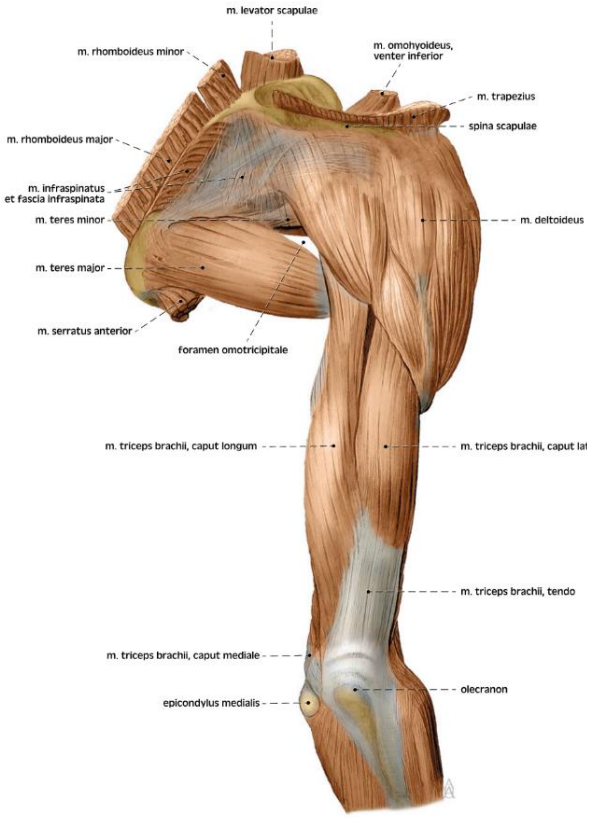

Fig. 6 Muscles of the shoulder and arm, posterior view [25]

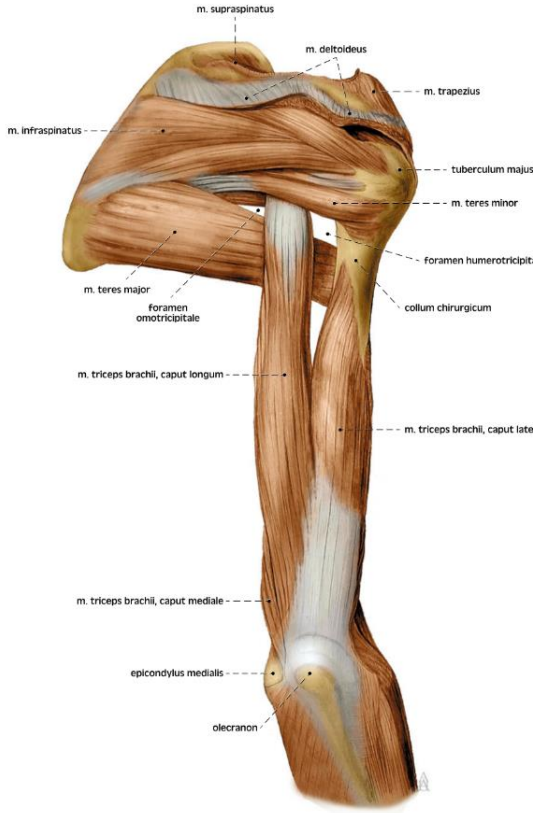

Fig. 7 Muscles of the shoulder and arm, the deltoid muscle removed, posterior view [25]

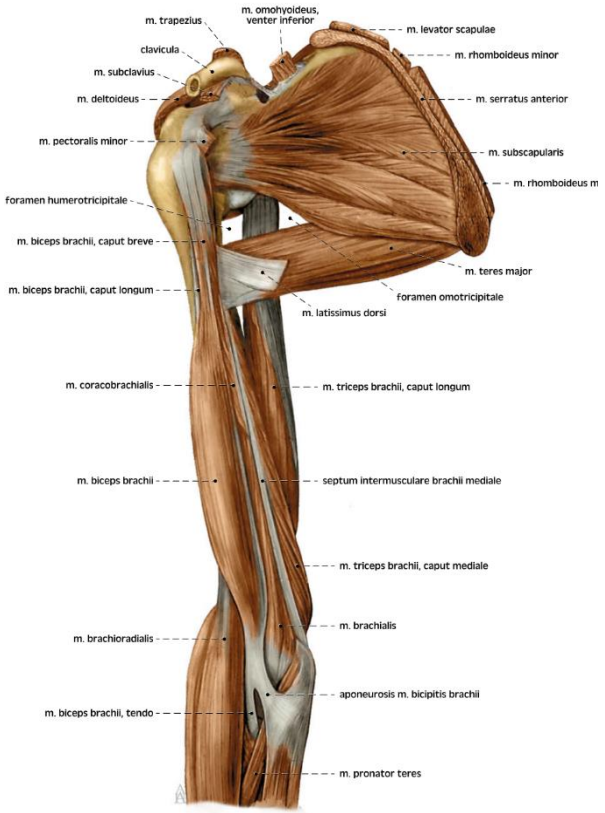

Fig. 8 Muscles of the shoulder and arm, the deltoid muscle removed, anterior view [25]

2.1.2 Movements

Six fundamental movements can be described within the glenohumeral joint (Fig. 9). Full ranges of movements in glenohumeral joint are not isolated and depend on the movements of other joints in shoulder complex (Fig. 1) [18].

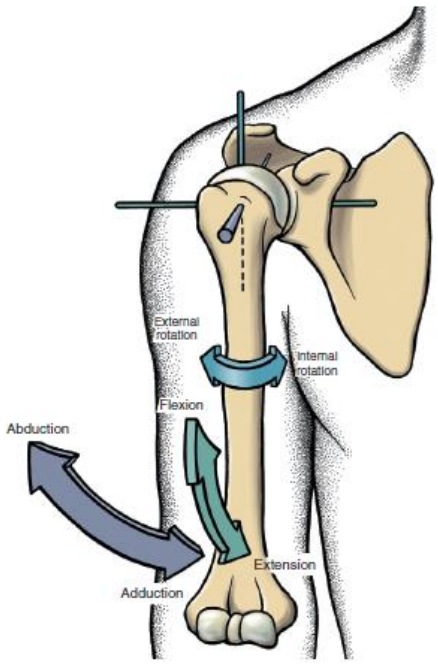

Fig. 9 Fundamental movements in glenohumeral joint [18]

2.1.2.1 Flexion

The arthrokinematics of flexion (Fig. 9) can be characterized as a rotational movement of the humeral head around the glenoid fossa, employing a medial-lateral axis of rotation with the arm moving anteriorly [18]. Muscles that traverse the anterior side of the glenohumeral joint play a role in shoulder flexion. The main flexors include the anterior deltoid and the clavicular segment of the pectoralis major (Fig. 10). Additionally, the coracobrachialis and the short head of the biceps brachii provide auxiliary support in the process of flexion [15]. The typical range of flexion observed in healthy general population approximates 160 degrees [26]. Approximately 120° of flexion can be achieved through the isolated movement of glenohumeral joint. Beyond this range, additional shoulder flexion involves upward rotation of the scapulothoracic joint. [27].

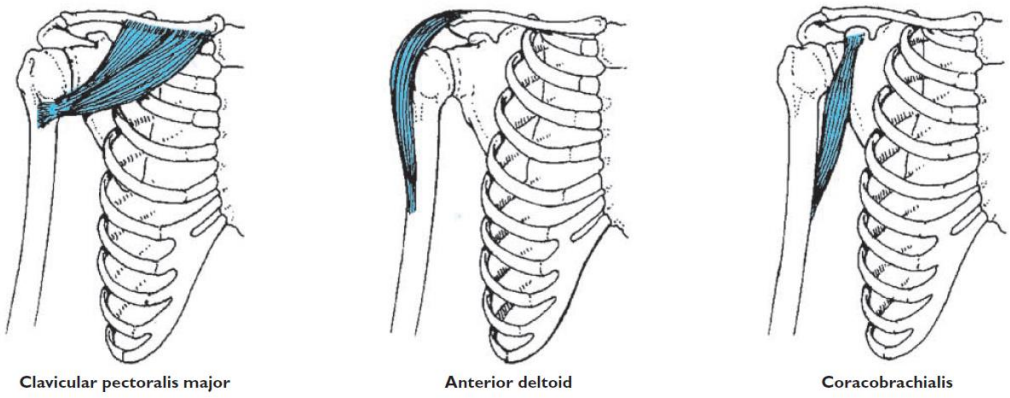

1

Fig. 10 The main flexors of the glenohumeral joint [15]

2.1.2.2 Extension

The arthrokinematics of extension (Fig. 9) mirror those of flexion, except for the arm's posterior movement [18]. In the absence of resistance, shoulder extension is primarily facilitated by gravitational force, and the eccentric contraction of the flexor muscles serves to regulate or decelerate this motion. However, when external resistance is encountered, the muscles located posterior to the glenohumeral joint, notably the sternocostal pectoralis, latissimus dorsi, and teres major, act to extend the humerus. The posterior deltoid contributes to extension, particularly in cases where the humerus is externally rotated. Additionally, the long head of the triceps brachii provides assistance, and its effectiveness is slightly enhanced when the elbow is in a flexed position, owing to its action across the elbow joint [15]. The extension range of motion extends to approximately 65 degrees posteriorly from the frontal plane [28].

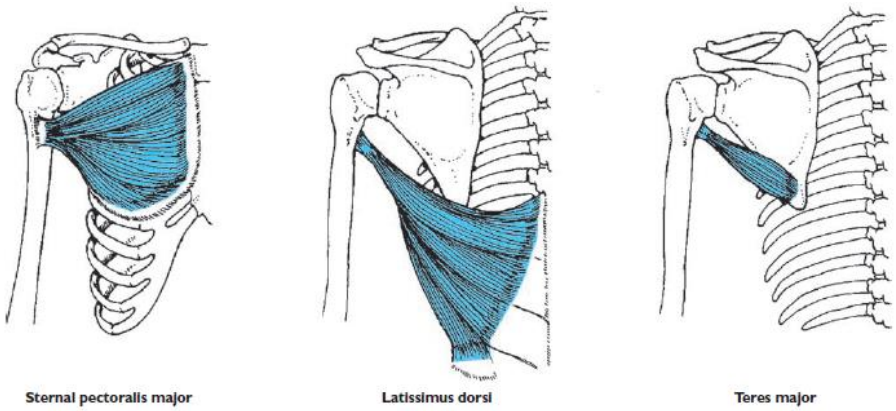

Fig. 11 The main extensors of the glenohumeral joint [15]

2.1.2.3 Abduction

Abduction can be characterized as a rotation of the humerus around the anterior-posterior axis with the arm moving laterally (Fig. 9). In this motion, the ball rolls superiorly while simultaneously sliding inferiorly (Fig. 13). This coordinated movement ensures continuous contact between the articulation surfaces throughout the entire range of abduction [18]. The main abductors of the humerus are the middle deltoid and supraspinatus muscles. The supraspinatus muscle, active during the initial 110 degrees of motion, initiates the process of abduction. Subsequently, in the range from approximately 90 degrees upwards of abduction, the middle deltoid muscle comes into play [15]. During this phase, the infraspinatus, subscapularis, and teres minor muscles act to counterbalance the component of force produced by the middle deltoid that would otherwise tend to dislocate the humerus superiorly [15]. The typical range of abduction observed in healthy general population approximates 150 degrees [26]. Scapulohumeral rhythm that occurs in abduction was reported by Inman et al., 1944 [29]. This classical study states that in a healthy shoulder is a natural kinematic rhythm between glenohumeral abduction and scapulothoracic upward rotation. It has been observed that after approximately 30 degrees of abduction, this rhythm remains consistently constant, manifesting at a ratio of 2:1 (meaning that every 2 degrees of glenohumeral abduction is accompanied by 1 degree of scapulothoracic upward rotation).

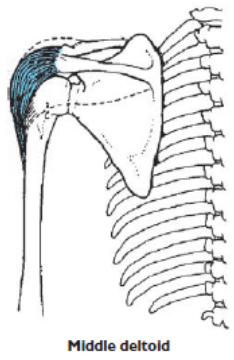

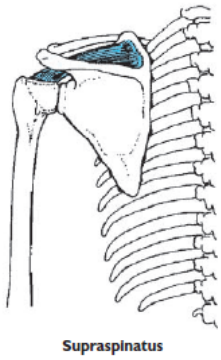

Fig. 12 The main abductors of the glenohumeral joint [15]

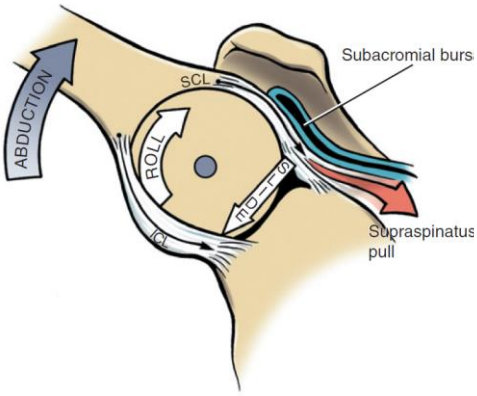

Fig. 13 The arthrokinematics of the glenohumeral joint during abduction [18]

2.1.2.4 Adduction

As is the case with shoulder extension, unresisted adduction at the shoulder primarily arises from gravitational force, with the abductor muscles serving to regulate the pace of the movement. The motion mirrors abduction with arm moving

medially [18]. When external resistance is introduced, the primary adductors are the latissimus dorsi, teres major, and sternocostal pectoralis muscle, situated on the inferior side of the joint. The short head of the biceps and the long head of the triceps provide minor supplementary support, and when the arm is elevated beyond 90 degrees, the coracobrachialis and subscapularis muscles also contribute to the adduction process [15].

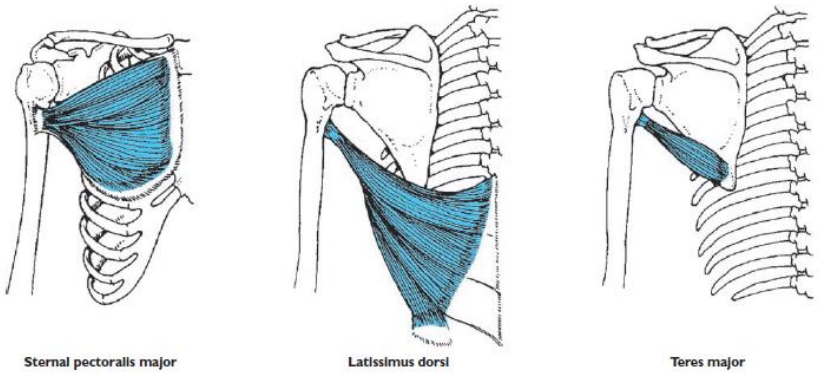

Fig. 14 The main adductors of the glenohumeral joint [15]

2.1.2.5 Internal and External Rotation

Internal (medial) and external (lateral) rotation at the glenohumeral joint is characterized by an axial rotation of the humerus in the transverse plane. This rotation takes place around the longitudinal axis of the humerus [18]. Internal rotation of the humerus is predominantly driven by the subscapularis and teres major muscles. These muscles are attached to the anterior side of the humerus, with the subscapularis having the most substantial mechanical advantage for facilitating medial rotation. Additionally, the anterior deltoid, both segments of the pectoralis major, the latissimus dorsi, and the short head of the biceps brachii play auxiliary roles, with the pectoralis major being the primary assisting muscle in this context. Conversely, muscles anchored to the posterior side of the humerus, notably the infraspinatus and teres minor, contribute to external rotation with some assistance from the posterior deltoid [15]. The typical range of lateral rotation observed in healthy general population approximates 60 degrees [26].

2.1.2.6 Circumduction

Circumduction is a coordinated sequence of shoulder movements that results in the hand following a circular path and the arm tracing a conical trajectory with apex in shoulder. This complex movement is achieved by sequentially combining shoulder flexion, abduction, extension, and abduction (or their reverse sequence).

Successful execution of circumduction involves the coordination of all muscles responsible for these individual movements, as well as the interaction of other joints within the pectoral girdle [30].

2.1.3 Stabilization

Unlike the hip joint, which possesses a ball-and-deep-socket configuration centered by the acetabulum, enveloping most of the femoral head and offering significant resistance to dislocation, the glenohumeral joint exhibits a different anatomical arrangement [31]. In the shoulder joint, a relatively small glenoid socket accommodates the much larger humeral head. In shallow joints like the knee, ligaments remain taut to stabilize the joint in all positions [32]. However, in the case of the shoulder joint, the ligaments must remain lax in most of the positions to enable a full range of motion. Consequently, alternative mechanisms are necessary to maintain stability in the glenohumeral joint [33].

Glenohumeral balance is a stabilizing mechanism where the glenoid is aligned to ensure that the net humeral joint reaction force passes through the glenoid fossa. When the humeroscapular position is configured to facilitate this alignment, no additional stabilizing mechanisms are required. This stability is effectively maintained within a range of directions, roughly spanning 60 degrees around the centerline of the glenoid (30 degrees anteriorly and 30 degrees posteriorly). Conditions such as hypoplasia, erosion, or glenoid rim fractures can reduce the stability angular range [34].

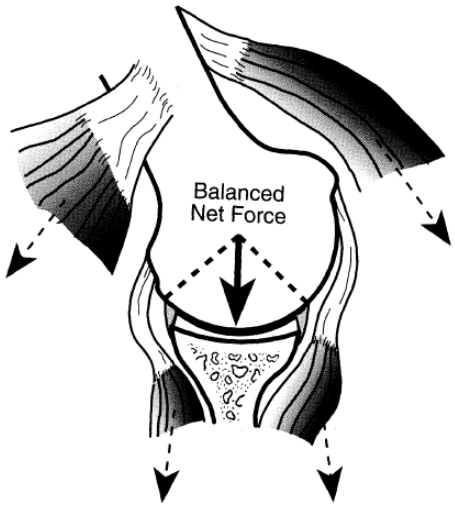

Fig. 15 The vector sum of muscle forces creates the net humeral joint reaction force [33].

Concave compression effect is present even though the glenoid fossa is notably shallow. Convex humeral head is pressed into a concave glenoid, thereby protects the joint from translation. This effect is also supported by the labrum glenoidale, which makes up approximately 50% of the effective depth of the glenoid (Fig. 16) [23].

Fig. 17 depicts the stability ratios of translation to compressive force in the glenohumeral joint, revealing significantly higher values in the superior-inferior direction compared to the anterior-posterior direction. This discrepancy arises from the greater width of the glenoid in the superior-inferior direction, which, given a constant radius, leads to increased depth. [34].

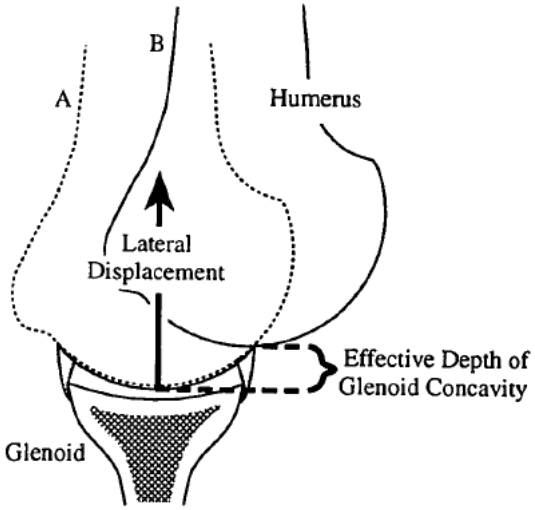

Fig. 16 The effective depth of gleoind is described as maximum lateral displacement of the humerus without losing a stability. Humeral head at center of glenoid (A) and at the glenoid rim (B) [34].

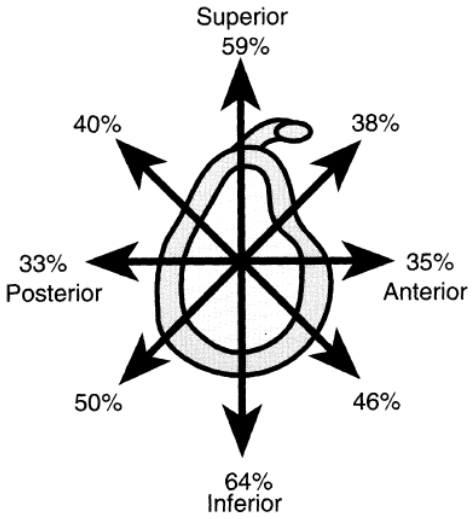

Fig. 17 Stability ratios for the glenohumeral joint under a 50 N compressive load with an intact labrum. [33].

Adhesion-cohesion functions as a mechanism binding the articulating surfaces through the molecular attraction present in the synovial fluid (cohesion) and adhesion of the synovial fluid to the cartilage. Also, mechanism like a suction cup operates within the glenohumeral joint. The glenoid surface exhibits greater flexibility at its edges than at the center. The peripheral structures, including the glenoid labrum and the capsule, contribute additional flexibility. This allows the socket to adapt and securely encase the humeral head. Notably, both adhesion-cohesion mechanisms operate independently of muscle tension [33]. Itoi et al., 1993 [35] reported intraarticular pressure around -76 cm H_2O in nine fresh frozen

cadaveric shoulders without load. This static negative pressure relates to the mechanisms mentioned above.

The shoulder muscles play a crucial role in providing dynamic stability. The activation of tension in one shoulder muscle often needs to be counteracted by the development of tension in its antagonist to prevent dislocation of the humeral head [15].

Most muscles spanning the shoulder contribute to dynamic stability in the joint, with the rotator cuff excelling in this regard. The rotator cuff, comprising the subscapularis, supraspinatus, infraspinatus, and teres minor (shown in Fig. 18) plays a crucial role in enhancing dynamic stability. A key function of the rotator cuff group is to compensate for the natural laxity and predisposition for instability in the glenohumeral joint [36]. The distal attachments of these muscles blend into the joint capsule before attaching to the humerus, creating a protective cuff around the joint. Forces primarily generated by the rotator cuff, along with their attachments into the capsule, not only actively rotate the humeral head but also stabilize and centralize it against the glenoid fossa [37].

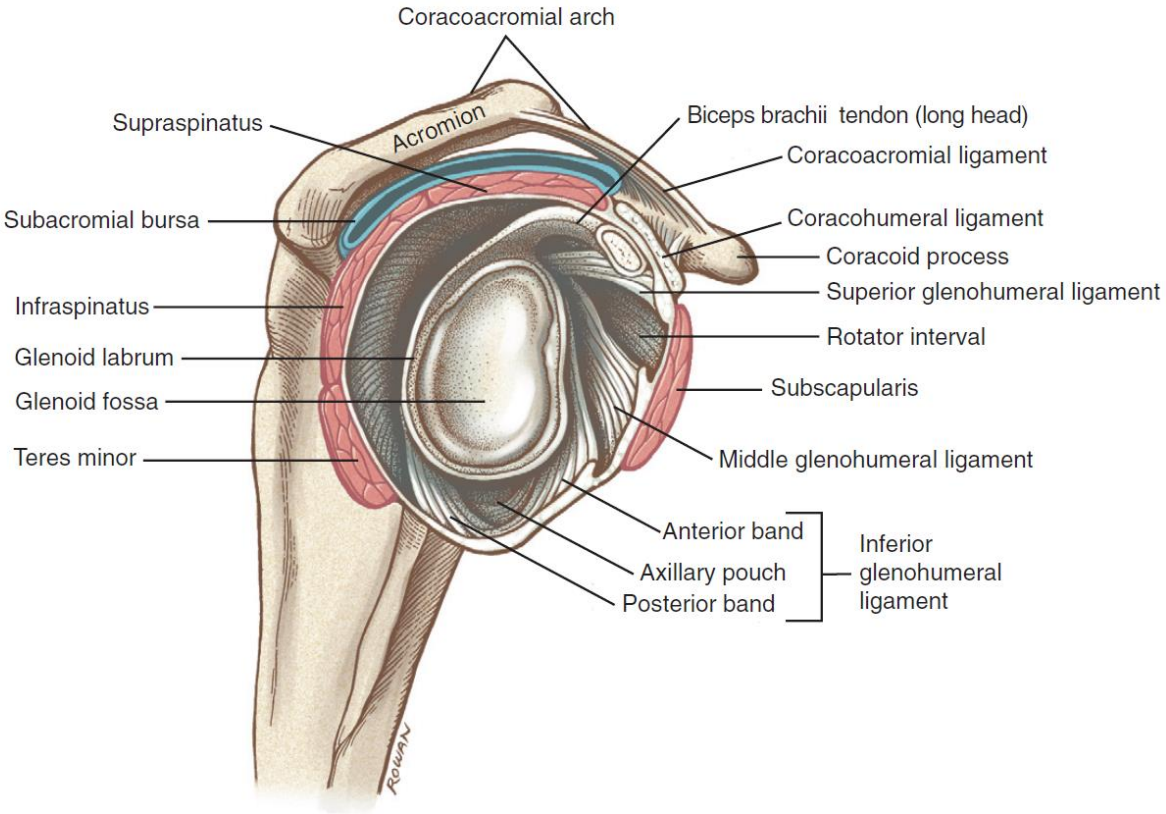

Fig. 18 Lateral view of the inner surface of the glenohumeral joint [18].

2.2 Reverse Total Shoulder Arthroplasty

The utilization of shoulder arthroplasty has witnessed significant expansion over the last decade, a trend supported by data from US databases. These statistics can be attributed, at least in part, to an aging population that aspires to maintain an active lifestyle [13]. In 2012, a total of 22,835 primary RTSA procedures were conducted [9]. In 2017, this number experienced a significant surge, nearly tripling to reach 62,705 RTSA procedures [9]. Over the same period, the count of anatomic total shoulder arthroplasty (TSA) procedures rose from 29,685 in 2012 to 40,665 in 2017 [9]. Conversely, the number of shoulder hemiarthroplasty procedures underwent a substantial decline, decreasing by almost half, from 11,695 in 2012 to 4,930 in 2017 [9].

Nowadays, total shoulder arthroplasty (TSA) is a common intervention for advanced glenohumeral joint osteoarthritis, demonstrating efficacy in terms of pain alleviation, functional enhancements, and a high rate of implant longevity in patients who maintain an intact rotator cuff [38]. On the other hand, RTSA has proven to be effective in reducing pain and optimizing functionality in patients with rotator cuff-deficient shoulders [39; 10]. Nevertheless, RTSA also serves as an effective treatment option for various other medical conditions. This includes the acute and delayed management of proximal humeral fractures [40], fracture malunion and non-union, cases of rheumatoid arthritis, tumor-related issues, fixed glenohumeral dislocation, revision arthroplasty [10] and severe glenoid bone wear [41].

2.2.1 Evolution and Design

In 1893, Jules Emile Péan introduced the initial implementation of total shoulder arthroplasty. The surgical procedure was conducted in Paris on a patient afflicted with tuberculosis in shoulder, who declined the option of amputation. This shoulder implant consisted of a platinum shaft, a hardened rubber sphere, and metallic loops, and it was conceived and fabricated by a dentist J. Porter Michaels [42]. It became the first metal implant within the human body, predating the initial metal total hip implant, which was introduced in 1953, and the first metal total knee implant, which was introduced in 1973 [43].

In 1955, Dr. Charles Neer unveiled his first hemiarthroplasty design crafted from vitallium (CoCrMo). This design prioritized the use of an inert material with elastic properties resembling bone tissue, faithfully replicating the natural anatomical

structure. Furthermore, it incorporates ample anchorage through a long stem within the bone to mitigate the risk of bone resorption [44].

In the 1970s, a polyethylene glenoid component was devised and integrated with Charles Neer's humeral replacement system [45]. Subsequent years witnessed advancements, encompassing not only material enhancements but also the modular aspects of the humeral components. [43].

It was observed that anatomical replacement alone proved insufficient for patients with deficient rotator cuff. In response to this, the reverse replacement technique was developed to address beyond this specific patient population.

Fig. 19 Platinum and rubber-based shoulder prosthesis by Péan [43].

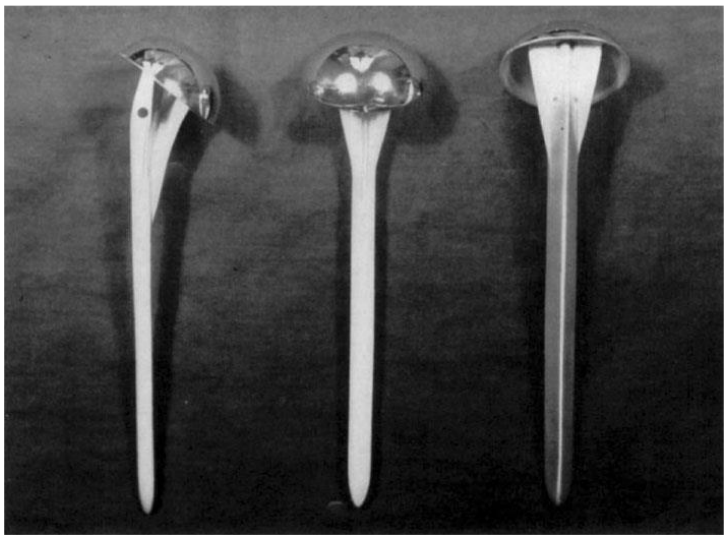

Fig. 20 Neer's initial vitallium prosthesis design, primarily intended for fracture cases in small, medium, and large version [44].

In the 1970s, several designs of RTSA were introduced. However, many of them faced challenges as they adhered to the anatomical COR, resulting in restricted motion. Consequently, these designs generated excessive torque and shear forces at the glenosphere-bone interface, leading to premature loosening. In most instances, the achievable functional active elevation was limited, often falling below 90 degrees, particularly in relation to scapulothoracic motion. Numerous models remained experimental and were eventually abandoned due to these failures [46]. Some of these designs are mentioned below.

In 1972, Neer and Averill [47] introduced three types of “Mark” reverse prothesis numbered I, II, and III. All types had fixed fulcrum. Mark I had an oversized ball to allow increased motion. Mark II had smaller ball to allow rotator cuff reconstruction,

and Mark III was also with smaller ball and rotating stem within a polyethylene sleeve to regain motion.

In the same year Reeves, 1972 [48] designed replacement with respect to anatomical CoR and with glenosphere fixed by divergent threaded peg (Fig. 21). This replacement was only experimental [46].

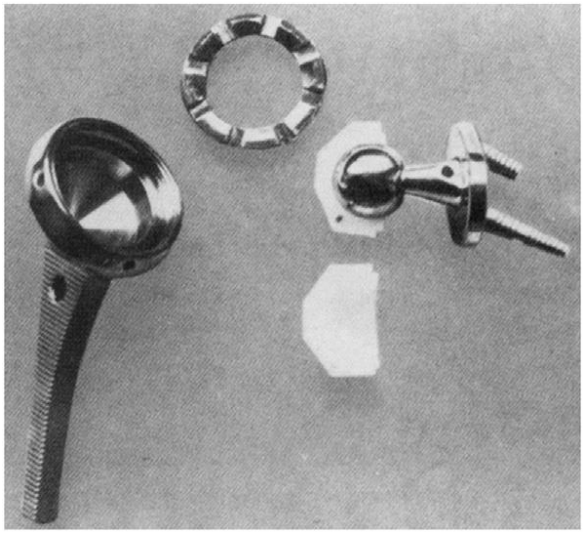

Fig. 21 The first reverse prosthesis developed by Reeves [43].

Fig. 22 Grammont's first design of a reverse prosthesis Delta also called „Trompette" [43].

Next year Kölbel and Friedebold, 1973 [49] presented an implant with a new designed to reduce bone removal from the glenoid. Scapular fixation was done by bolted flange with central screw and two plates with the screws directed toward the coracoid process and/or the base of the scapular spine. It occurred functional in stress transfer as well.

Kessel et al., 1979 [50] introduced his design in 1973. In this model, the glenosphere was secured to the glenoid using a large central screw and the humeral stem was affixed with bone cement.

Fenlin, 1975 [51] proposed a design aimed at enhancing deltoid function through a larger glenosphere with an expanded ball-and-socket construct, intended to compensate for the absence of the rotator cuff. The glenosphere was constructed from polyethylene to reduce the implant's weight, while the humeral cup was metallic.

Buechel et al., 1978 [52] introduced replacement with floating fulcrum provided with two spheres supporting system, featuring a small glenosphere articulating

with a larger and mobile intermediate polyethylene cup, along with the humeral head, enabling additional motion.

In 1981, Paul Grammont introduced the concept of medializing the COR. This involves also shifting the COR of the glenohumeral joint inferiorly and thereby increasing the lever arm of the deltoid. This adjustment aims to compensate for the absence of the rotator cuff muscles [53]. The initial prototype by Grammont, introduced in 1985, was named Delta (referring to deltoideus) (Fig. 22). It comprised only two components: a metallic or ceramic glenosphere with a diameter of 42 mm without a neck, and a polyethylene socket for the humeral component. The stem of the humeral component had a trumpet-shaped design, leading to the prosthesis being dubbed "Trompette". Cementation was employed to anchor both the humeral and glenoid sides of the prosthesis [54].

Between years 1991 and 1994, three generations of Delta III prosthesis were introduced. The third generation consisted of five parts: the glenoid baseplate, the glenosphere, the polyethylene humeral cup, the humeral neck, and the humeral stem. The Delta III prosthesis (DePuy International Limited, Leeds, England) has been used for the last 25 years worldwide [55]. The Delta III also presents drawbacks, such as scapular notching. This occurs due to the absence of a prosthetic neck on the glenosphere and the horizontal orientation of the humeral cup. The notching is a result of the impingement of the medial aspect of the polyethylene humeral cup on the scapular neck, both inferiorly and posteriorly. [56]. Additionally, there is a limitation in the rotation of the glenohumeral joint caused by the medialization of the humeral component, leading to increased medial impingement against the scapula. The medialization of the COR also diminishes the strength of the posterior and anterior deltoid fibers [57]. Other issues, such as instability or acromial fracture, are linked to inadequate deltoid tension [58].

Most of the RTSA systems that were introduced after Grammont's prosthesis are grounded in its principles and and aim to address its inherent shortcomings. In 1998, Frankle developed the reverse prosthesis (ENCORE Medical, Austin, Texas, USA). Positioned less medially than Grammont's Delta, it had the COR closer to its typical anatomical location. Consequently, there was an improvement in the range of rotation, although abduction was compromised. [59]. In 2001, the Duocentric® reverse prosthesis (Aston Medical) drew inspiration from the "Trompette" and Delta® (DePuy). This system key elements are a spherical inferior overhang to

prevent scapular notching and variously sized fixation pegs to preserve the glenoid bone stock [60]. In 2003, Lima Corporate introduced a reverse shoulder prosthesis with a modular shoulder replacement system (SMR™) [61]. This system allows conversion to reverse shoulder arthroplasty without changing the humeral stem, and the glenoid metal back helps avoid the risk of sacrificing bone [62].

Aequalis Ascend™ Flex (Tornier SASWright Medical Inc., Bloomington, MN, USA) was introduced in 2012. It was a novel reverse shoulder prosthesis featuring an a short, uncemented, and convertible humeral stem. It was designed to meet specific criteria: preserving bone stock with a short stem, preventing scapular notching by employing a 145° angle derived from the summation of the stem and polyethylene liner angles, and facilitating easier humeral revision. [63].

Fig. 23 SMR prothesis (Lima Corporate SMR™) [46].

Fig. 24 The Aequalis Ascend™ Flex (Tornier SAS-Wright Medical Inc., Bloomington, MN, USA) prothesis with short stem [46].

2.2.2 Biomechanics of Reverse Total Shoulder Arthroplasty

In RTSA, the COR is medially and inferiorly shifted, influencing the biomechanical characteristics of the deltoid muscle (Fig. 25 and Fig. 26) and the remaining rotator cuff. The medialization of the COR elevates deltoid tension, crucial for prosthetic stability and improved efficacy during abduction [64]. Deltoid elongation, approximately 20% greater than that of a normal shoulder, is more pronounced in shoulders with cuff tear arthropathy. The abduction moment arm of the deltoid significantly increases by up to 40 mm, impacting its capacity to generate abductional forces [65]. The displacement of the humerus also affects the biomechanics of the remaining rotator cuff. In patients with cuff tear arthropathy, the supraspinatus and infraspinatus are frequently affected, resulting in compromised humeral rotation postoperatively [66]. Following conventional RTSA, rotational moment arms of the teres minor and subscapularis experience a substantial decrease. Muscle tension in these muscles decreases, and overall muscle length diminishes after surgery [67]. One potential strategy for mitigating these unfavorable biomechanical properties is to laterally shift the COR compared to conventional RTSA. However, it's important to note that this approach also addresses specific biomechanical disadvantages. Lateralized RTSA preserves rotational moment arms and prevents significant reductions in muscle tension for both the subscapularis and teres minor [68]. However, overall joint reaction forces in RTSA are reduced by approximately 30% compared to a normal shoulder, primarily in glenoid compression forces, while shear forces may increase with flexion [64].

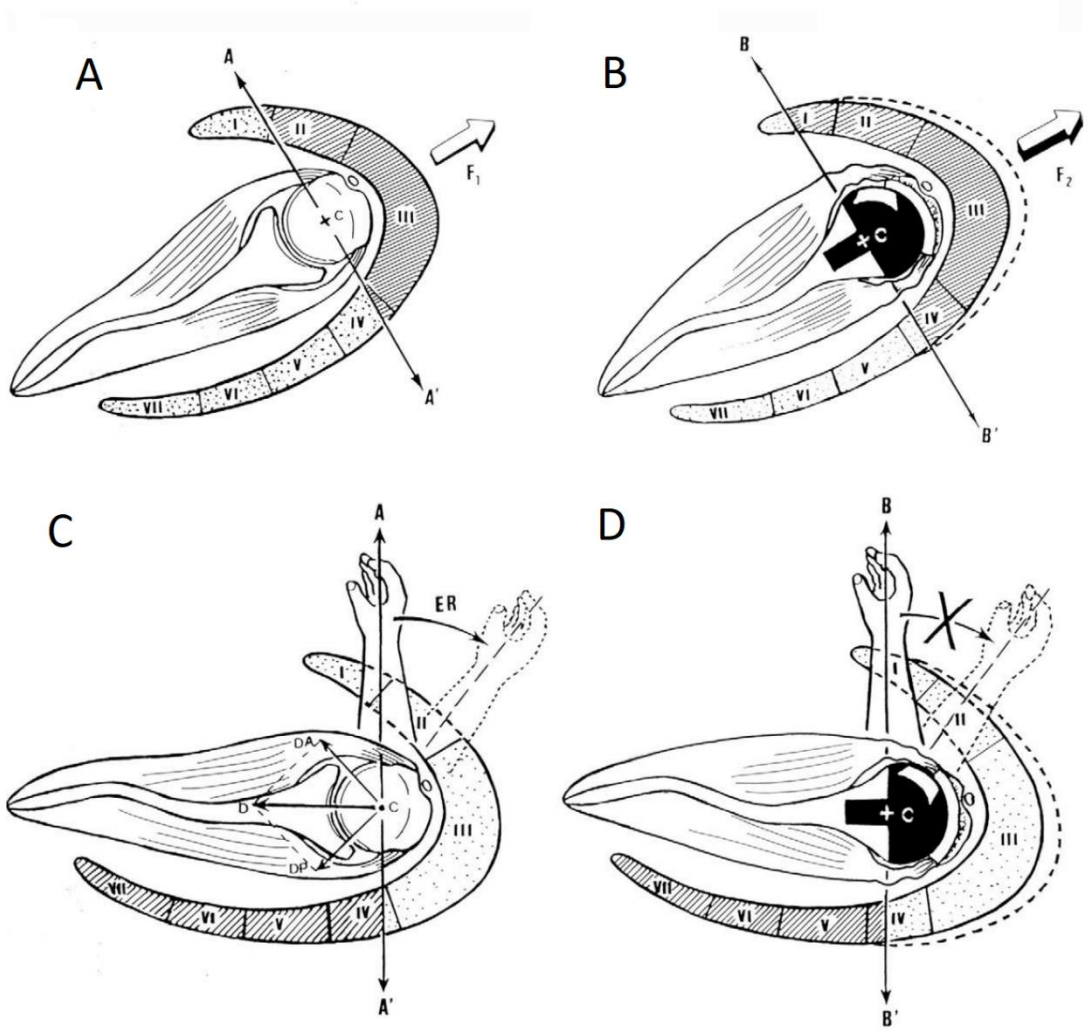

Fig. 25 In a normal shoulder, active elevation involves only the middle deltoid and a portion of the anterior deltoid segment (A); following RTSA, the medialization of COR engages more of the deltoid fibers for active elevation (B). Conversely, RTSA alters the dynamics in external rotation (ER), resulting in a reduced utilization of the posterior deltoid (D) compared to a normal shoulder (C). [11].

While the normal glenohumeral joint relies on dynamic stabilizers, such as the rotator cuff muscles, for stability, patients undergoing RTSA lack this natural dynamic stabilization. Consequently, maintaining the relative position of the humerus against the glenoid becomes crucial. The RTSA design strategically positions the convex surface on the glenoid and the concave surface on the humerus, effectively constraining the joint and preventing superior translation during deltoid contraction. This modification allows for a broader deviation angle of the joint force vector without the risk of dislocation. To enhance the stability of the RTSA, increasing the ratio between the diameters of the glenosphere and humeral socket is advocated [69]. Additionally, adjusting the depth of the humerosocket can

contribute to stability, although this must be carefully balanced with the impingement-free range of motion [70].

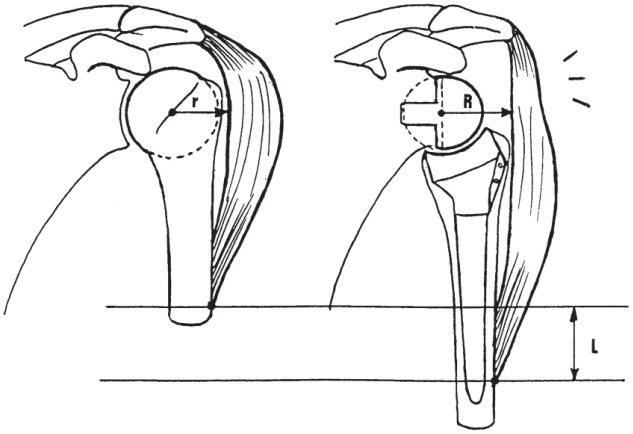

Fig. 26 The lever arm for deltoid contraction during elevation initiation is extended in RTSA due to the medialization of COR ($R > r$). Furthermore, the strength of the deltoid is increased by the prolonging of the humerus (L), leading to the elongation of deltoid fibers [11].

Another approach to boost deltoid efficiency is to pretension the muscle by increasing its resting length, achieved in the RTSA by distalizing the humeral insertion of the deltoid muscle (Fig. 26). Studies suggest that even a 1 cm distalization can yield an additional 30% efficiency [69]. This not only aids in deltoid torque production but also enhances joint stability. Optimal deltoid lengthening remains a subject of investigation, but studies indicate improved functional outcomes with arm lengthening rather than shortening. However, potential complications, including neuropraxia and acromial stress fractures, need careful consideration in the context of over-lengthening of the deltoid muscle [71; 72].

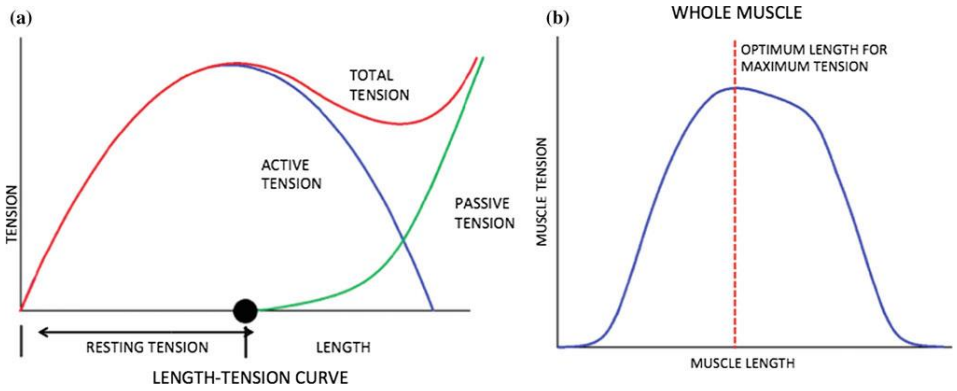

Fig. 27 Length–Tension Relationship: The total tension generated by a muscle comprises both its active tension during contraction and passive tension (a). Enhancing the passive tension of a muscle is achievable by increasing its resting length (b), thereby contributing to an overall improvement in the force generated by the muscle [73].

2.3 Musculoskeletal models

The musculoskeletal modeling of the shoulder mechanism, which includes the thorax, clavicle, scapula, and humerus, is particularly challenging due to its complexity. Since the work of Inman et al., 1944 [29], various musculoskeletal mathematical models of the glenohumeral joint have been developed for clinical applications. The following provides an overview of selected musculoskeletal models that specifically examine loading in the glenohumeral joint during abduction.

2.3.1 Poppen and Walker, 1978

A two-dimensional biomechanical model based on X-ray images of normal subjects. Relative angles of the humerus, glenoid and the thorax, were found from a radiographic study as well as the COR in the middle of humeral ball. An electromyographic study of 37 normal subjects provided information of the integrated signals of the muscles around the shoulder for isometric abduction in the plane of the scapula. The muscle vectors and their lines of action and lever arms about the COR were determined from three fresh cadaveric upper quarter specimens from normal males [74].

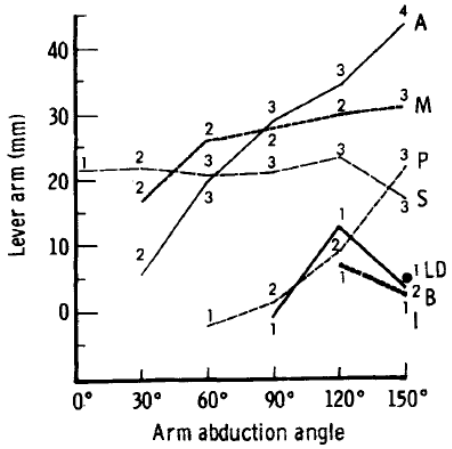

Fig. 28 The lever arms and level of muscle activity (1–4) at different abduction angles. S = supraspinatus; A = anterior deltoid; M = middle deltoid; P = posterior deltoid; B = subscapularis; I = infraspinatus; LD = latissimus dorsi [74].

From an electromyographic study, it was utilized that all heads of deltoid muscle (anterior, middle, and posterior), supraspinatus, infraspinatus, subscapularis and latissimus dorsi are active during abduction and a muscle activation rated from 1 to 4 was evaluated (Fig. 28). Therefore, the glenohumeral joint load was calculated with reflection only to these muscles (Fig. 32) [74].

2.3.2 van der Helm, 1994

A three-dimensional musculoskeletal model of shoulder mechanism which represented the gross morphological structures by finite elements of simple geometry. It uses 3 types of elements to model the shoulder joint (Fig. 29). It consists of 31 shoulder and elbow muscles [75].

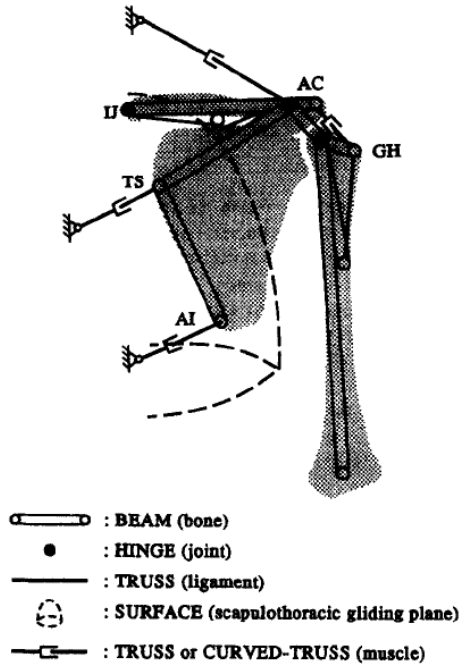

Fig. 29 The shoulder mechanism described by finite elements, featuring a representation with one ligament and a limited number of muscle elements [75].

Input variables to the inverse dynamic model of the shoulder mechanism includes the position, velocity, and acceleration, along with external forces. The model's output variables comprise muscle forces, determined through an optimization criterion of minimizing the sum of quadratic muscle stresses. Model parameters, acquired from an extensive cadaver study involving both shoulders of seven cadavers [76; 77; 78], fall into three categories: inertia parameters (translational and rotational inertia of segments), muscle contraction parameters (maximal force based on physiological cross-sectional area), and geometry parameters (describing joint COR, muscle and ligament attachments, bony contours, and landmarks) [75]. The resulting glenohumeral joint load during abduction is illustrated in Fig. 32.

2.3.3 Favre et al., 2005

In the Algorithm for Shoulder Force Estimation (ASFE), a three-dimensional numerical musculoskeletal model, an external moment applied at the joint COR undergoes decomposition into three orthogonal components to predict the muscle forces required for shoulder joint equilibrium. This algorithm employs a recruitment strategy that prioritizes muscles with a relative mechanical advantage, defined by the muscle lever arms for the current position multiplied by muscle cross-section, along with a corresponding set of muscles counterbalancing secondary joint moments. Muscles outside these two categories remain inactive during the current step.

A detailed segmentation of shoulder muscles is implemented to account for their distinct actions, addressing the varied moment arm length and tendon action direction within muscles with broad insertions. The muscle's maximal force capacity is constrained by factors including its optimal length, contraction velocity, fiber type composition, and notably, the physiological cross-sectional area (PCSA). The resulting glenohumeral joint load during abduction is illustrated in Fig. 32.

2.3.4 Terrier et al., 2008

A two-dimensional numerical musculoskeletal model of the shoulder, incorporating a feedback algorithm for muscle activation control during shoulder abduction, was developed to facilitate and predict the natural translation of the humerus. The model encompasses six muscles: middle deltoid, anterior deltoid, posterior deltoid, supraspinatus, subscapularis, and infraspinatus combined with teres minor (Fig. 30). Muscle origin and insertion points were determined through cadaver shoulder dissection. The muscles were treated as cables with high longitudinal stiffness and no bending stiffness.

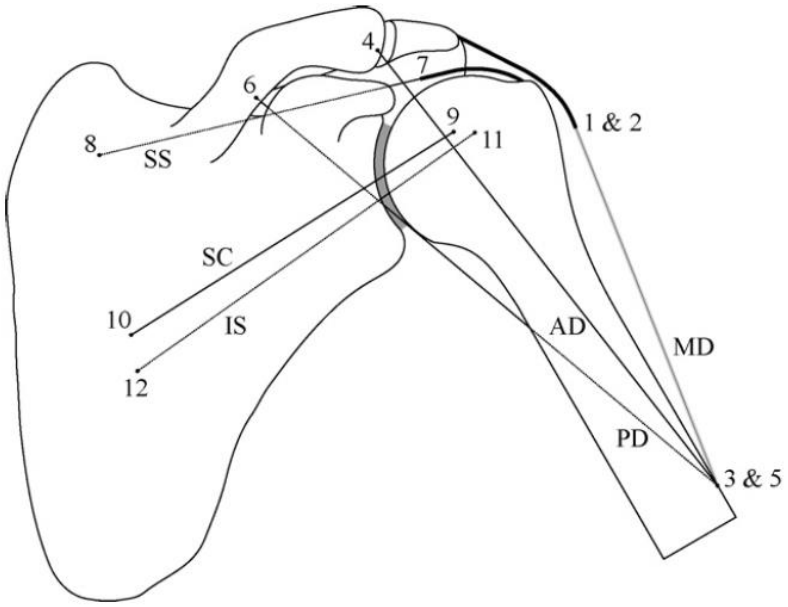

Fig. 30 Numerical shoulder model showing the muscles. The heavy black curves represent the deformable parts of the MD and the SS, which may be in contact with the humerus and wrap on it. MD = middle deltoid, AD = anterior deltoid, PD = posterior deltoid, SS = supraspinatus, SC = subscapularis, and IS = infraspinatus combined with teres minor [79].

The muscle indeterminacy was characterized by five ratios, correlating the magnitude of each muscle force with that of the middle deltoid—a chosen reference muscle due to its prominent role in shoulder abduction. This synchronization of muscle forces was achieved through a feedback mechanism regulated by the length of the middle deltoid, a key determinant of arm abduction. When lifting the arm, the middle deltoid's length decreased, prompting a reactive force within it. This force was systematically propagated to the remaining five muscles based on predetermined ratios. The resultant glenohumeral joint load during abduction is illustrated in Fig. 32.

2.3.5 AnyBody Shoulder Model

This three-dimensional musculoskeletal model of the shoulder is available from the AnyBody Modeling System (AnyBody Technology A/S, Aalborg, Denmark) repository (AnyBody Managed Model Repository, v. 1.6.2). The model is constructed based on the combined shoulder and forearm morphologies from the Delft shoulder group [77] [78] [80]. It depicts the average European male with a weight of 75 kg, height of 1.80m, and includes the representation of 32 muscles using 118 musculotendinous fibers (Fig. 31) [81].

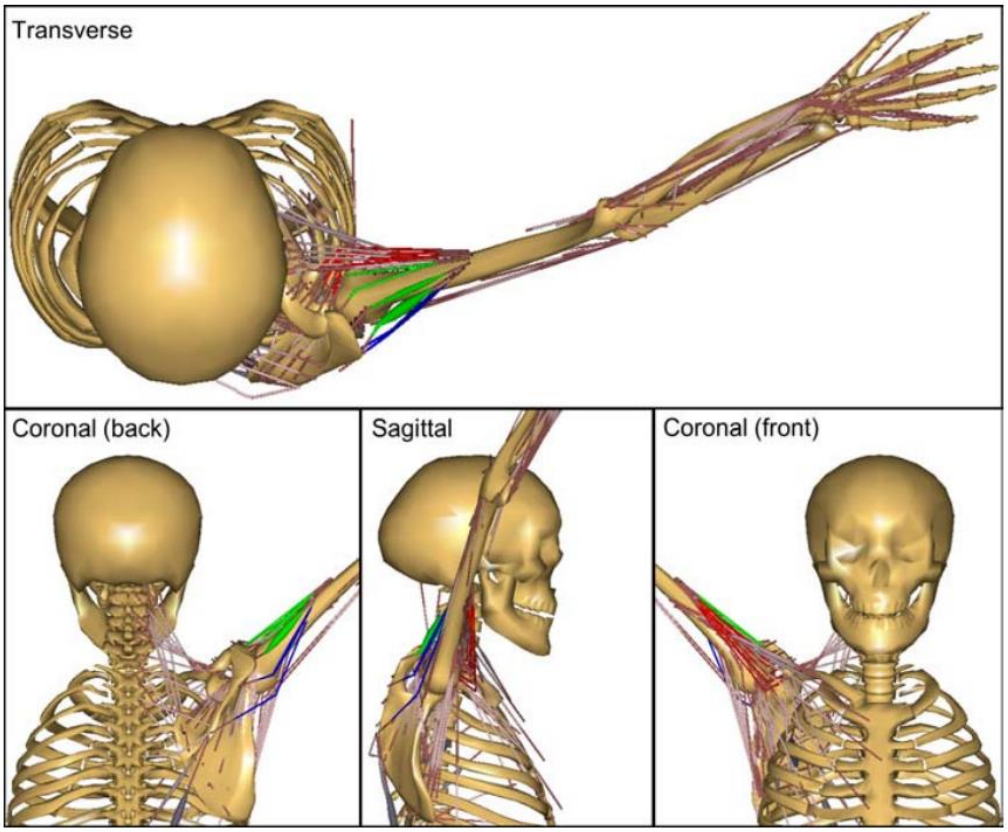

Fig. 31 The AnyBody Modeling System's shoulder model utilizes multiple fibers for the deltoid, with the posterior fibers in blue, middle fibers in green, and anterior fibers in red. The model depicts the shoulder in an abducted position. [82].

In this model, the segments defining bones serve visual purposes only, and, as such, there is no actual glenohumeral contact. The system enforces two constraints at the glenohumeral joint for stability. The first constraint treats the glenohumeral joint as a ball and socket joint with three rotational DOF, preventing humeral head translations. The second constraint, known as the stability constraint, ensures that the glenohumeral joint reaction force direction remains within the glenoid cavity. To achieve this, a circle representing the glenoid implant surface is positioned to approximate the glenoid plane. The reaction force is defined as the sum of virtual contracted muscles located on this circle, preventing the resultant force from exiting the glenoid implant cavity. [83]. The resultant glenohumeral joint load during abduction (from 15° to 120° in 60 steps) is illustrated in Fig. 32.

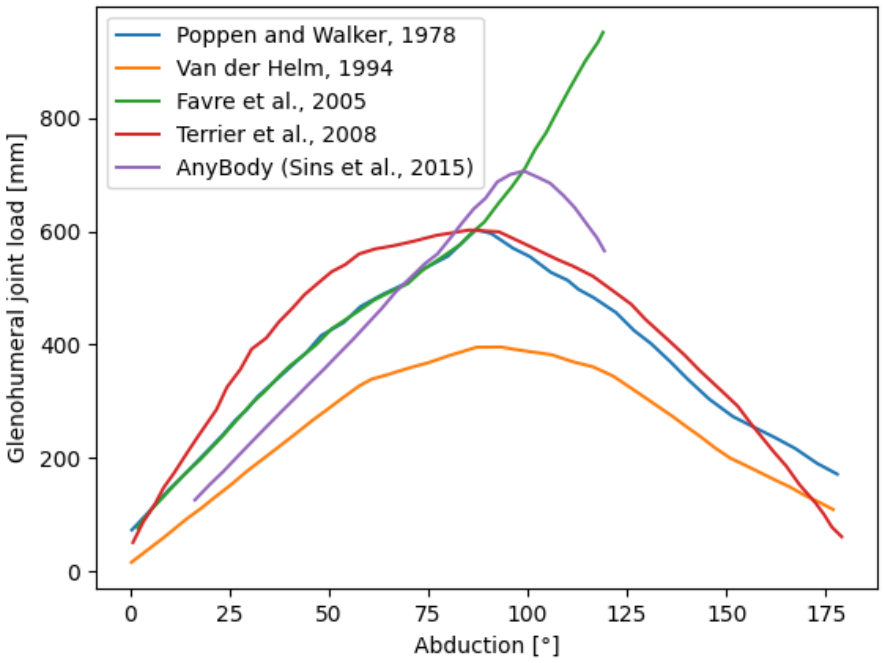

Fig. 32 Comparison of glenohumeral joint load during abduction in different musculoskeletal models. Data was obtained from [84] for Favre et al. 2005 and from [81] for the other models.

2.3.6 In vivo measurements

Bergmann et al., 2007 [85] adapted a clinically established shoulder implant (Biomodular, Biomet Inc., USA) to capture all six components of forces and moments exerted on the humeral head after shoulder hemiarthroplasty (Fig. 33). The recorded data is conveniently accessible on the www.orthoload.com database [86], encompassing information from six subjects engaging in diverse activities within each patient. The resultant glenohumeral joint load during abduction for all 6 subjects is illustrated in Fig. 34. The group of subjects consisted of 3 males and 3 females, all right handed with 5 right shoulder surgeries and one left. The average age of subjects at time of examination was 71 years (ranging from 63 to 81 years), the average weight was 83.5 kg (ranging from 50 to 103 kg) [87].

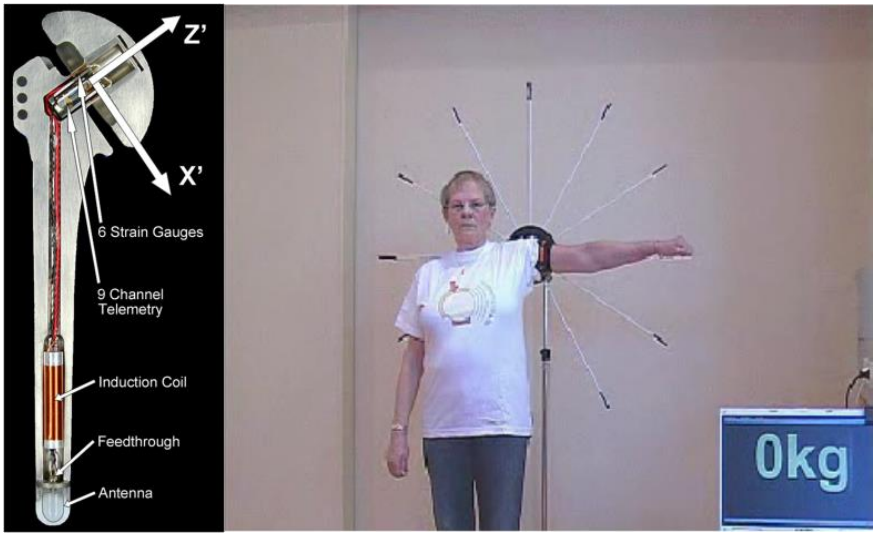

Fig. 33 Instrumented humeral shooulder component implant (left) [85], and in vivo examination of patient s3l with arm in abducted position (right) [86].

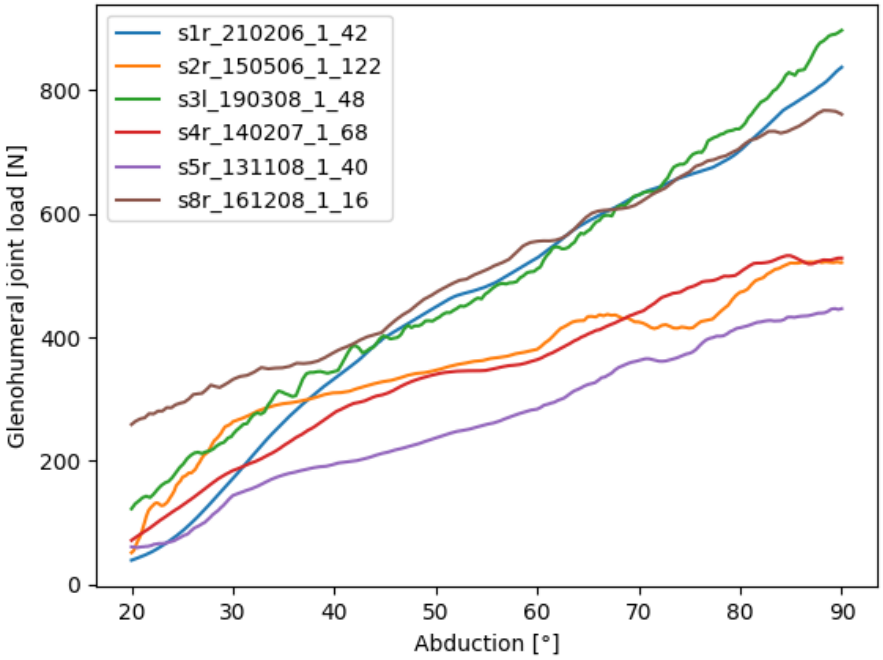

Fig. 34 In vivo measurments of glenohumeral joint load during abduction in six patients (s1–s5 + s8); r,l = right/left shoulder. Data is obtained from www.orthoload.com.

3 Aims of the Thesis

Existing studies addressing RTSA predominantly focuses on clinical outcomes rather than conducting in-depth biomechanical analyses. In instances where biomechanical analysis is considered, it often emphasizes changes in COR while overlooking the significant aspect of humeral prolongation. Humeral prolongation is crucial in the biomechanical context as it induces prestressing of shoulder muscles, thereby influencing force patterns in the shoulder, alongside with the shift of COR.

Assessing changes in musculoskeletal geometry post-RTSA presents a complex challenge requiring specific clinical data. Many studies addressing musculoskeletal changes utilize custom-created data, such as full-arm X-rays, not standard in routine RTSA examinations. While preoperative and postoperative CT scans would be ideal, postoperative CT is not standard, necessitating the use of X-rays. In addition, the role of passive structures in musculoskeletal models of RTSA is usually neglected although it responds for joint stability. It is not clear whether and to which extend humeral lengthening contributes to overall joint load.

This dissertation aims to develop a comprehensive biomechanical analysis of RTSA, incorporating humeral prolongation and COR shift, utilizing widely available clinical data from preoperative and postoperative examinations of patients who have undergone RTSA. We hypothesize, that humeral prolongation along with the center of rotation change would reduce muscle forces and decrease joint loading.

Specific aim of the thesis is to develop an accurate method for evaluating musculoskeletal changes after RTSA based on routinely available clinical data, including preoperative CT and X-ray, along with postoperative X-ray. The initial step involves determining the precise magnification of X-rays, considering the hypothesis that the commonly used 5% magnification for shoulder radiographs may be higher and vary among patients. Secondly, a method must be devised to ascertain changes in musculoskeletal geometry, not just the shift of the COR but, crucially, the humeral lengthening after RTSA. This lengthening significantly influences muscle force ratios, impacting glenohumeral joint load and shoulder mobility. The method is applied in a clinical study and effect of patients' sex, weight, and age on the postoperative change in musculoskeletal geometry will be evaluated.

To understand glenohumeral joint load comprehensively, a musculoskeletal model of shoulder with a muscle model should be employed with modelling the muscles as Hill active units. Various Hill muscle models could be utilized to assess their impact on the resulting muscle force and glenohumeral load. We suggest that the formulations of the Hill-type models will considerably influence predicted glenohumeral load. The appropriate model should be verified to experimental measurements. Based on parametric analysis of RTSA surgery, a "safe zone" for humeral lengthening during RTSA could possibly be defined. We expect that the safe zone will indicate the permissible amount of humeral elongation during surgery without overloading the glenohumeral joint and its structures.

4 Methods

To achieve the goals of this thesis, we encountered several challenges. The initial challenge was to ascertain the radiographical magnification in the shoulder region. Subsequently, we needed to devise a method for accurately determining the actual humerus lengthening in patients who underwent RTSA. Both challenges included clinical studies involving human participants. While these studies were non-interventional and retrospective, relying on anonymized datasets, that did not require ethics committee approval, we obtained authorization for our studies from the Ethics Committee of the Faculty Hospital in Motol (Reference No. EK-1204/18). The decision is detailed in the attached annex A.

4.1 Radiographical Magnification in Shoulder Joint Region

A retrospective study included patients that have previously undergone total glenoid arthroplasty at the Motol University Hospital, Czechia. The implants analysed included only SMR Reverse Shoulder System (Lima Corporate, San Daniele del Friuli, Italy) [61]. The inclusion criteria for the study were as follows: unilateral RTSA, documented implant size and type, documented patient height and weight, digital AP (anterior-posterior) radiographs of the shoulder in neutral position obtained from archives, completely visible humeral and glenoid component of RTSA. 98 digital AP radiographs from 98 patients after the glenoid arthroplasty at the first follow-up were obtained as digital images (DICOM files). 3 patients were excluded from the study due to obvious rotation in the position of the arm, one patient was excluded due to missing information on the radiographic setup in the DICOM file. The final cohort included 94 patients (62 female and 32 male). The average age of patients at time of surgery was 69,4 years (± 8,7 years, range 38 – 85 years). The data were collected during period spanning from 2014 to 2017.

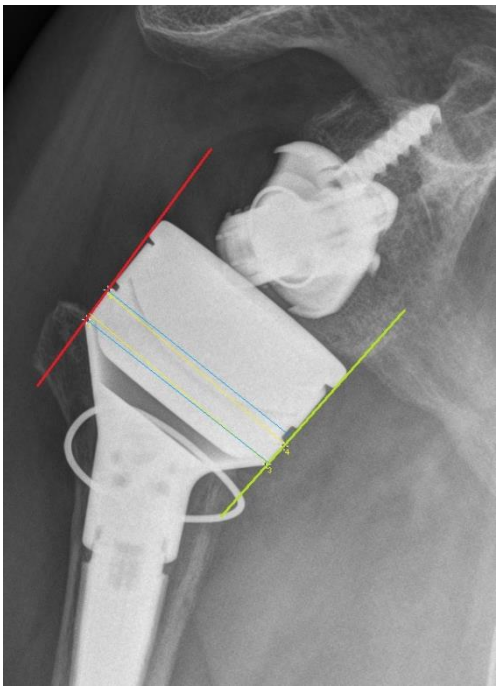

Fig. 35 Estimation of reverse humeral body dimension from standard AP shoulder radiograph. The lateral edge (highlighted in red) and the medial edge (highlighted in yellow) of the component were defined. The transverse size of the humeral body was determined as the mean perpendicular distance between the edges [I].

The diameter of the proximal part of reverse humeral body (component no. 1352.20.010) was used as reference (Fig. 35). The component is cylindrical in shape and its diameter is hence invariant to internal or external rotation. The cylindrical geometry was verified by fitting a cylinder to 3D scan of non-implanted specimen using optical coordinate measuring system (Omnilux, RedLux Ltd, Romsey, UK). The physical diameter of 36.6 mm was obtained from cylindrical fit and confirmed by measuring of component using digital calliper (Mahr GmbH, Göttingen, Germany). The component dimension on radiograph was estimated from DICOM files using Fiji platform for biological-image analysis [88] as follows: two points on each side of cylinder portion of the component were defined and used to construct the lateral and the medial edge of the component. A custom Matlab script (Matlab R2020b, The Mathworks, Inc., Natick, MA, USA) was programmed to calculate the diameter of the component as a mean perpendicular distance between the lines measured at defined points (Fig. 35). One observer (A.K.) analysed all radiographs. To assess the validity of the method for radiographic magnification estimation, five independent and blinded observers (postgraduate students of biomechanics at CTU in Prague) analysed a set of 20 randomly selected radiographs [I, V].

The radiographic magnification (M) of the implants was calculated as shown in equation (1).

$$M[\%] = \left(\frac{measured\ dimension}{true\ dimension} - 1\right) \cdot 100\% \quad (1)$$

where 0% magnification correspond to exact match between the image size and implant size.

4.2 Determination of Changes in Musculoskeletal Geometry after RTSA

Identifying changes in musculoskeletal geometry for patients undergoing RTSA poses a significant challenge. The surgical procedure involves a medial and inferior shift in the COR of the glenohumeral joint, accompanied by humerus lengthening. These alterations impact strength ratios in shoulder muscles, thereby influencing mobility, range of motion, stability, and the lifespan of the replaced joint. To address this complexity, we have devised a semi-automatic method utilizing preoperative and postoperative X-rays, along with a preoperative computed tomography scan (Fig. 36). Our method was validated through virtual surgeries, detailed in chapter 4.2.11. Additionally, a sensitivity analysis was conducted, and its findings are outlined in chapter 4.2.12.

Establishing the resection line poses a significant challenge as it varies among patients and affects humeral lengthening determination. Standard preoperative and postoperative anteroposterior radiographs may not provide a clear view, considering the fixed arm position postoperatively and thus unknown rotation in the shoulder. To address this, we utilized preoperative CT scans alongside X-rays. The 3D model created from the CT scan can be rotated to match the humerus positions in preoperative and postoperative X-rays, facilitating a cohesive comparison. Another challenge is X-ray magnification variation between preoperative and postoperative states, potentially introducing errors. To mitigate this, our method determines radiographical magnification in the shoulder joint. This involves estimating postoperative X-ray magnification using a replacement as a reference object, followed by evaluating preoperative magnification by aligning the preoperative clavicle contour with the postoperative clavicle contour. The detailed steps of the evaluation process are outlined below.

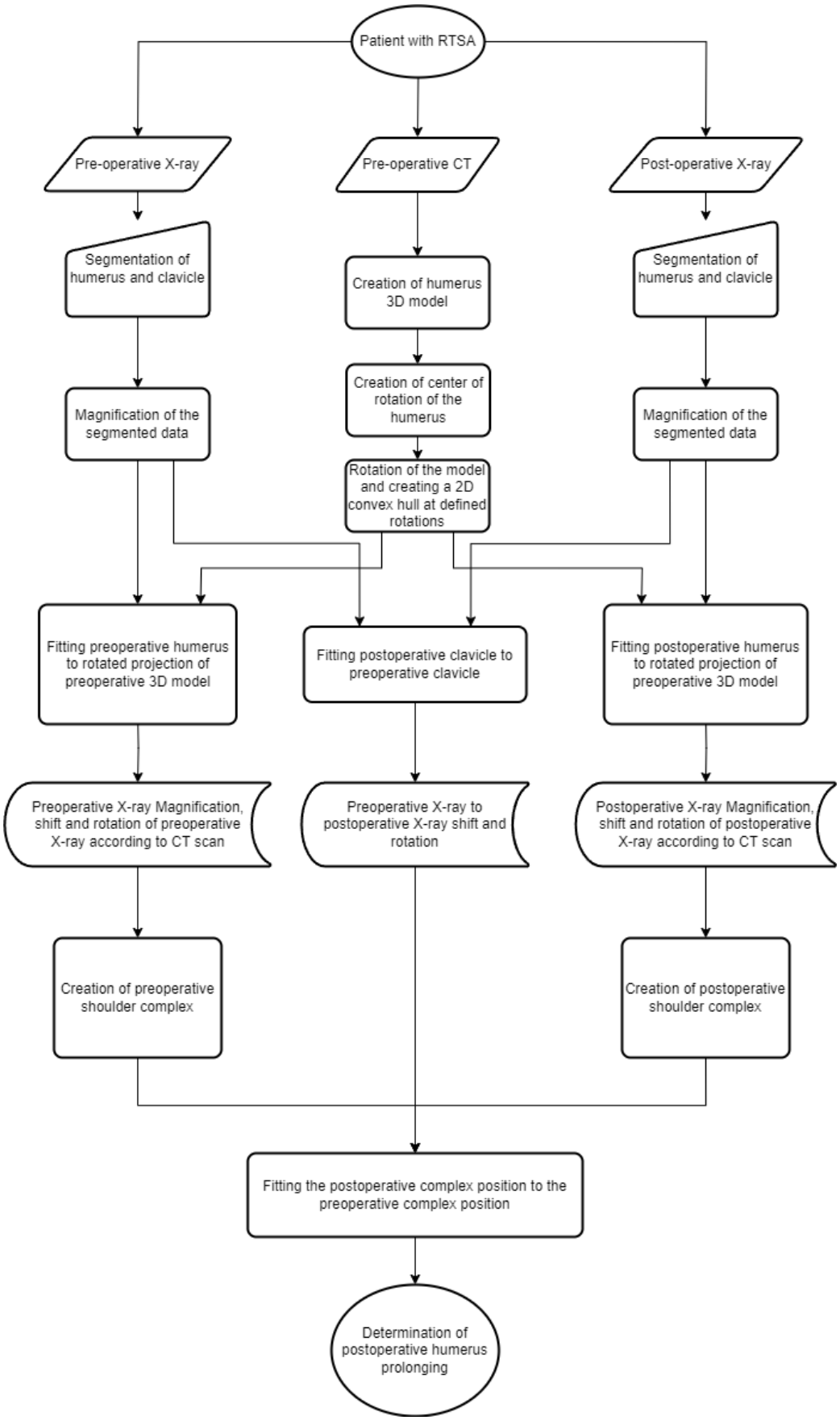

Fig. 36 Workflow diagram of method for determination of changes in musculoskeletal geometry after RTSA

4.2.1 Study shoulders

A total of 34 patients who underwent RTSA at the Faculty Hospital in Motol, performed by one of six senior surgeons, were included. The study spanned the period between 2012 and 2020. Three patients were excluded due to suboptimal radiographic quality, resulting in the evaluation of 31 patients (32 shoulders). The surgical indications encompassed cuff tear arthropathy (CTA) in 20 shoulders, omarthrosis (OA) in 7, post-traumatic deformity (PTD) in 3, rheumatoid arthritis (RA) in 2, osteochondrodysplasia (OCD) in 1, and psoriatic arthritis (PA) in 1. Among the patient cohort, there were 20 females and 11 males, with a mean age of 67.2 years (± 8.8 years, ranging from 42 to 82) and a mean BMI 29.1 (± 5.5, ranging from 17.7 to 45.8) at the time of surgery. All patients underwent implantation of a RTSA using SMR Reverse Shoulder System (Lima Ltd, San Daniele del Friuli, Italy) [61].

4.2.2 Segmentation of X-rays

Each patient enrolled in the study was required to have in the archives both preoperative and postoperative X-rays in DICOM file format. An X-ray machine from Phillips Medical Systems manufacturer was used for imaging with following settings – resolution 2667x1945, pixel spacing 0.136/0.136 with pixel aspect ratio 1/1.

The archives for most patients contained more than one postoperative X-ray. In such instances, the X-ray exhibiting the arm position and clavicle rotation most closely resembling those in the preoperative X-ray was selected to achieve the best possible fit. Manual segmentation of the humerus and clavicle on both radiographs was conducted using the Fiji platform for biological image analysis [88]. Multiple points along the edges of the chosen bones were selected to form their contours (Fig. 37 and Fig. 38). To ascertain the position of the replacement components, points were selected on the postoperative X-ray. Ten points were utilized to define edges of the cylindrical portion of the humeral component, and an additional ten points were employed to determine edges of the cylindrical anchor part of the glenosphere. These points were subsequently saved in a CSV format file for future reference. The segmentation process was performed by four proficient operators.

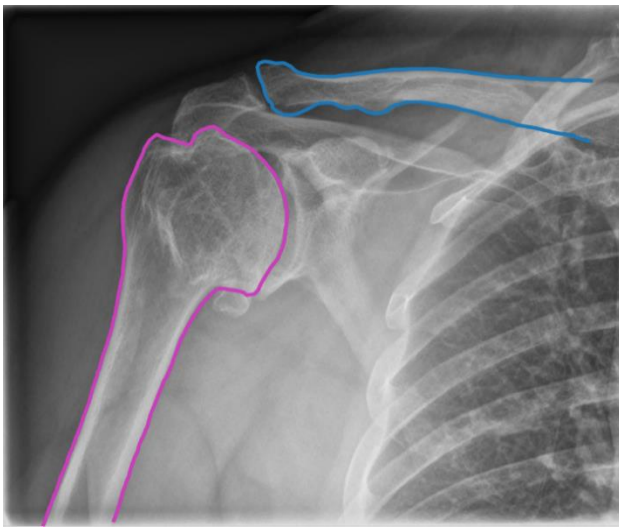

Fig. 37 Selected bone contours on preoperative X-ray. Pink line defines humerus and blue line defines clavicle.

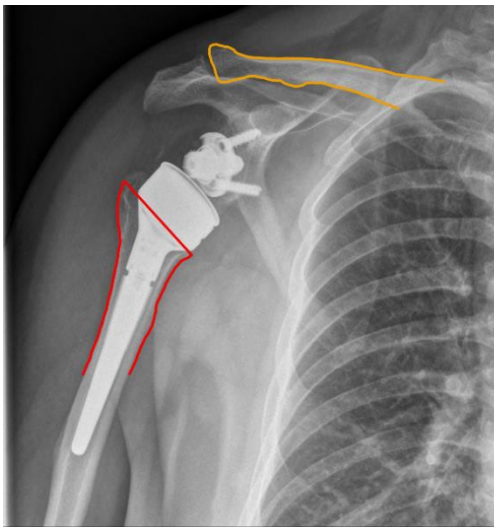

Fig. 38 Selected bone contours on postoperative X-ray. Red line defines humerus and orange line defines clavicle.

4.2.3 Creation of 3D model from CT scan

Every participant in the study underwent a preoperative CT scan, from which a 3D model of the humerus was generated. A CT scan in DICOM file format was required for each patient. X-ray images within the transverse plane, with a 5 mm interval between each, were employed for model creation. The raw resolution resulted in steps on the model's surface. (Fig. 39). The CT scans were taken on single workplace on Siemens Definition CT scanner with following settings – slice thickness 1.5 mm, resolution 512x512, and pixel spacing 0.39/0.39.

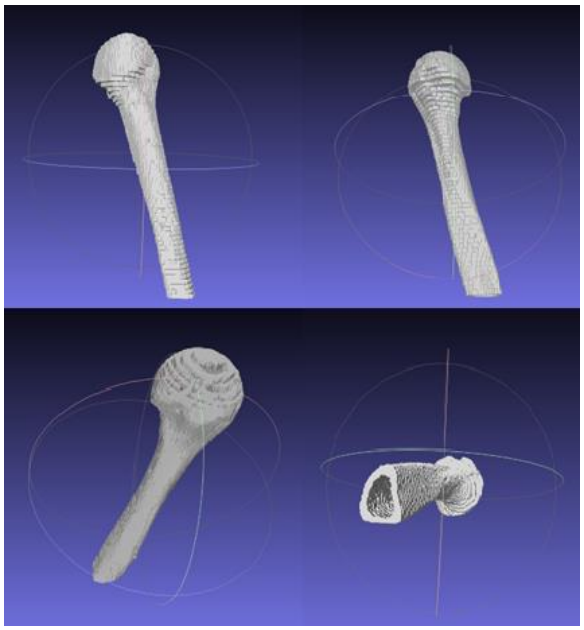

Fig. 39 A 3D model of the humerus created using preoperative CT scan.

For the semiautomatic segmentation of the CT scans and the creation of a 3D model in STL file format, we utilized the 3D Slicer software [89]. The model's simplification, achieved through quadric edge collapse decimation [90], was carried out using the MeshLab software [91].

4.2.4 Determination of Center of Rotation of the Reverse Replacement

We assessed the displacement of the COR based on establishing the axes of the replacement components by segmenting the edges of the replacement from the postoperative X-rays. The segmented components are cylindrical and, therefore, symmetrical, while the articulation surfaces are spherical with the same radius of curvature. Consequently, the intersection of the axes of the components lies at the COR (Fig. 40) [IV].

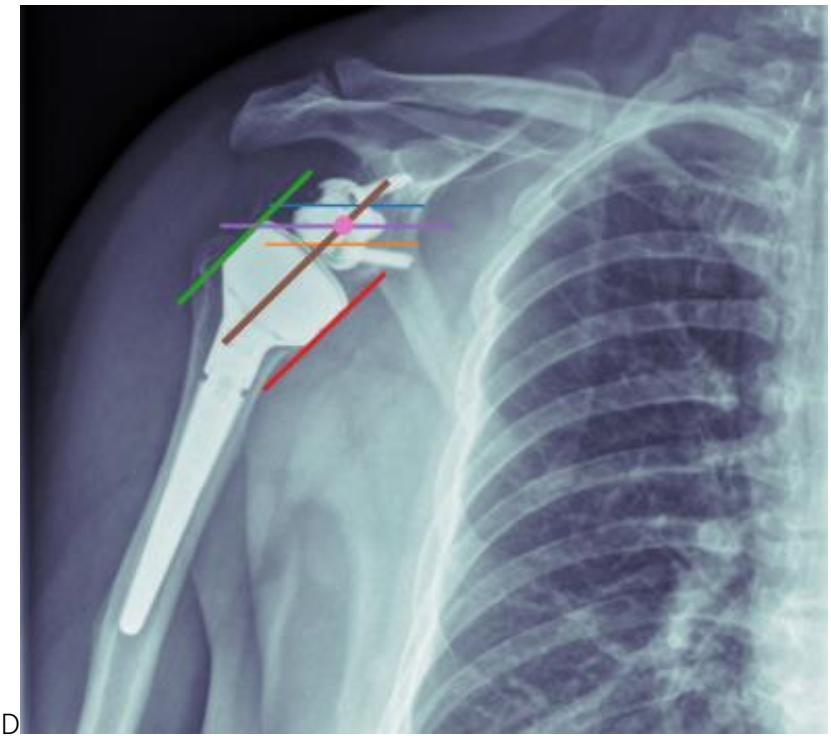

Fig. 40 Determination of the COR of reverse shoulder replacement from standard AP shoulder radiograph. The lateral edge (highlighted in green) and the medial edge (highlighted in red) of the humeral component created axis of humeral component (brown line). The superior edge (highlighted in blue) and the inferior edge (highlighted in orange) of the anchoring component of the glenosphere created axis of glenoidal component (purple line). Intersection of the axis of the components creates CoR of the revers shoulder replacement (pink dot) [IV].

The real COR of the reverse shoulder replacement was verified by fitting a sphere to 3D scan (Fig. 41) of non-implanted glenosphere component using optical coordinate measuring system (Omnilux, RedLux Ltd, Romsey, UK).

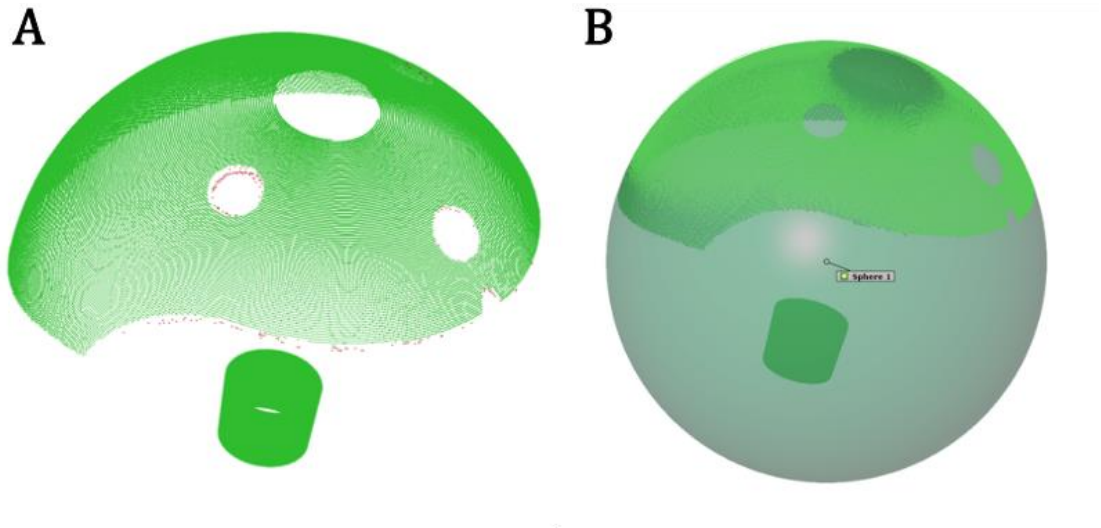

Fig. 41 3D scan of non-implanted glenosphere component using optical coordinate measuring system (A) and sphere fitted to the 3D scan to evaluate the COR (B).

The glenosphere component is produced in two variants based on its eccentricity. The first variant is concentric with the anchoring element, eliminating the need for any compensation, as the axis of the glenosphere aligns with the axis of the anchoring element. The second version is shifted 4 mm inferiorly, requiring a corresponding inferior shift in the axis of the glenosphere component.

4.2.5 Determination of Center of Humeral Head and Longitudinal Axis of Humerus

To determine the preoperative COR of the glenohumeral joint, which can be approximated to the middle of the humeral head [18], we employed a sphere-fitting approach. A sphere was fitted to the humeral head of each patient, and the center of this fitted sphere served as the preoperative COR (Fig. 42). The least squares method was utilized for the purpose of sphere fitting [92].

The general equation of a sphere in x, y, and z coordinates is defined by Eq. (2), where the center point of the sphere, with a radius r, is located at the point (x0, y0, z0).

$$(x - x_0)^2 + (y - y_0)^2 + (z - z_0)^2 = r^2 \quad (2)$$

To apply the least squares method, it is necessary to reorganize the terms of equation (2) as

$$x^2 + y^2 + z^2 = 2xx_0 + 2yy_0 + 2zz_0 + r^2 - x_0^2 - y_0^2 - y_0^2 \tag{3}$$

Upon expanding and reorganizing the terms, the revised equation (3) can be represented in vector/matrix notation as (4).

$$\vec{f} = A\vec{c} \tag{4}$$

where

$$\vec{f} = \begin{bmatrix} x_i^2 + y_i^2 + z_i^2 \\ x_{i+1}^2 + y_{i+1}^2 + z_{i+1}^2 \\ \vdots \\ x_n^2 + y_n^2 + z_n^2 \end{bmatrix} \tag{5}$$

$$A = \begin{bmatrix} 2x_i & 2y_i & 2z_i & 1 \\ 2x_{i+1} & 2y_{i+1} & 2z_{i+1} & 1 \\ \vdots & \vdots & \vdots & \vdots \\ 2x_n & 2y_n & 2z_n & 1 \end{bmatrix} \tag{6}$$

$$\vec{c} = \begin{bmatrix} x_0 \\ y_0 \\ z_0 \\ r^2 - x_0^2 - y_0^2 - z_0^2 \end{bmatrix} \tag{7}$$

We obtain an over-determined system suitable for employing the least squares method for a spherical fit. The fit aims to determine the optimal values for the parameter vector, denoted as $\vec{c}$ based on the available data points. Subsequently, we can calculate the radius of the sphere using the terms in the parameter vector $\vec{c}$.

The first point for establishing the longitudinal axis of the humerus is the center of the fitted sphere. The second point is identified as the midpoint within a point set located at the distal end of the 3D model, specifically in the diaphysis of the humerus (Fig. 43). To guarantee that the second point resides at the midpoint of the cross-section of the diaphysis, we calculate a mean position from points with a horizontal distance ranging from 10 to 20 mm from the distal end of the 3D model.

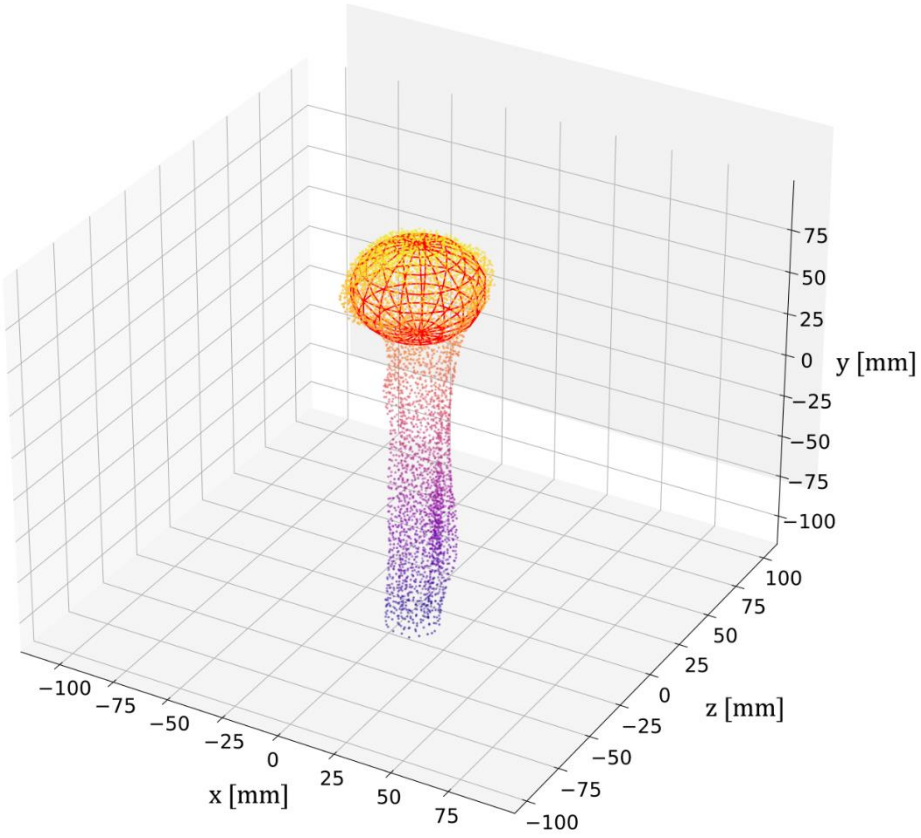

Fig. 42 A sphere fitted to the head of the preoperative model of humerus to determine the preoperative CoR. Fitted sphere is highlithed in red. Points varieted from yellow to blue color are points of stl model of humerus.

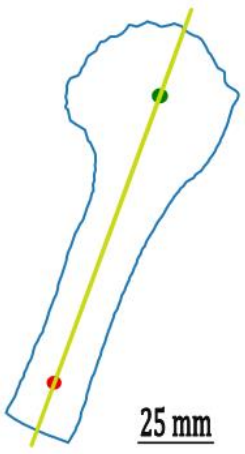

Fig. 43 2D projection of the preoperative 3D model with center of fitted sphere to the humeral head (green point), center of the diaphysis cross-section (red point) and longitudinal axis of humerus (yellow line).

4.2.6 Creation of the Convex Hull of the 3D model of Humerus in Given Rotations

Following the establishment of the longitudinal axis, the 3D model is rotated using this axis as the pivot. The rotation spans a complete circle in increments of 5 degrees. During each rotation, a 2D convex hull operation is applied to the rotated 3D model, generating distinct 2D projections of the 3D model at varying rotational angles (Fig. 44) [VIII].

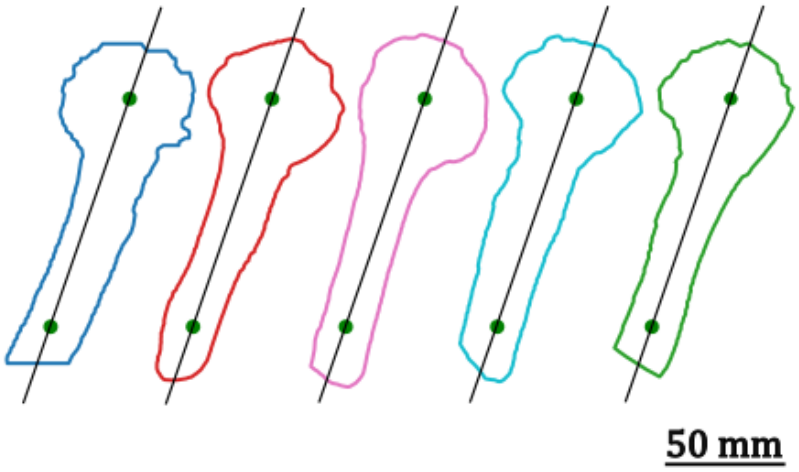

Fig. 44 Convex hulls of the rotated 3D model (different colours) of the humerus by 60 degrees throughout a complete circle.

4.2.7 Fitting X-ray Segmentation Data on Rotated 3D model

An automated script was employed to align the segmentations of preoperative and postoperative humerus contours onto the rotated 2D projections of the 3D preoperative model. This alignment process involves identifying the maximal intersection of areas created by the humerus contour from the radiograph and the convex hull of the 2D projection of the humerus 3D model. The problem was defined as optimization task and optimum solution was estimated using Nelder-Mead method [93], where the optimized parameters are two-dimensional displacement and rotation. The algorithm underwent iterative fitting of contours from the radiograph to each rotation of the 3D model, covering a range of magnifications set between predefined values with specified increments. The magnification range employed in the optimization process was determined using our method for assessing radiographical magnification in the shoulder region as described in

chapter 4.1. This fitting procedure is executed independently for both preoperative and postoperative radiographs (Fig. 45 and Fig. 46) [VIII].

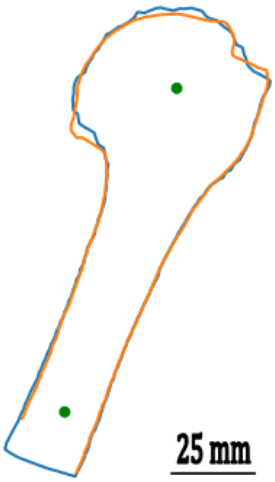

Fig. 45 Fitted preoperative humerus contour from radiograph (orange line) to the 2D projection of rotated 3D model (blue line). Green dots are representing humeral longitudinal axis [VIII].

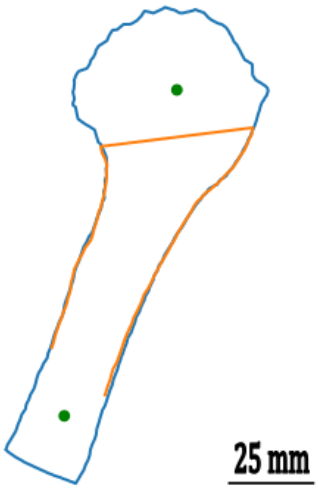

Fig. 46 Fitted postoperative humerus contour from radiograph (orange line) to the 2D projection of rotated 3D model (blue line). Green dots are representing humeral longitudinal axis [VIII].

4.2.8 Fitting Preoperative and Postoperative Clavicle Contours

A procedure alike to the one described in chapter 4.2.7 is applied to fit preoperative and postoperative clavicle contours. Initially, the geometric center of the postoperative segmentation is adjusted to align with the geometric center of the preoperative segmentation. Subsequently, the Nelder-Mead method [93] is employed to ascertain the maximum achievable intersection of the areas created by both segmentations (Fig. 47). This fitting process involves exploring various mutual magnifications, defaultly ranging from 90% to 110% in increments of 1% [VIII].

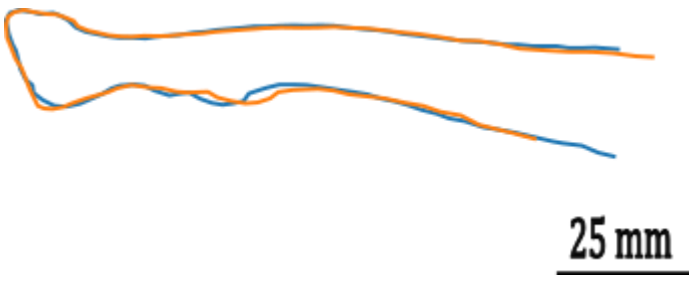

Fig. 47 Fitted preoperative clavicle contour from radiograph (blue line) to the postoperative clavicle contour from radiograph (orange line) [VIII].

4.2.9 Creation of the Shoulder Complex

To construct the shoulder complex encompassing both the preoperative and postoperative states of the patient's glenohumeral joint, data from preceding chapters are utilized. In order to align the postoperative state with the preoperative state, transformations done in the previous chapters are employed to integrate all the data cohesively, as illustrated in Fig. 48 [VIII].

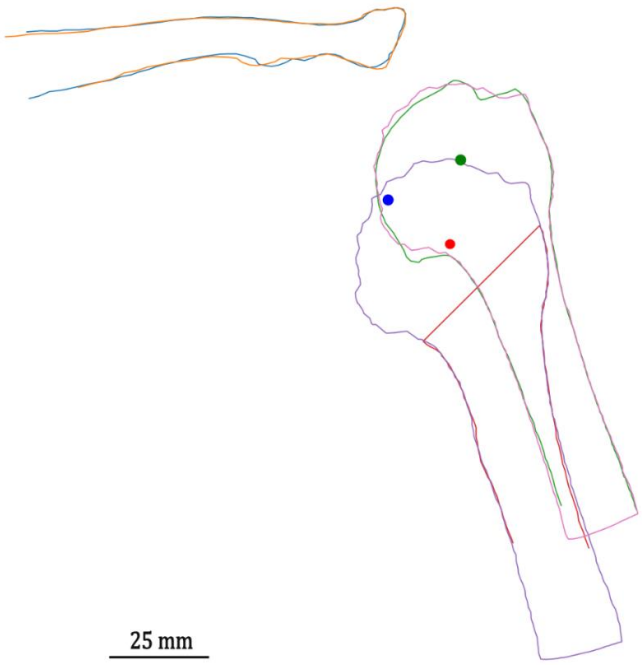

Fig. 48 Shoulder complex with both states – preoperative and postoperative. Preopertative clavicle (blue line), postoperative clavicle (orange line), preoperative humerus (green line) with fitted 2D projection of preoperative humerus model (pink line), postoperative humerus (red line) with fitted 2D projection of preoperative humerus model (purple line), preoperative CoR (green dot), postoperative CoR (blue dot), and projection of preoperative CoR to postoperative state (red dot) [VIII].

4.2.10 Determination of Changes in Musculoskeletal geometry after RTSA

After creating the shoulder complex, the changes in the glenohumeral geometry can be determined as shown in Fig. 49. Overall change of the musculoskeletal geometry is assessed together with shift of COR and prolonging of humerus [VIII].

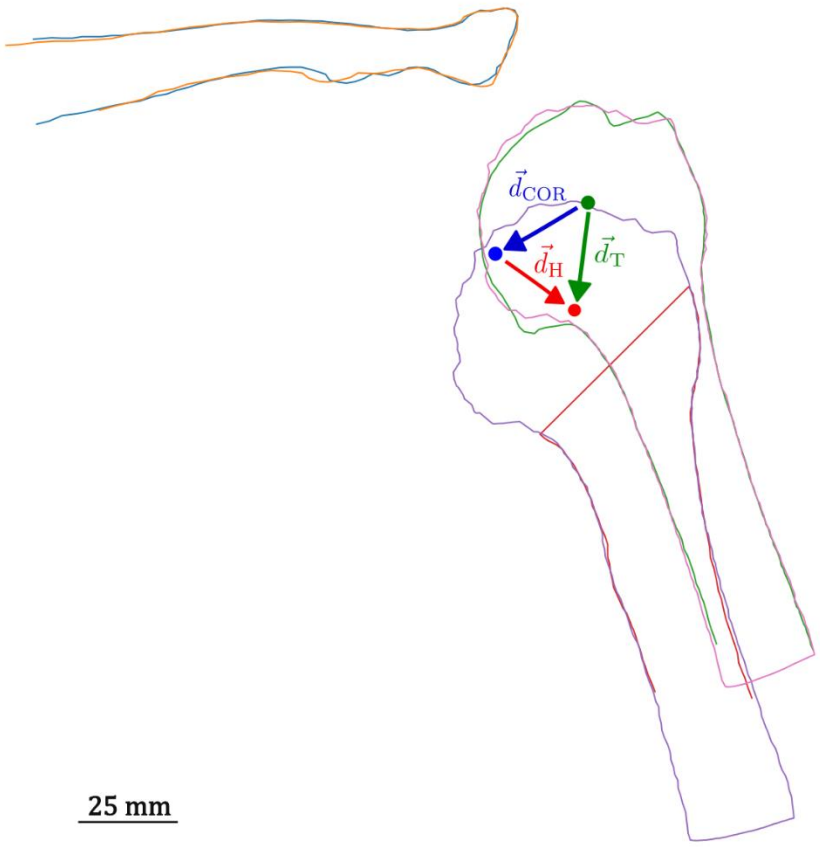

Fig. 49 Assessment of alterations in musculoskeletal geometry following RTSA. The blue arrow indicates the shift of COR ($\vec{d}_{COR}$), the red arrow indicates the lengthening of the humerus ($\vec{d}_{H}$), and the green arrow indicates the total change in musculoskeletal geometry ($\vec{d}_{T}$) [VIII].

4.2.11 Verification of the Method

The verification of the method for assessing total change of musculoskeletal geometry (shift) post-RTSA involved virtual surgeries. Fictitious removal of the humeral head was simulated in five patients to mimic RTSA. Subsequently, our method for evaluating changes in glenohumeral geometry was applied, and the extent of lengthening, expected to be close to zero, was calculated. The verification results are presented in Tab. 2.

Tab. 2 Total changes in musculoskeletal geometry in virtual surgeries (verification method).

Patient	Inferior shift [mm]	Medial shift [mm]	$\boldsymbol{d_T}$ [mm]
A	0.15	1.18	1.19
B	-0.65	0.35	0.74
C	-0.29	1.87	1.89
D	-2.16	-1.57	2.67
E	-0.41	-1.50	1.56
MEAN	-0.67	0.07	1.61
SD	± 0.88	± 1.56	± 0.73

Note: SD represents standard deviation, and a negative inferior shift indicates a superior shift.

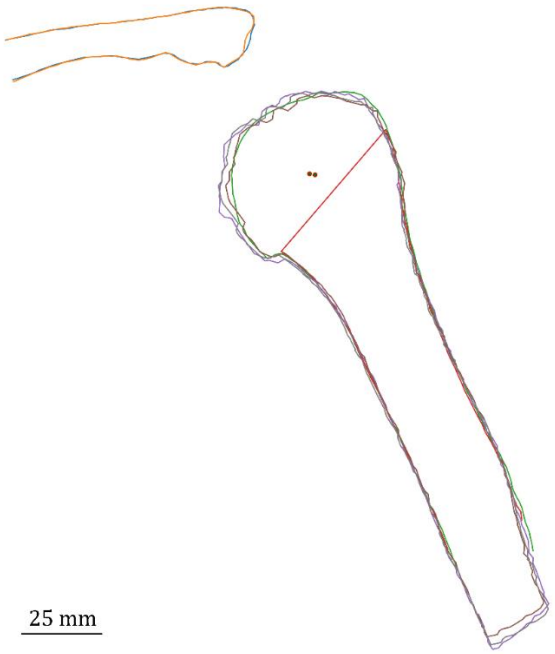

Fig. 50 Shoulder complex with both states before and after the virtual surgery of patient C.

The overall mean humeral lengthening after the virtual surgeries is 1.61 mm, a value below the potential errors attributed to radiographic resolution.

4.2.12 Sensitivity analysis of the method

In our approach, numerous steps have the potential to introduce errors to the results. Therefore, we conducted a sensitivity analysis to assess the potential errors to overall change in musculoskeletal geometry associated with each step. These steps include the rotation increment during the creation of 2D projections of the

humeral 3D model, magnification of the humerus and clavicle, fitting of the sphere to the humeral head and the subsequent creation of the longitudinal axis of the humerus, as well as the simplification of the 3D model. Three patients were randomly selected and evaluated in the sensitivity analysis.

4.2.12.1 Effect of Rotation Increment

To evaluate the effect of rotation increment, the 3D models of humerus of each patient were rotated in full circle with different numbers of steps. Results are shown in Tab. 3 and in Fig. 51. The values of total change in musculoskeletal geometry became stable with increasing number of rotation increments as shown in Fig. 51. The actual number of increments was chosen according to precision and calculating time of our program, which is highly dependent on the number of rotational increments.

Tab. 3 Effect of rotation increment on total change in musculoskeletal geometry.

Number of increments to full circle	Increment size	$\boldsymbol{d_T}$ [mm]		
		Patient A	Patient B	Patient C
18	20°	21.29	14.63	16.28
24	15°	17.82	16.28	17.02
30	12°	25.43	16.16	15.29
36	10°	24.32	16.30	16.28
45	8°	27.44	15.22	17.42
72	5°	25.13	16.60	17.38
120	3°	25.55	16.27	16.53
180	2°	25.34	16.03	16.94
360	1°	25.13	16.09	16.94

Note: The actual numbers of increments used in our approach are indicated in green.

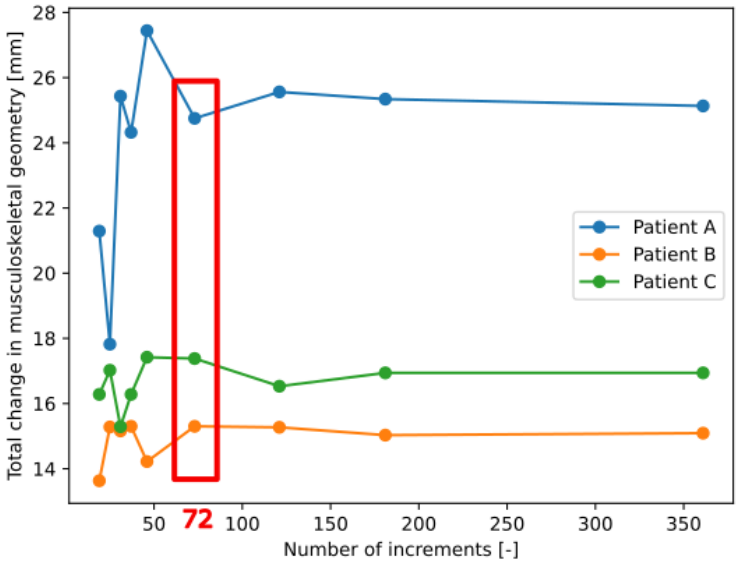

Fig. 51 Total change in musculoskeletal geometry based on the quantity of rotation increments. The red rectangle highlights the number of increments employed in our approach.

4.2.12.2 Effect of Radiographical Magnification

To assess the impact of radiographical magnification, we employed various magnification levels regardless of the optimization process. This part of evaluation effects the magnification of humerus contour and thereby fitting process of preoperative and postoperative humerus on the 3D model. The outcomes are presented in Tab. 4 and in Fig. 52. The actual radiograph magnifications used for each patient was chosen according to the best fit of the preoperative and postoperative humerus contour on the 3D model.

Tab. 4 Effect of radiographical magnification on total change in musculoskeletal geometry.

Magnification	d_T [mm]		
	Patient A	Patient B	Patient C
80 %	24.11	5.96	12.48
85 %	24.69	18.76	16.65
87 %	30.50	12.20	17.38
90 %	25.49	16.60	18.83
93 %	25.13	19.31	21.28
95 %	27.01	21.36	23.73
100 %	26.42	25.12	x
105 %	24.26	29.55	x

Note: The actual radiograph magnifications for each patient are indicated in green, "-" indicates a lack of convergence.

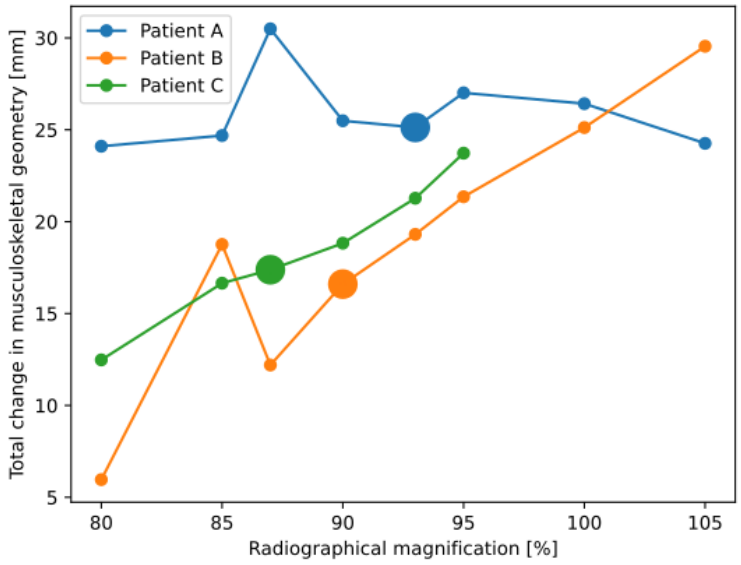

Fig. 52 Total change in musculoskeletal geometry according to the humerus magnification. Highlighted points represent the actual radiograph magnification.

4.2.12.3 Effect of Difference in Radiographical Magnification

To evaluate the influence of difference in radiographical magnification, signifying variations in magnification between the preoperative and postoperative radiographs, we utilized different magnification levels without considering the optimization process. The results are depicted in Tab. 5 and in Fig. 53. The actual radiographical magnifications used for each patient was chosen according to the best fit of the preoperative and postoperative clavicle contour on each other.

Tab. 5 Effect of difference in radiographical magnification on total change in musculoskeletal geometry.

Magnification	d_T [mm]		
	Patient A	Patient B	Patient C
91 %	-	-	14.76
94 %	-	-	16.79
95 %	x	x	17.38
97 %	23.73	-	18.75
100 %	24.27	-	20.64
102%	x	16.60	x
103 %	24.51	15.76	23.09
104 %	25.13	x	x
106 %	26.43	17.18	-
109 %	28.03	18.58	-
112 %	28.04	19.94	-
115 %	28.36	21.23	-

Note: "-" indicates a lack of convergence, and "x" signifies a value that has not been calculated. The actual postoperative radiograph magnification according to preoperative radiograph magnifications are indicated in green.

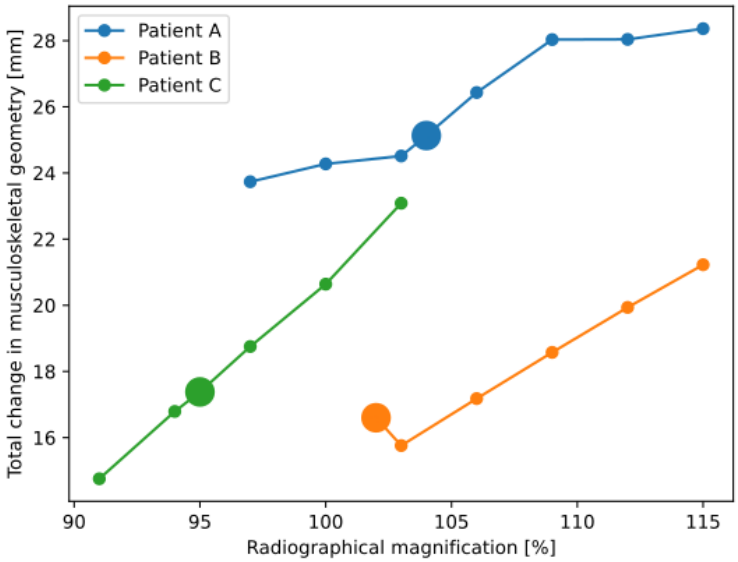

Fig. 53 Total change in musculoskeletal geometry according to the clavicle magnification. Highlighted points represent the actual postoperative radiograph magnification according to preoperative radiograph magnification.

4.2.12.4 Effect of Sphere Fitting

We assessed the impact of the sphere fitting process, examining how the outcome is influenced by the extent of the humeral head area considered for fitting. The fitting area is determined by the points' vertical distance from the top of the humeral head. The outcomes are presented in Tab. 6 and in Fig. 54. The actual area used for sphere fitting for each patient was chosen according to the best fit of the sphere to the head of the 3D model of humerus.

Tab. 6 Effect of sphere fitting on total change in musculoskeletal geometry.

Area used for fitting defined by points' vertical distance from the top of the humeral head [mm]	d_T [mm]		
	Patient A	Patient B	Patient C
5	56.96	16.90	17.82
10	55.46	16.54	17.61
15	55.42	16.39	17.55
20	55.25	16.30	17.42
25	55.13	16.60	17.38
30	54.97	16.34	17.36
35	54.63	16.41	17.28
40	54.00	16.32	17.03
50	53.07	16.23	16.56
60	50.59	16.07	15.41
80	48.02	16.09	14.11
100	56.96	16.90	17.82

Note: The actual areas used in our approach are indicated in green.

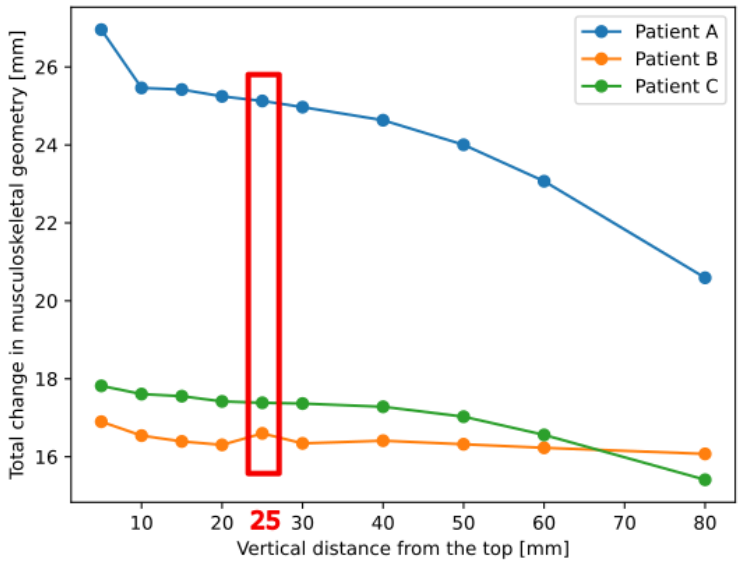

Fig. 54 Total change in musculoskeletal geometry according to the sphere fit adjustments. The red rectangle highlights the settings our approach.

4.2.12.5 Effect of Model Simplification

To improve the calculating time of the method, we simplified the surface mesh of the 3D model as described in chapter 4.2.3. The effect of number of nodes of the model is shown in Tab. 7 and in Fig. 55. The actual number of nodes that defined the 3D model of humerus used for each patient was optimized with respect to the original geometry of the humerus and calculation time of our algorithm.

Tab. 7 Effect of the humerus 3D model simplification on total change in musculoskeletal geometry.

Number of nodes	d_T [mm]		
	Patient A	Patient B	Patient C
60000	55.98	15.95	15.85
45000	55.71	15.65	14.89
30000	55.22	15.84	17.90
15000	55.85	15.88	16.27
10000	55.13	16.60	17.38
8000	56.17	17.49	18.59

Note: The actual numbers of nodes used in our approach are indicated in green.

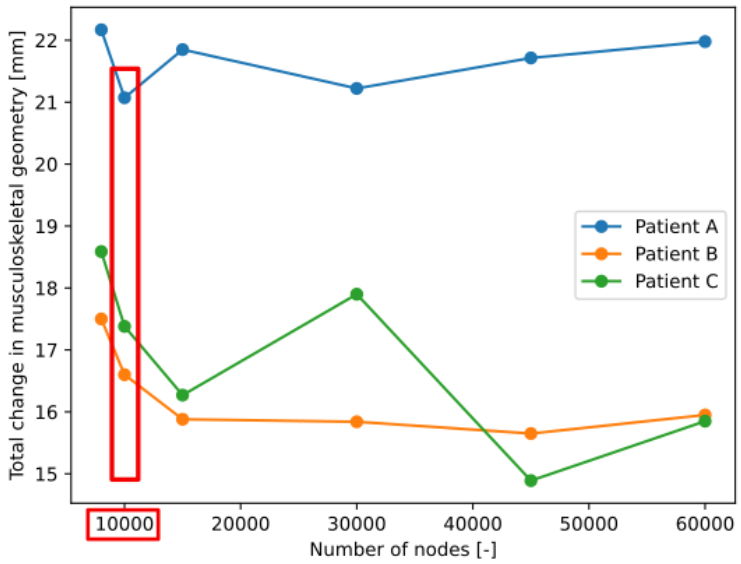

Fig. 55 Total change in musculoskeletal geometry according to the number of nodes of the simplified humerus 3D model. The red rectangle highlights the settings our approach.

4.3 Musculoskeletal Model and Kinematics

We utilized the musculoskeletal model of the human shoulder (Fig. 56) proposed by Seth et al., 2019 [94]. This model, implemented in the OpenSim software [95], consisting of 16 muscles (33 muscle segments) integrates a swift and precise skeletal representation of scapulothoracic kinematics, as introduced by Seth et al., 2016 [96]. The muscle paths and architecture are derived from the work of Klein Breteler et al., 1999 [97]. In order to enhance computational efficiency and simplify the model, muscle bundles from van der Helm, 1994 [75] were consolidated, and their parameters were integrated (Tab. 9). Additionally, adjustments are made to the muscle paths of the model, including wrapping surfaces and geometry, to align with moment arms constrained by measurements from cadaver experiments conducted by Ackland et al., 2008 [98], thereby reducing complexity.

Three muscles, namely the subscapularis, supraspinatus, and long head of the biceps brachii, were deemed inadequate for inclusion in the musculoskeletal model. In cuff tear arthropathy, a prevalent indication for RTSA, the subscapularis and supraspinatus muscles often face irreparable conditions [99]. Additionally, the long head of the biceps brachii is typically interrupted during surgery and subsequently reconstructed adjacent to the short head, diminishing its primary contributions to shoulder movement and stability [100].

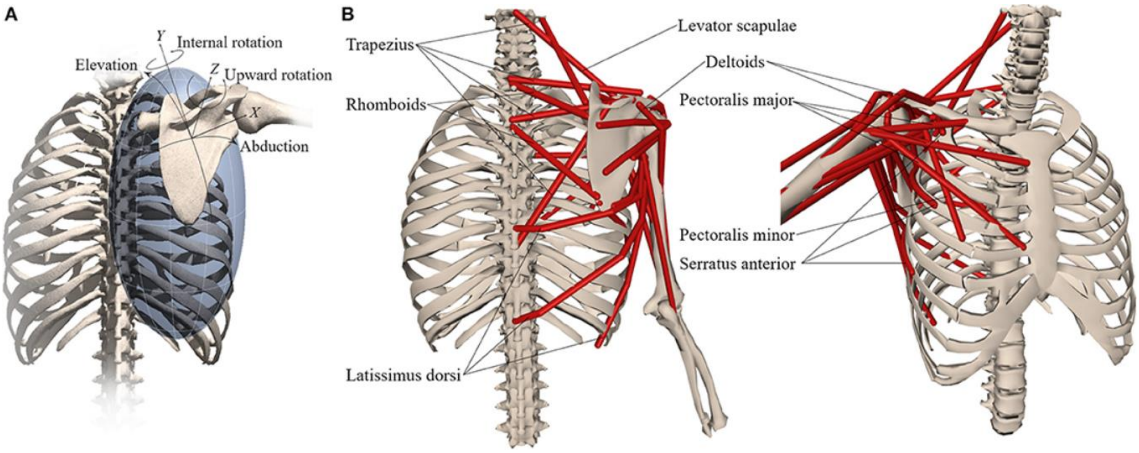

Fig. 56 Musculoskeletal model with (A) wrapping ellipsoid of thorax and scapula DOF and (B) selected muscles that control scapula [94].

The datasets of arm kinematics were obtained from database OpenSim available at https://simtk.org/projects/scapulothoracic. The process of data acquisition and processing is described in detail in Seth et al., 2019 [94]. Briefly, electromagnetic tracking kinematics of thorax, scapula, and humerus were obtained

using Ascension 3D trakSTAR (Ascension Technology Corp, USA) and Motion Monitor software (Innovative Sports Training, Chicago, Illinois) at a sampling rate of 120 Hz. The ISB shoulder protocol (Wu et al., 2005 [101]) was used to collect data based on the recorded sensor and digitized landmark locations were used to perform an inverse kinematical analysis in OpenSim (version 4.1) [95]. Three trials of shoulder shrugging, forward flexion, and abduction without weight, for a total of 9 trials from the dominant shoulder (right) of a 26-year-old healthy female subject (height: 162 cm, weight: 52 kg) [94].

The arm position in abduction and flexion was described by an elevation angle. Elevation angle is defined as an angle between the vertical and arm axis running through the COR of glenohumeral joint and the center of gravity of hand (Fig. 57 and Fig. 58). The motion in shrugging is described by vertical displacement of the COR of glenohumeral joint (Fig. 59). The studied motions are described in Tab. 8 and the kinematics are depicted in Fig. 61.

Local coordinate system of the humerus was used for evaluation of the changes in musculoskeletal geometry as shown in Fig. 60.

Tab. 8 Description of studied motions, definition of coordinate frame is based on ISB recommendation for global coordinate system stated in Wu et al., 2005 [101].

Motion	Description	Glenoid motion
Abduction	Starting from neutral position, humerus abducted to 90° in the coronal plane; elbow fully extended	Rotation around x-axis
Flexion	Starting from neutral position, humerus abducted to 90° in the sagittal plane; elbow fully extended	Rotation around z-axis
Shrug	Starting from neutral position, shoulder raise; elbow fully extended	Translation in +y axis

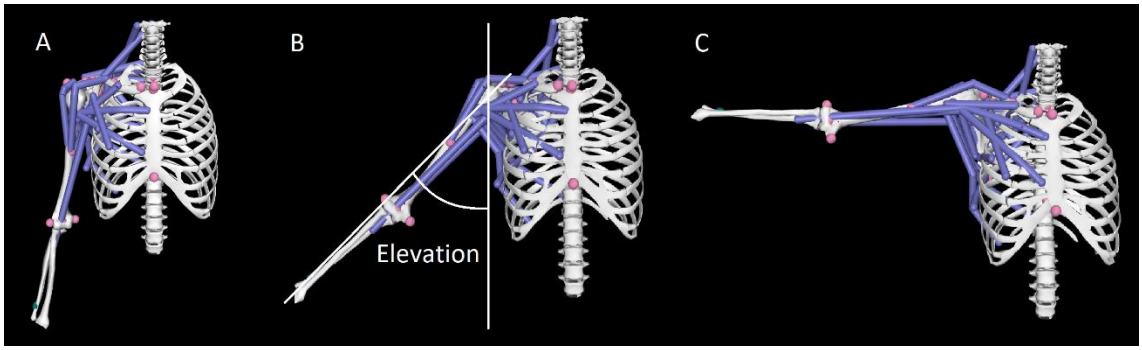

Fig. 57 Kinematics of abduction in OpenSim software in three positions: initial position (A), 45 degrees (B), and 90 degrees (C).

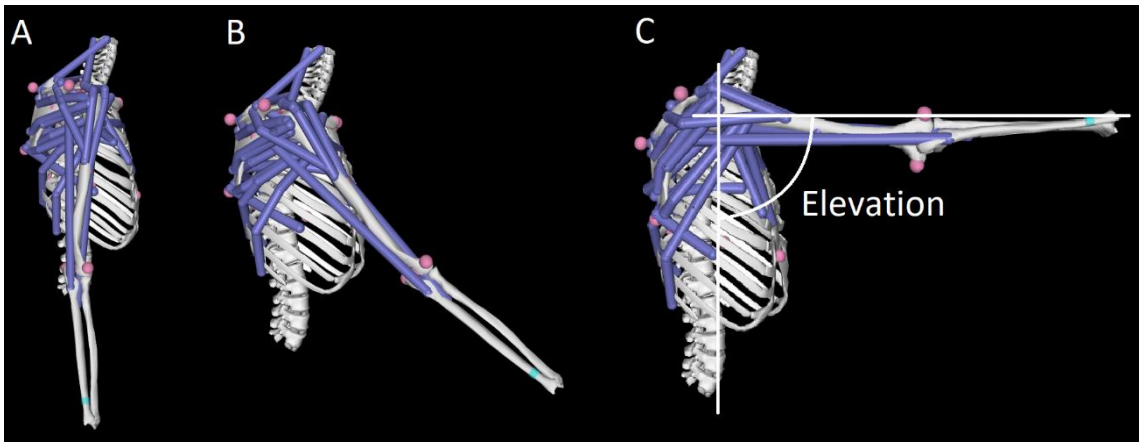

Fig. 58 Kinematics of flexion in OpenSim software in three positions: initial position (A), 45 degrees (B), and 90 degrees (C).

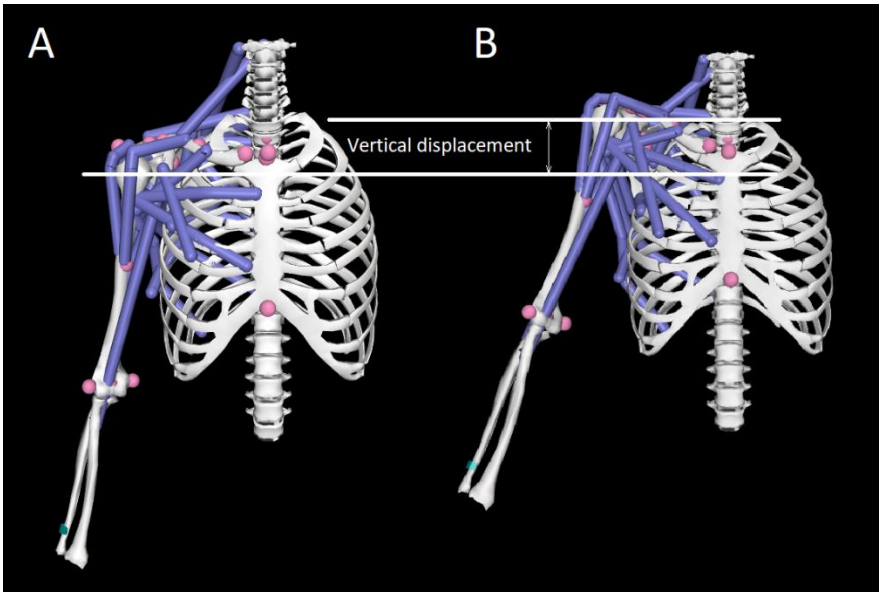

Fig. 59 Kinematics of shrug in OpenSim software in two positions: initial position of shoulder (A) and top peak position of shoulder (B).

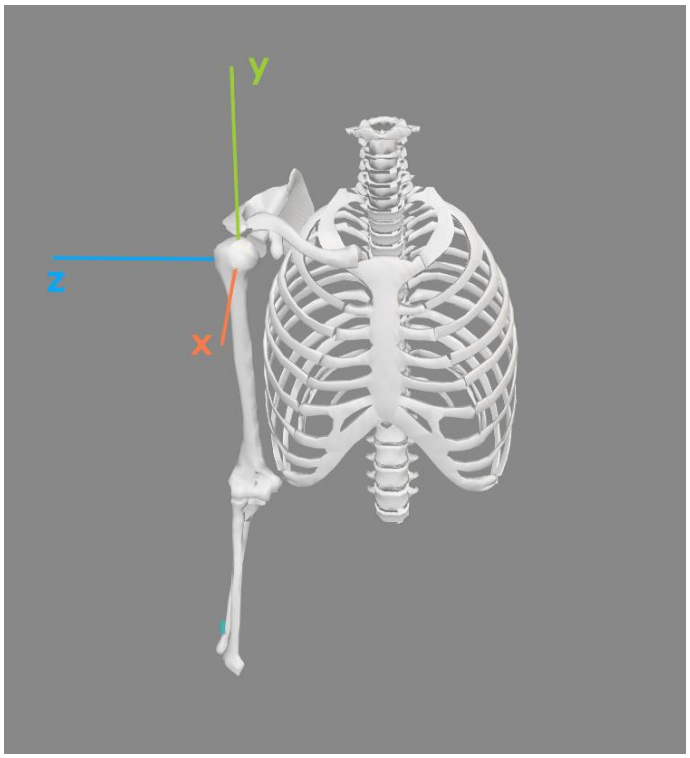

Fig. 60 The local coordinate system of humerus according to Wu et al., 2005 [101]. X-axis is in anterior-posterior meaning, y-axis is in superior-inferior meaning and z-axis in medialis-lateralis meaning.

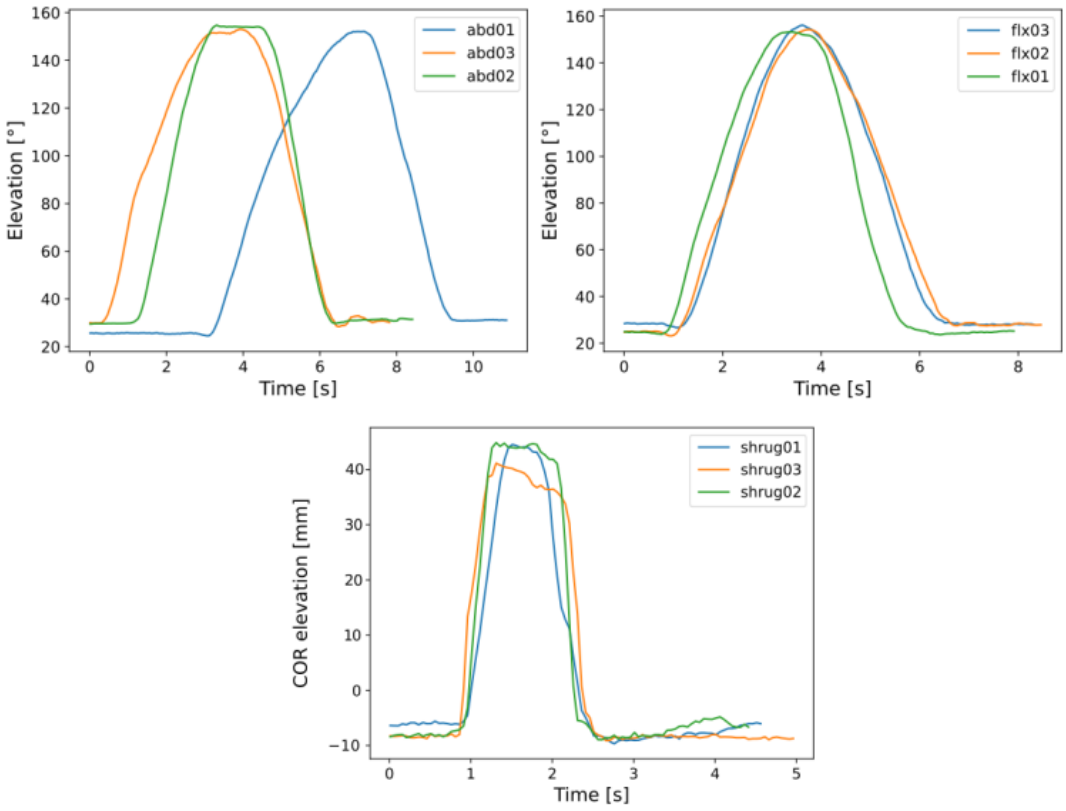

Fig. 61 Kinematics of shoulder abduction (upper-left), forward flexion (upper-right), and shrugging (lower) without weight. Three trials of each motion were examined.

Tab. 9 Muscle parameters for the musculoskeletal shoulder model adapted from Klein Breteler et al., 1999 [97] with aggregated bundles from van der Helm, 1994 [75].

Muscle	Group	Maximal isomeric force [N]	Optimal fiber length [m]	Tendon slack length [m]	Pennation angle [°]	Van der Helm bundles
Trapezius	Scapula superior	1043	0.1127	0.027	0	1–6
	Scapula middle	470.4	0.0832	0.032	0	7–9
	Scapula inferior	414.4	0.1264	0.035	0	10–12
	Clavicle	201.6	0.1116	0.027	0	C1, C2
Serratus anterior	Superior	387.8	0.0945	0	0	9–12
	Middle	508	0.1538	0.012	0	5–8
	Inferior	430	0.1587	0	0	1–4
Rhomboideus	Superior	200.2	0.0986	0.015	0	1, 2
	Inferior	407.4	0.1152	0.028	0	3, 4
Levator scapulae		280	0.1578	0.019	0	All
Coracobrachialis		648.2	0.0683	0.104	0	All
Deltoideus	Anterior	707.7	0.0940	0.088	5	C1–C4
	Middle	2597.8	0.0748	0.064	5	4–11
	Posterior	1324.4	0.0949	0.076	5	1–3
Latissimus Dorsi	Superior	201.6	0.2109	0.081	0	1, 2
	Middle	315	0.2656	0.095	0	3, 4
	Inferior	270.2	0.3062	0.062	0	5, 6
Pectoralis Major	Clavicle	408.8	0.1087	0.014		C1, C2
	Thorax middle	683.2	0.1500	0.026	0	4–6
	Thorax inferior	571.2	0.1830	0.043	0	1–3
Teres Major		851.2	0.1410	0.006	0	All
Infraspinatus	Superior	967.4	0.0698	0.050		4–6
	Inferior	1037.4	0.0677	0.084	0	1–3
Pectoralis minor		429.8	0.1183	0.032	0	All
Teres minor		695.8	0.0550	0.051	0	All
Subscapularis*	Superior	540.4	0.0676	0.059	5	1–3
	Middle	609	0.0744	0.055	5	4, 5, 10
	Inferior	854	0.0721	0.059	0	6–9, 11
Supraspinatus*	Anterior	543.2	0.0554	0.031	0	3, 4
	Posterior	326.2	0.0591	0.025	0	1, 2
Triceps long		1580.6	0.0969	0.241	10	All
Biceps	Long*	485.8	0.1412	0.257	0	All
	Brevis	693	0.1264	0.212	0	All

Note: Muscles marked with asterisk were excluded from RTSA analysis.

4.4 Muscle Models

The principle of humerus prolongation is based on utilization of passive muscle response in order to improve RTSA stability. However, different biomechanical studies adopt diverse muscle models. To assess the impact of the muscle model on the predicted glenohumeral load, we employed four different muscle models. Three Hill-type muscle models comprising three elements (Fig. 62) and one Hill-type muscle model comprising four elements (Fig. 63).

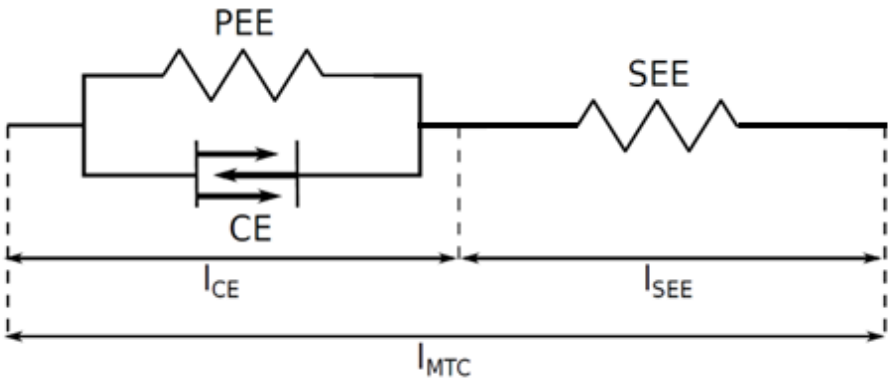

Fig. 62 The configuration of the three elements MTC

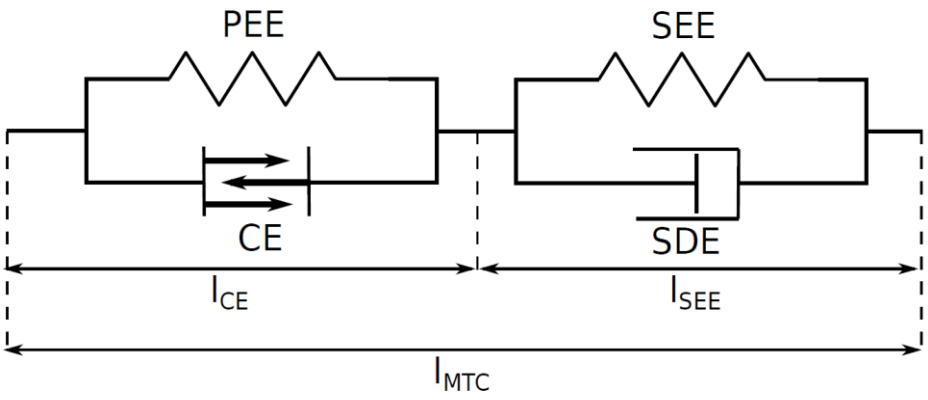

Fig. 63 The configuration of the four elements MTC as presented by Haeufle et al., 2014 [102].

The kinematics of the movements were addressed by employing slow movements, allowing for a quasi-static analysis of slow motion. Consequently, parameters associated with contraction velocity could be disregarded.

All the muscle tendon complexes (MTC) consist of active (muscle) and passive (tendon) part. The active part includes contractile element (CE), responsible for active force production and parallel elastic element (PEE), aligned parallel to the CE

and which simulates passive response of the muscle fibres. The passive part includes serial elastic element (SEE), positioned in series with the CE and simulating the elastic response of tendon. In four elements MTC, the passive part also includes serial damping element, operating in parallel to the SEE, which simulates the force-velocity response of the tendon, which is highly dependent on the velocity of the fast contractions. [103]. The pennation angle was applied to all muscle models by multiplying the resultant force by the cosine of the pennation angle.

Forces in the MTCs are F_{max}, maximum isometrical force (optimized parameter), F_{CE}, contractile element force (calculated), F_{SEE}, serial element force (calculated), F_{PEE}, parallel element force (calculated), and F_M, total muscle force (calculated). Together, these elements uphold force equilibrium as shown in equation (8).

$$F_M = F_{CE} + F_{PEE} = F_{SEE} \tag{8}$$

Lengths in the MTCs are l_{MTC}, total muscle tendon complex length (calculated), l_{CE}, contractile element length (calculated) initialized to l_{CE}^{opt}, optimal contractile element length (optimized parameter), l_{SEE}, serial element length (calculated), l_{PEE}, parallel element length (calculated), l_{CE}^{slack}, muscle slack length (optimized parameter), l_{SEE}^{slack}, tendon slack length (optimized parameter). The kinematic relations in MTC between the elements are $l_{PEE} = l_{CE}$, and $l_{MTC} = l_{SEE} + l_{CE}$.

4.4.1 Contractile element

The contractile element characterizes the active fibre bundles in the muscle. The force exerted by the CE is contingent on the present length of the muscle fibres.

Haeufle et al., 2014 [102] utilizes equation (9) to describe force-length relationship.

$$F_{CE} = exp\left\{-\left|\frac{l_{CE}/l_{CE}^{opt} - 1}{w}\right|^{\upsilon_{CE}}\right\} \tag{9}$$

In this context, l_{CE}^{opt} represents the optimal fibre length at which F_{CE} achieves its maximum ($F_{CE} = F_{max}$), w is a shape factor, which signifies the width of the normalized bell curve, and υ_{CE} denotes its exponent.

Equation (10) represents the normalized force-length relationship of the CE, expressed by Thelen, 2003 [104].

$$\bar{F}_{CE} = exp\left[-\frac{\left(\bar{l}_{CE} - 1\right)^2}{w}\right] \tag{10}$$

where $\bar{l}_{CE}$ is the normalized muscle fiber length, relative to the optimal muscle fiber length (l_{CE}^{opt}), at which maximal force can be generated. $\bar{l}_{CE}$ is then expressed by equation (11).

$$\bar{l}_{CE} = \frac{l_{CE}}{l_{CE}^{opt}} \tag{11}$$

The shape factor (w) was selected as 0.45, approximating the force-length relationship of individual sarcomeres [105]. The resultant force is derived by multiplying $\bar{F}_{CE}$ by the maximum isometric muscle force, F_{max}.

McLean et al., 2003 [106] describe the force-length relationship of the CE as a function of muscle length by a quadratic function defined in equation (12)

$$F_{CE} = max\begin{Bmatrix} F_{CE}^{min} \\ F_{max}\left[1 - \left(\frac{l_{CE} - l_{CE}^{opt}}{w l_{CE}^{opt}}\right)^2\right] \end{Bmatrix} \tag{12}$$

For numerical stability, a minimum force level F_{CE}^{min} is introduced, with McLean, 2003 [106] setting $W = 1$ and $F_{Mmin} = 10\ N$.

Force-length relationship of CE used by Geyer et al., 2010 [107] muscle model, which was previously published by Geyer et al., 2003 [108] is defined in equation (13).

$$F_{CE} = exp\left[c\left|\frac{\bar{l}_{CE} - l_{CE}^{opt}}{w l_{CE}^{opt}}\right|^3\right] \tag{13}$$

where $\bar{l}_{CE}$ is defined by equation (11) and and $c = ln(0.05)$ fulfilling $F_{CE}\left(l_{CE}^{opt}(1 \pm w)\right)$.

4.4.2 Parallel Elastic Element

The parallel elastic element characterizes the passive response fibre bundles in the muscle.

The attributes of the parallel elastic element as formulated in Haeufle et al., 2014 [102] muscle model are depict in equation (14).

$$F_{PEE} = \begin{cases} 0, l_{CE} < l_{PEE} \\ k_{PEE}\left(l_{CE} - l_{PEE}^{opt}\right)^{\nu_{PEE}}, l_{CE} \geq l_{PEE} \end{cases} \quad (14)$$

where k_{PEE} is defined by equation (15) and l_{PEE}^{opt} by equation (16).

$$k_{PEE} = \mathcal{F}_{PEE} \frac{F_{max}}{\left(l_{CE}^{opt}(w + 1 - \mathcal{L}_{PEE})\right)^{\nu_{PEE}}} \quad (15)$$

$$l_{PEE}^{opt} = \mathcal{L}_{PEE} l_{CE}^{opt} \quad (16)$$

where $\mathcal{F}_{PEE}$, $\mathcal{L}_{PEE,0}$, and ν_{PEE} are free parameters [103].

The normalized force of the parallel element of Thelen, 2003 [104] muscle model is represented as a function of muscle length (normalized by the optimal muscle fiber length) shown in equation (17).

$$\bar{F}_{PEE} = \frac{exp\left[k_{PEE}\left(\bar{l}_{CE} - 1\right)/\epsilon_{CE}\right] - 1}{exp(k_{PEE}) - 1} \quad (17)$$

where k_{PEE} is a stiffness parameter characterizing the parallel element and $\epsilon_{CE}$is the passive muscle strain due to maximum isometric force expressed by equation (18).

$$\epsilon_{CE} = \frac{l_{CE} - l_{CE}^{slack}}{l_{CE}^{slack}} \quad (18)$$

where l_{CE}^{slack} is the muscle slack length. Thelen, 2003 [104] adopted $l_{CE}^{slack} = l_{CE}^{opt}$, $k_{PEE} = 5$, and $\epsilon_{CE} = 0.6$ for young adults ($\epsilon_{CE} = 0.5$ for old adults). The actual force produced is obtained multiplying $\bar{F}_{PEE}$ by the maximum isometric muscle force, F_{max}.

McLean et al., 2003 [106] express the force of the parallel element of the muscle as a function of muscle length by a quadratic function as in equation (19).

$$F_{PEE} = \begin{cases} 0, l_{CE} \leq l_{CE}^{slack} \\ k_{PEE}\left(l_{CE} - l_{CE}^{slack}\right)^2, l_{CE} > l_{CE}^{slack} \end{cases} \quad (19)$$

where k_{PEE} is outlined in equation (20).

$$k_{PEE} = \frac{F_{max}}{\left(w l_{CE}^{opt}\right)^2} \quad (20)$$

McLean, 2003 [106] adopted $l_{CE}^{slack} = l_{CE}^{opt}$.

Force in parallel element in Geyer et al., 2010 [107] muscle model is computed according to equation (21).

$$F_{PEE} = F_{max}\left(\frac{\bar{l}_{CE} - l_{CE}^{opt}}{w l_{CE}^{opt}}\right)^2 \tag{21}$$

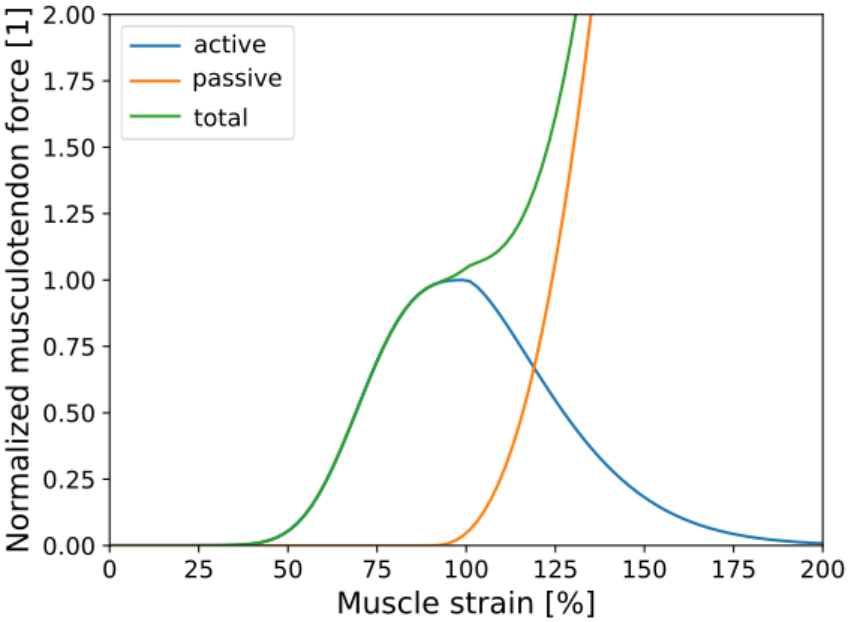

Fig. 64 Force-length relation of the contractile element (CE, blue line) and the parallel elastic element (PEE, orange line) starting at $0.95 l_{CE,opt}$ in Haeufle et al., 2014 [102] muscle model. Green line indicates total muscle force. Data is shown for middle deltoid with 100 % activation.

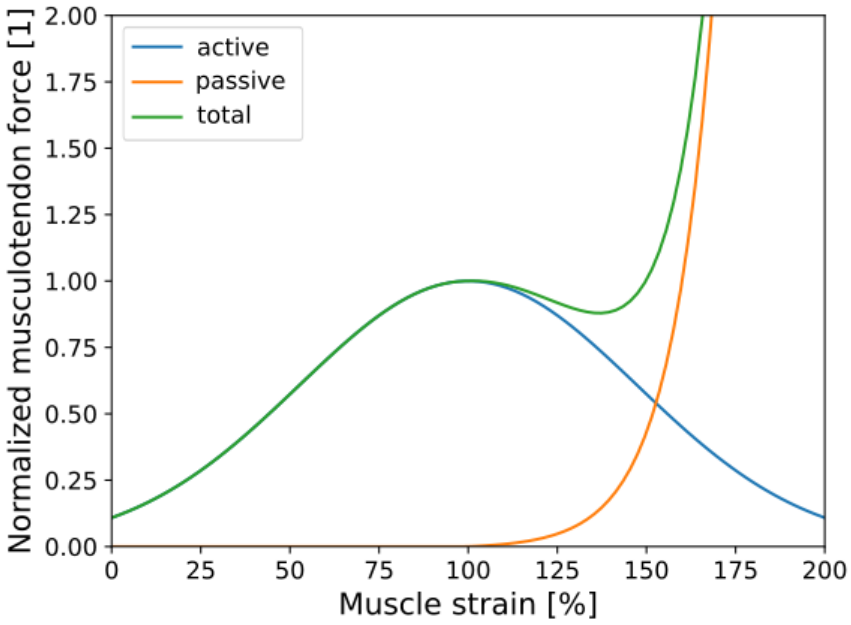

Fig. 65 Force-length relation of the contractile element (CE, blue line) and the parallel elastic element (PEE, orange line) in Thelen, 2003 [104] muscle model. Green line indicates total muscle force. Data is shown for middle deltoid with 100 % activation.

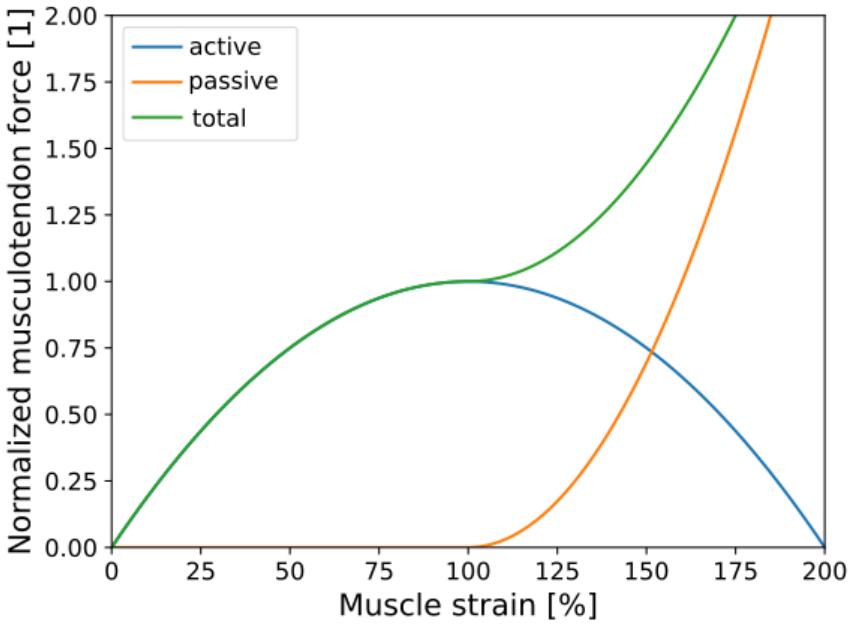

Fig. 66 Force-length relation of the contractile element (CE, blue line) and the parallel elastic element (PEE, orange line) in McLean et al., 2003 [106] muscle model. Green line indicates total muscle force. Data is shown for middle deltoid with 100 % activation.

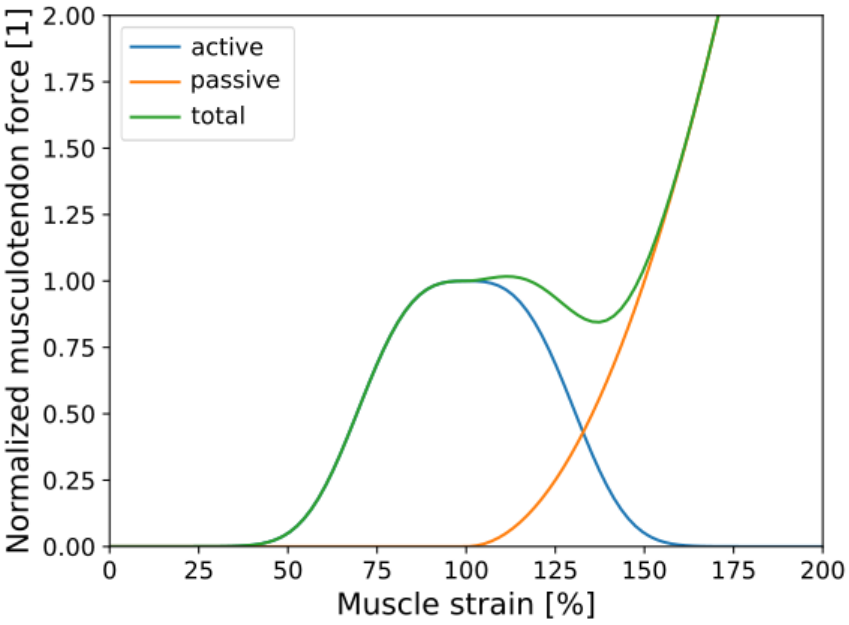

Fig. 67 Force-length relation of the contractile element (CE, blue line) and the parallel elastic element (PEE, orange line) in Geyer et al., 2003 [108] muscle model. Green line indicates total muscle force. Data is shown for middle deltoid with 100 % activation.

4.4.3 Serial Elastic Element

The force F_{SEE} exerted in the serial elastic element in Haeufle et al., 2014 [102] is represented by a non-linear toe zone followed by a linear continuation as presented by Günther et al., 2007 [103]:

$$F_{SEE} = \begin{cases} 0, l_{SEE} < l_{SEE}^{slack} \\ k_{SEE}^{nll} \left(l_{SEE} - l_{SEE}^{slack}\right)^{\nu_{SEE}}, l_{SEE} < l_{SEE}^{nll} \\ \Delta F_{SEE}^{lin} + k_{SEE}^{lin} \left(l_{SEE} - l_{SEE}^{nll}\right), l_{SEE} \geq l_{SEE}^{nll} \end{cases} \quad (22)$$

All parameters introduced in Equation (22) can be deduced from the parameters l_{SEE}^{slack}, tendon slack length, ΔU_{SEE}^{nll}, relative stretch at non-linear–linear transition, ΔF_{SEE}^{lin} both force at the transition and force increase in the linear part, and ΔU_{SEE}^{lin} relative additional stretch in the linear part providing a force increase of ΔF_{SEE}^{lin}:

$$l_{SEE}^{nll} = \left(1 + \Delta U_{SEE}^{nll}\right) l_{SEE}^{slack} \quad (23)$$

$$\nu_{SEE} = \Delta U_{SEE}^{nl} / \Delta U_{SEE}^{lin} \quad (24)$$

$$k_{SEE}^{nll} = \Delta F_{SEE}^{lin} / \left(\Delta U_{SEE}^{nll}\, l_{SEE}^{slack}\right)^{\nu_{SEE}} \quad (25)$$

$$k_{SEE}^{lin} = \Delta F_{SEE}^{lin} / \left(\Delta U_{SEE}^{lin}\, l_{SEE}^{slack}\right) \quad (26)$$

The tendon force in Thelen, 2003 [104] (equation (27)) is represented by a function of the normalized tendon length (in fact, tendon strain) by an exponential function during an initial nonlinear toe region and by a linear function thereafter.

$$\bar{F}_{SEE} = \begin{cases} \frac{\bar{F}_{SEE}^{toe}}{exp(k_{SEE}^{toe}) - 1}[exp(k_{SEE}^{toe}\epsilon_{SEE}/\epsilon_{SEE}^{toe}) - 1], \epsilon_{SEE} \leq \epsilon_{SEE}^{toe} \\ k_{SEE}^{lin}(\epsilon_{SEE} - \epsilon_{SEE}^{toe}) + \bar{F}_{SEE}^{toe}, \epsilon_{SEE} > \epsilon_{SEE}^{toe} \end{cases} \quad (27)$$

where ϵ_{SEE} is the tendon strain.

$$\epsilon_{SEE} = \frac{l_{SEE} - l_{SEE}^{slack}}{l_{SEE}^{slack}} \quad (28)$$

where ϵ_{SEE}^{toe} is the tendon strain above which the tendon exhibits linear behavior, k_{SEE}^{toe} is an exponential shape factor, and k_{SEE}^{lin} is a linear scale factor. The parameters are chosen such that the tendon elongation at the normalized maximal isometric force of the muscle is 4% of the tendon length ($\epsilon_{SEE}^{isom} = 0.04$). Thelen2003Muscle adopted $k_{SEE}^{toe} = 3$ and the transition from nonlinear to linear behavior occurs for normalized tendon forces greater than $\bar{F}_{SEE}^{toe} = 0.33$. For continuity of slopes at the transition, $\epsilon_{SEE}^{toe} = 0.609\epsilon_{SEE}^{isom}$ and $k_{SEE}^{lin} = 1.712/\epsilon_{SEE}^{isom}$. The actual force produced is obtained multiplying $\bar{F}_{SEE}$ by the maximum isometric muscle force, F_{max}.

The tendon force of the serial element in McLean et al., 2003 [106] is expressed as a quadratic function of the tendon length (equation (29)), mirroring the quadratic function employed for the force of the passive muscle element.

$$F_{SEE} = \begin{cases} 0, l_{SEE} \leq l_{SEE}^{slack} \\ k_{SEE}\left(l_{SEE} - l_{SEE}^{slack}\right)^2, l_{SEE} > l_{SEE}^{slack} \end{cases} \quad (29)$$

where k_{SEE} is determined to achieve a tendon elongation of 4% at the maximum isometric force. Specifically, $k_{SEE} = \left(1/\epsilon_{SEE}^{isom}\right)^2 = 625$ for $F_{max} = 1$.

Passive force produced in Geyer et al., 2010 [107] by the elastic elements F_{SEE} is modelled as non-linear spring based on its lengths as written in equation (30).

$$F_{SEE} = \begin{cases} \left(\frac{\epsilon_{SEE}}{\epsilon_{SEE}^{ref}}\right)^2, & \epsilon_{SEE} > 0 \\ 0, & \epsilon_{SEE} \leq 0 \end{cases} \quad (30)$$

where tendon strain ϵ_{SEE} is computed as written in equation (28) and ϵ_{SEE}^{ref} is tendon reference strain with $F_{SEE}\left(\epsilon_{ref}\right) = 1$.

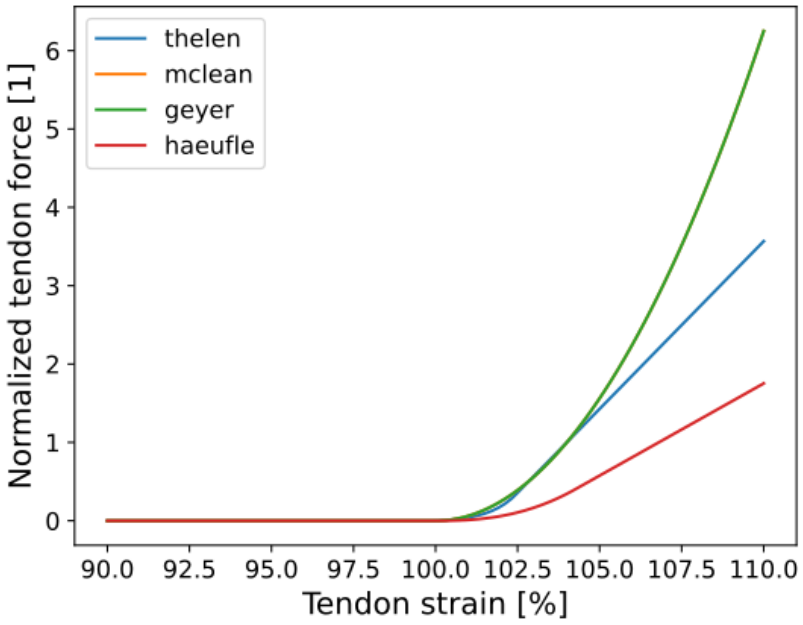

Fig. 68 Comparasion of force-length relations of the serial elastic element in all four muscle models. Data for McLean et al., 2003 [106] and Geyer et al., 2003 [108] mirrors each other. Data is shown for middle deltoid.

4.5 Estimation of Glenohumeral Load

The estimation of glenohumeral load was conducted through a mathematical model that considers the equilibrium of forces and torques within the joint. Muscles were represented as active fibers running from proximal to distal attachment points, with parameters based on the cadaveric study by Klein Breteler et al., 1999 [97], as detailed in Tab. 9. Muscle paths, including wrapping points, were aligned with moment arms estimated from cadaver experiments (Ackland et al., 2008 [98]). Effective moment arms and muscle vectors were derived from OpenSim (version 4.1) [95] using the MuscleForceDirection plugin [109], while the musculotendon length was obtained using MuscleAnalysis tool. Segment masses were extracted from an arm reference model described by Wu et al., 2016 [110] as listed in Tab. 10, and center of gravity positions were sourced from a model by Seth et al., 2019 [94]. During motion, gravitational torques on individual body segments were balanced by muscle actions.

Tab. 10 The masses of individual segments taken from Wu et al., 2016 [110].

Body segment	Mass [kg]
humerus	2.035
ulna	0.6075
radius	0.6075
hand	0.4575

A static biomechanical analysis was employed, deemed acceptable for slow motions where the velocity of body parts could be neglected. This approach facilitated the comparison of individual trials at specific body positions. The glenohumeral joint was estimated using both passive and active approaches. In the former, muscle activation was set to zero, and muscle force was generated by nonlinear springs of parallel and serial elastic elements. In the latter, addressing the issue of muscle redundancy involved solving equilibrium torques in the shoulder joint. The model, with more active muscle forces (Tab. 9) than torque equilibrium equations, was statically indeterminate. Optimization, using the sum of squared muscle activation as the criterion [111] , was employed, considering equilibrium torque equations and muscle force generation capacity as constraints. Muscle force generation was influenced by musculotendon length, with muscle fiber and tendon lengths calculated for each muscle based on force and deformation transmission in the hill model at a given level of activation. Consequently, glenohumeral force was derived from the force equilibrium of the upper extremity [IX].

4.6 Simulation of Humeral Lengthening

The generic musculoskeletal model underwent modifications to account for changes in humeral geometry after RTSA [II]. The adjustments involved considering alterations in the rotation of the glenoidal joint, as well as changes in the position and length of the humerus. Rotational alteration was implemented by adjusting the position of the COR in the glenohumeral joint (Fig. 69). For humerus lengthening, adjustments were made to the muscle attachment points by introducing a vector representing humeral displacement to the original attachment points in the humerus coordinate system [101] (Fig. 70).

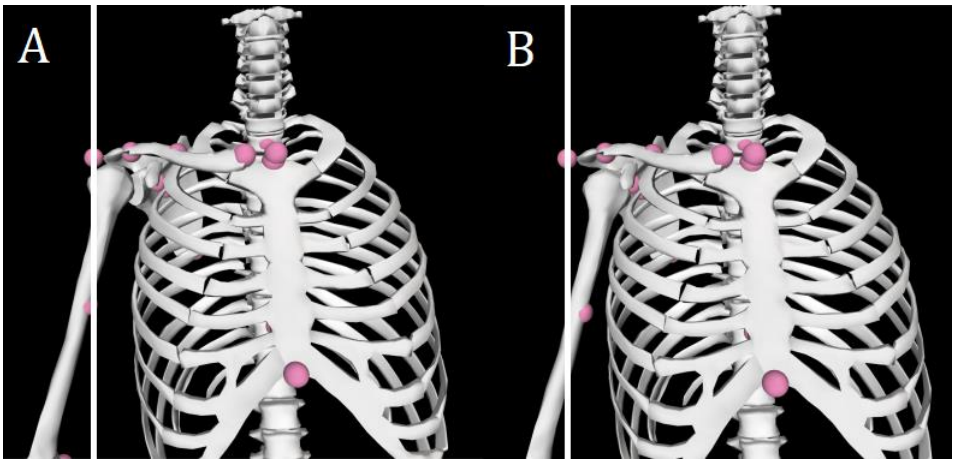

Fig. 69 Vizualization of medial shift of COR according to acromial marker. Shown in neutral position (A) and shifted medialy after RTSA (B).

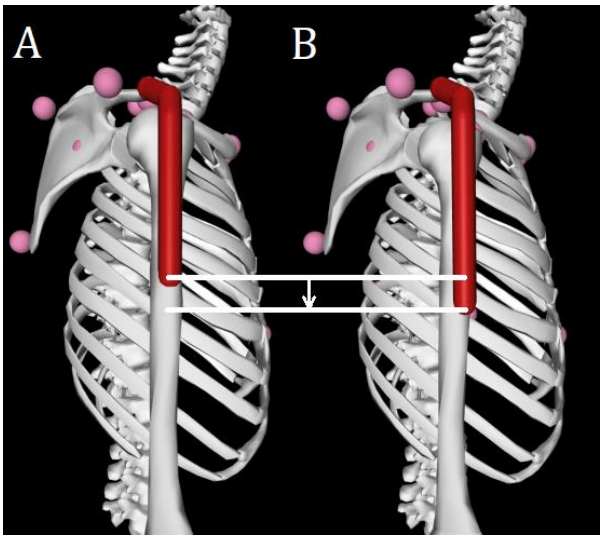

Fig. 70 Vizualization of humeral prolongation shown on middle deltoideus. Shown in neutral position (A) and prolonged after RTSA (B).

4.7 Statistical analyses

Data analysis was performed utilizing R (R Foundation for Statistical Computing, Vienna, Austria, version 4.1.2). To assess inter-observer variability, the intra-class correlation coefficient (ICC) was calculated using model 2.1 as described by Shrout and Fleiss [112]. The Shapiro-Wilk test was employed to assess the normal distribution of data. The analysis was conducted for the entire cohort as well as separately for male and female patients. The Welch Two Sample t-test and one way analysis of variance (ANOVA) followed by Tukey's post hoc test for normally distributed data were used to evaluate the differences between cohorts. Multiple linear regression was employed to investigate whether patients' weight and height significantly predicted magnification [113]. The computation of 95% confidence

intervals (CIs) and p-values was carried out using the Wald approximation. An alpha of 0.05 was applied for evaluating statistical significance. In the post-hoc power analysis, based on the sample size for the primary outcome, the power was determined to be 0.99 for a two-tailed comparison, with an effect size of 0.5 and an α error of 0.05.

A Pearson correlation coefficient was computed to assess the linear relationship between humeral prolongation and age, humeral prolongation and BMI, humeral prolongation and height, and humeral prolongation and weight. Correlations between patient characteristics and measured changes in musculoskeletal geometry were also evaluated using Pearson correlation coefficients.

5 Results

5.1 Radiographical Magnification in Shoulder Joint Region

There was an excellent agreement between the observers in evaluation the magnification of radiographs (inter-rater ICC = 0.997, 95% confidence interval 0.991-0.999). The average magnification factor was 11.91% (standard deviation 3.24%, range 5.74%–20.31%) [I, V]. The magnification factor was normally distributed (Shapiro-Wilk normality test p = 0.209) as shown in Fig. 71.

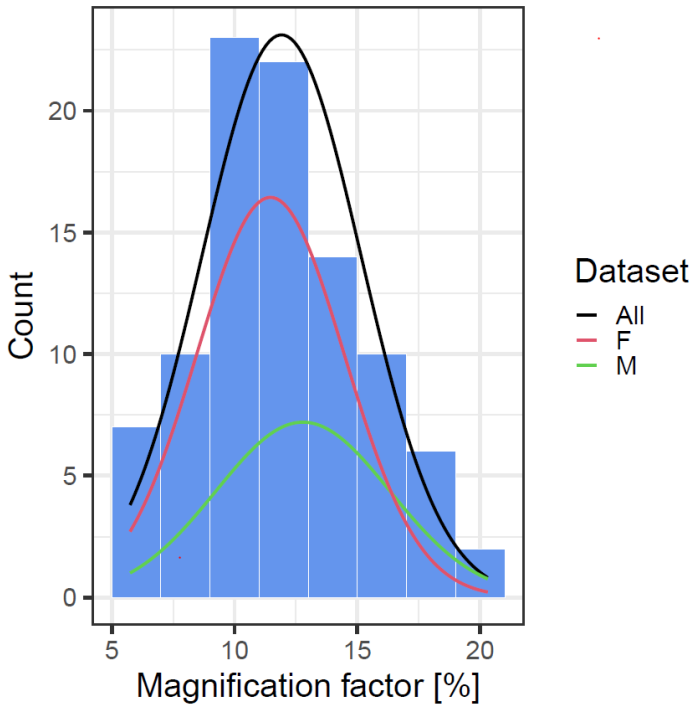

Fig. 71 Histogram of magnification factor for all patients and fitted Gaussian curves for all patients (All), female (F) and male (M) [I].

A slightly higher radiographic magnification was observed in male (mean 12.7%, standard deviation 3.5%) than in female patients (mean 11.4%, standard deviation 3.1%), the difference was not significant (Welch Two Sample t-test p=0.077). A linear model was fitted to predict radiographic magnification with patients' height and weight. The model's explanatory power is weak (R = 0.09) indicating large inter-individual variability among patients (Fig. 72). The effect of weight is statistically

significant and positive (p = 0.017), while the effect of height is statistically non-significant (p = 0.648) [I, V].

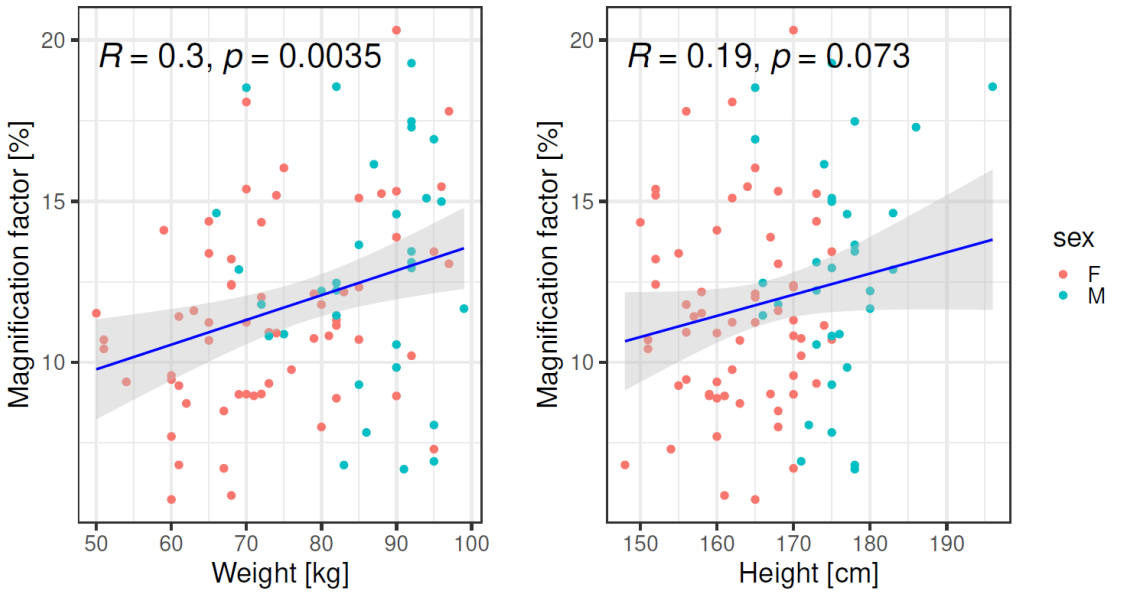

Fig. 72 Linear regression model (highlighted in blue) and a 95% confidence area (shaded area) illustrating the association between patients' weight (left) and height (right) with the magnification factor across all patients. In each plot, the Pearson correlation coefficient and corresponding p-value are provided to quantify the strength and significance of the observed relationships [I].

5.2 Changes in Musculoskeletal geometry after RTSA

Three changes of musculoskeletal geometry after RTSA were determined as shown in Fig. 49. The average shift of COR was 19.9 mm medially (standard deviation 7.9 mm, range 2.9–36.9 mm) and 6.2 mm inferiorly (standard deviation 7.4 mm, range -11.6–18.3 mm) [IV]. The medial and inferior shift of COR was normally distributed among patients (Shapiro-Wilk normality test W = 0.98139, p = 0.839 and W = 0.96839, p = 0.4562, respectively) as shown in Fig. 73.

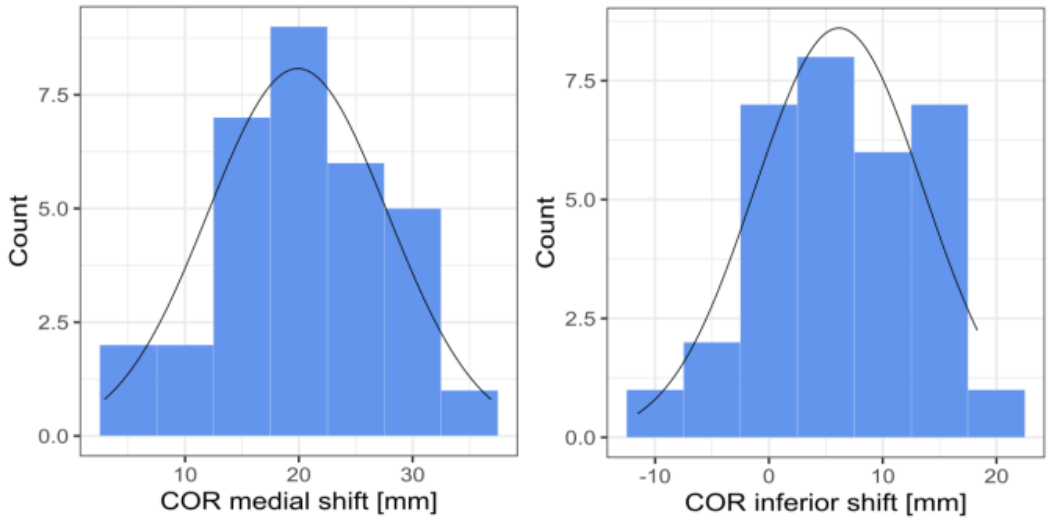

Fig. 73 Histogram of COR shift for all patients and fitted Gaussian curve.

The average prolonging of humerus in the direction of longitudinal axis of the humerus was 15.2 mm (standard deviation 6.2 mm, range 1.8–30.6 mm) and in lateral meaning (perpendicularly to the longitudinal axis of humerus) 11.8 mm (standard deviation 4.5 mm, range 1.3–17.9 mm), which resulted in average total prolonging of 19.7 mm (standard deviation 6.4 mm, range 2.2–35.2 mm) [III]. The inferior, lateral, and total prolonging of humerus was normally distributed among patients (Shapiro-Wilk normality test W = 0.98857, p = 0.9774; W = 0.92197, p = 0.02352; and W = 0.97215, p = 0.5606, respectively) as shown in Fig. 74. The distribution of data in humerus lateral shift might be influenced by the geometry of the replacement [VII].

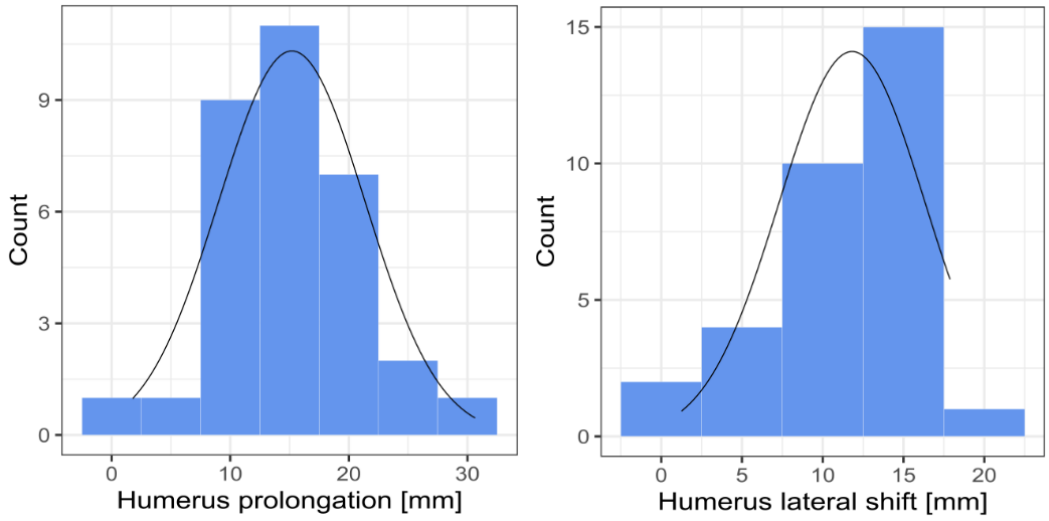

Fig. 74 Histogram of humerus prolongation and lateral shift for all patients and fitted Gaussian curves.

The average change in musculoskeletal geometry was 4.2 mm medially (standard deviation 7.5 mm, range -9.2–21.4 mm) and 17.2 mm inferiorly (standard deviation 9.8 mm, range -6.4–37.9 mm), which resulted in average total change in musculoskeletal geometry of 19.7 mm (standard deviation 9.8 mm, range 6.4–37.9 mm) [III]. The total change in musculoskeletal geometry was normally distributed among patients (Shapiro-Wilk normality test W = 0.94066, p = 0.07817).

The Welch Two Sample t-test testing the difference of humerus prolongation by sex (mean in females = 16.44, mean in males = 12.02 (Fig. 75)) suggests that the effect is positive, statistically not significant, and large (difference = 4.43, 95% CI [-0.37, 9.22], t(15.76) = 1.96, p = 0.068; Cohen's d = 0.99, 95% CI [-0.07, 2.02]).

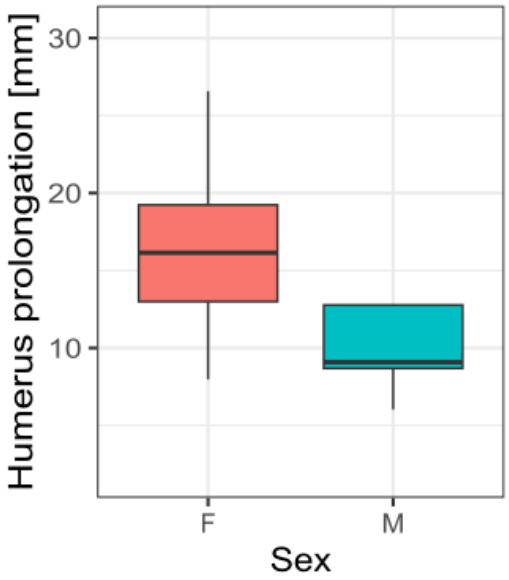

Fig. 75 The difference of humerus prolongation effected by sex. F = female, M = male.

The Welch Two Sample t-test testing the difference of humerus prolongation by the operated side (mean in left group = 16.73, mean in right group = 14.01 (Fig. 76)) suggests that the effect is positive, statistically not significant, and small (difference = 2.71, 95% CI [-1.89, 7.32], t(25.24) = 1.21, p = 0.236; Cohen's d = 0.48, 95% CI [-0.31, 1.27]).

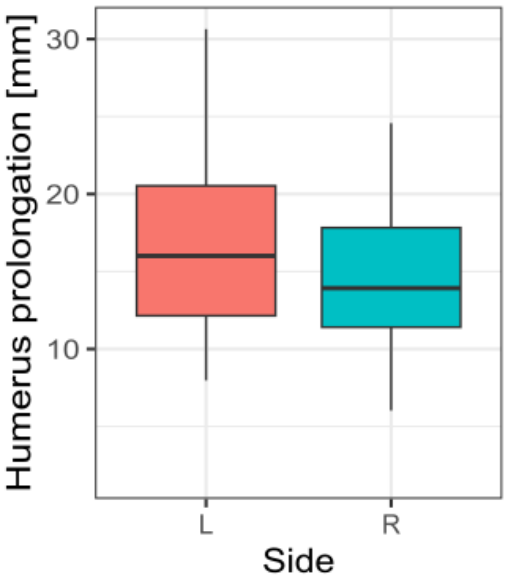

Fig. 76 The difference of humerus prolongation effected by operated side. L = left, R = right.

The Welch Two Sample t-test testing the difference of humerus prolongation by eccentricity of the glenosphere (mean in concentric group = 14.42, mean in 4 mm eccentric group = 17.97) suggests that the effect is negative, statistically not significant, and medium (difference = -3.55, 95% CI [-11.54, 4.44], t(7.34) = -1.04, p = 0.331; Cohen's d = -0.77, 95% CI [-2.24, 0.75]).

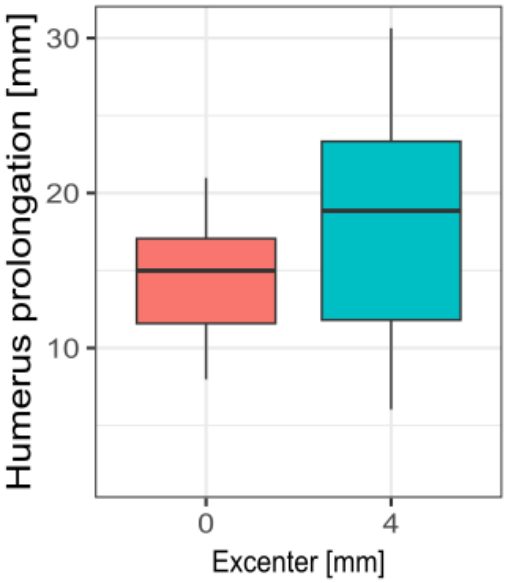

Fig. 77 The difference of humerus prolongation effected by eccentricity of the glenosphere.

A one-way ANOVA was performed to compare the effect of indication on humerus prolongation (Fig. 78). It was revealed that there was not a statistically

significant difference in humeral prolongation between at least two groups (F (5, 26) = 1.00, p = 0.435). Tukey's HSD Test for multiple comparisons found that the mean value of humerus prolongation was not significantly different between any of two groups (the highest difference was observed between RA and OCD groups, p = 0.422, 95% C.I. = [-8.85, 37.69]).

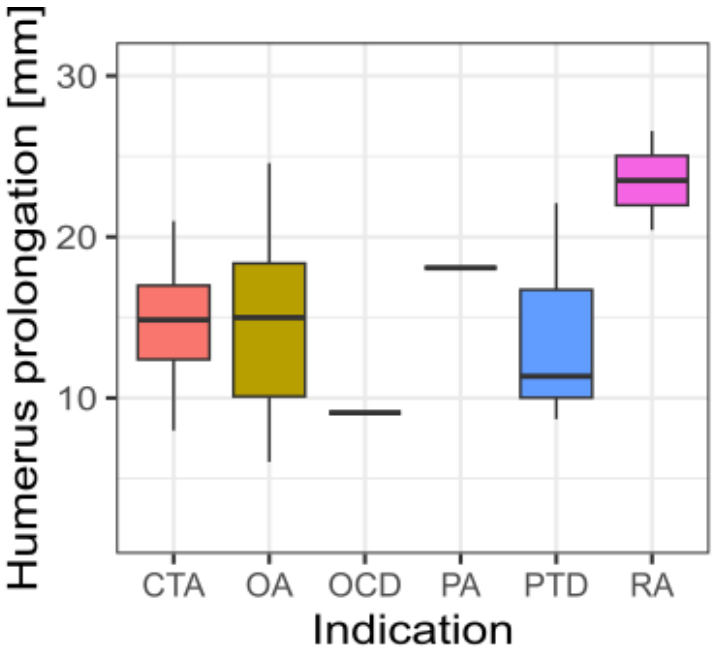

Fig. 78 The difference of humerus prolongation effected by surgical indication. CTA = cuff tear arthropathy, OA = omarthrosis, OCD = osteochondrodysplasia, PA = psoriatic arthritis, PTD = post-traumatic deformity, RA = rheumatoid arthritis.

A one-way ANOVA was performed to compare the effect of surgeon on humerus prolongation (Fig. 79). It was revealed that there was a statistically significant difference in humeral prolongation between at least two groups (F(3, 26) = 3.20, p = 0.040). Tukey's HSD Test for multiple comparisons found that the mean value of humerus prolongation was significantly different between 1 and 3 (p = 0.026, 95% C.I. = [0.60, 12.11]).

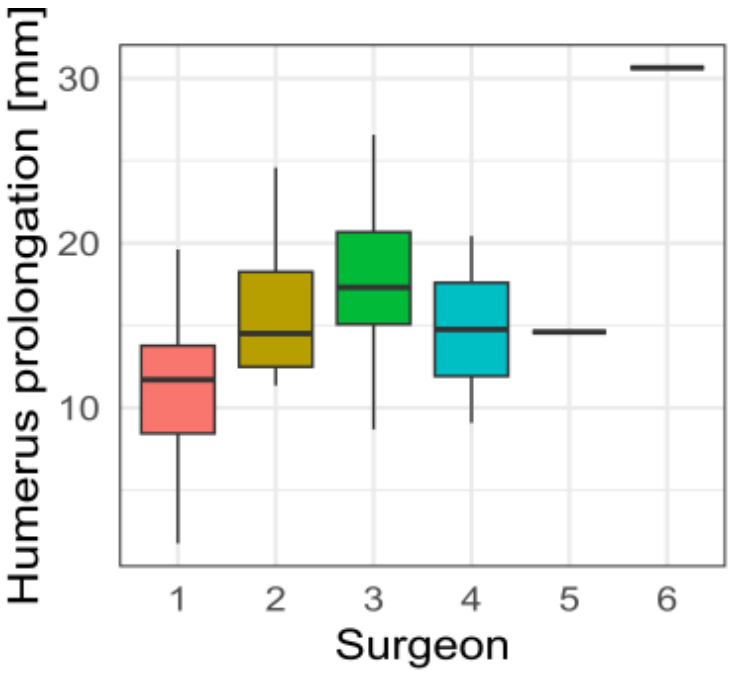

Fig. 79 The difference of humerus prolongation effected by surgeon.

A Pearson correlation coefficient was computed to assess the linear relationship between humeral prolongation and age, humeral prolongation and BMI, humeral prolongation and height, and humeral prolongation and weight (Fig. 80). There was a positive correlation between humeral prolongation and age, R(30) = 0.029, p = 0.88. Between humeral prolongation and BMI was a negative correlation, R(30) = -0.045, p = 0.81. Between humeral prolongation and height was a negative correlation, R(30) = -0.19, p = 0.31 and between humeral prolongation and weight was a negative correlation, R(30) = -0.15, p = 0.4. The p-value indicates weak correlations in all examined instances.

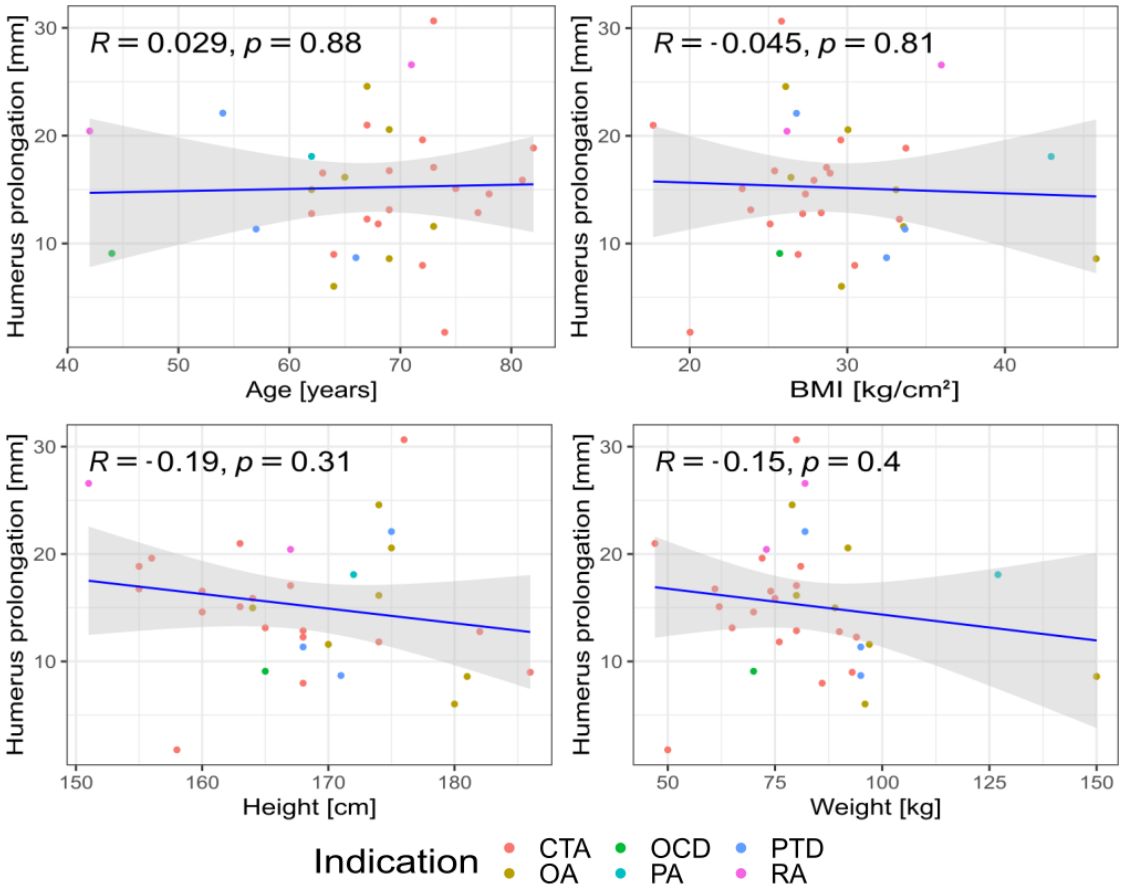

Fig. 80 Linear relationship using Pearson correlation coefficient between humeral prolongation and age (up left), humeral prolongation and BMI (up right), humeral prolongation and height (down left), and humeral prolongation and weight (down right). CTA = cuff tear arthropathy, OA = omarthrosis, OCD = osteochondrodysplasia, PA = psoriatic arthritis, PTD = post-traumatic deformity, RA = rheumatoid arthritis.

The correlation between the remaining variables is depicted in the correlation matrix (Fig. 81). Correlations between patient characteristics and measured changes in musculoskeletal geometry, using Pearson correlation coefficients, are provided along with p-values in the matrix squares.

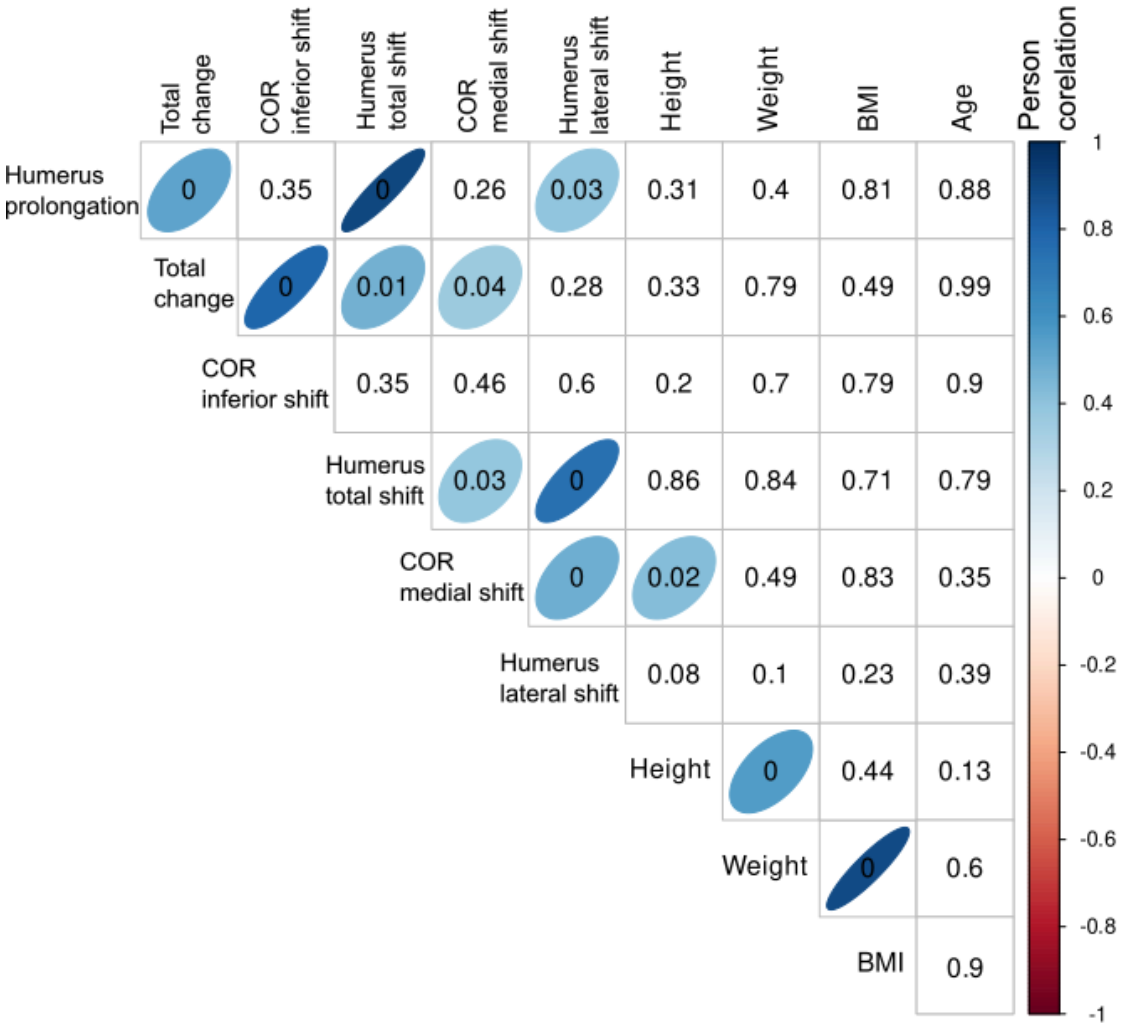

Fig. 81 Correlation matrix illustrating patient characteristics and measured changes in musculoskeletal geometry. Pearson correlation coefficients are provided, with numbers in boxes indicating p-values. Non-significant correlations ($p > 0.05$) are depicted without correlation ellipses. P-values under 0.01 are denoted as 0. The ellipses indicate the correlation rate, and their inclination and colour signify whether the correlation is positive or negative. Total change stands for overall alteration in musculoskeletal geometry after RTSA with both COR shift and humerus prolongation.

5.3 Influence of Muscle Model on Glenohumeral Joint Load

To assess the impact of muscle models on glenohumeral joint load, four different muscle models were employed in three distinct motions. Both passive and active motions were used to evaluate reaction forces, with passive motion representing no muscle activity and no gravitational influence, assessing passive forces alone. Active motion reflected real motion with the weights of body

segments and active muscle engagement. The influence of the muscle model was evaluated with the glenohumeral joint in its anatomical position for comparability with existing literature. As depicted in Fig. 82 for abduction, in Fig. 83 for forward flexion, and in Fig. 84 for shrugging, the choice of muscle model significantly impacted glenohumeral joint load. The highest load in all movements occurred when employing the Haeufle et al., 2014 [102] muscle model, while the lowest forces were observed with the Thelen, 2003 [104] muscle model. Although the muscle models showed the same qualitative trend, they varied quantitatively [XI].

Based on these results, the Thelen, 2003 [104] muscle model was chosen as a reference for all subsequent evaluations due to its widespread citation and close resemblance to in vivo measurements by Bergmann et al., 2007 [85] and Bergmann et al., 2011 [87].

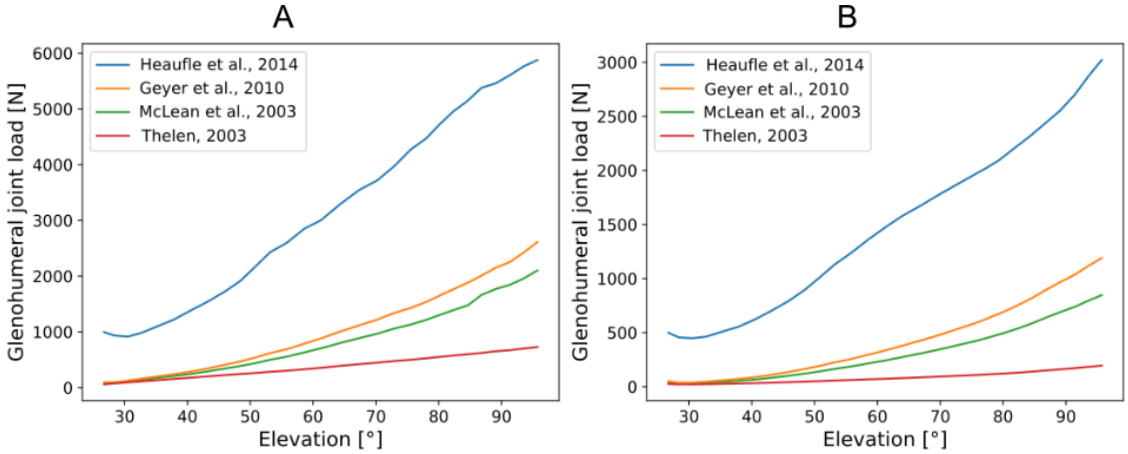

Fig. 82 The effect of formulation of Hill-type muscle model on glenohumeral joint load during active abduction (A) and passive abduction (B) [XI].

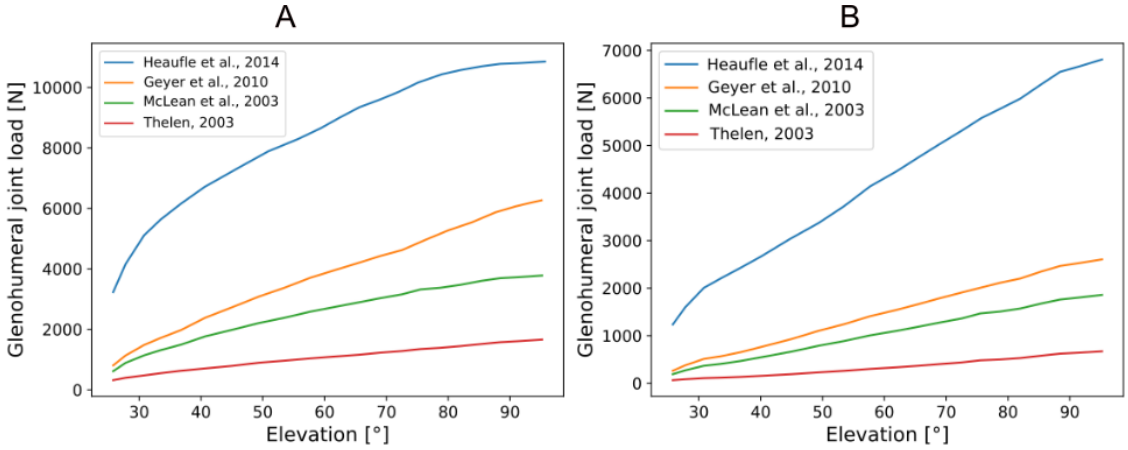

Fig. 83 The effect of formulation of Hill-type muscle model on glenohumeral joint load during active forward flexion (A) and passive forward flexion (B) [XI].

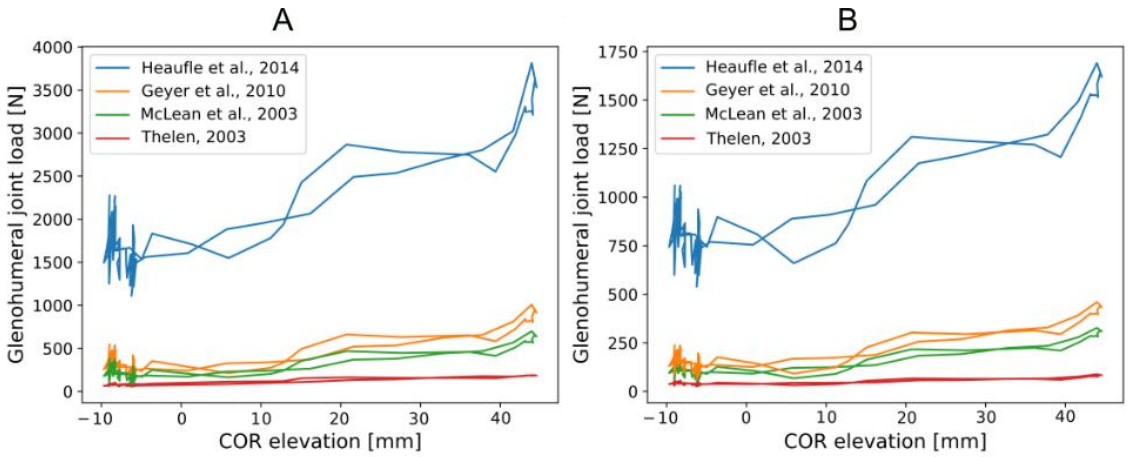

Fig. 84 The effect of formulation of Hill-type muscle model on glenohumeral joint load during active shrugging (A) and passive shrugging (B) [XI].

Muscle forces in each muscle during active and passive motions with glenohumeral joint in anatomical position were also determined. In abduction (Fig. 85), the most active muscle during active motion was middle deltoid. On the other hand, long head of triceps brachii and coracobrachialis contribute by the same force in both, passive and active motion. That signifies, that those muscles are not contributing actively to the abduction and their contribution arises form only from elongation during the motion. Deltoideus, supraspinatus, infraspinatus, and partly pectoralis major are the primary contributors to active abduction up to 90 degrees [X].

In active forward flexion (Fig. 86) the middle deltoid remained the most active muscle, with additional contributions from coracobrachialis and biceps brachii (mainly brevis head). Supraspinatus and infraspinatus were not active in forward flexion, and the long head of triceps exhibited a similar pattern to abduction but with higher contribution. Anterior deltoid became active in forward flexion, while posterior deltoid contributed only passively. The load was higher in forward flexion compared to abduction [X].

In active shrugging (Fig. 87), the middle deltoid was again the most active muscle, and supraspinatus, subscapularis, and pectoralis major were active contributors. Infraspinatus and teres minor mainly contributed passively. The glenohumeral joint load was significantly lower in shrugging than in abduction and forward flexion [X].

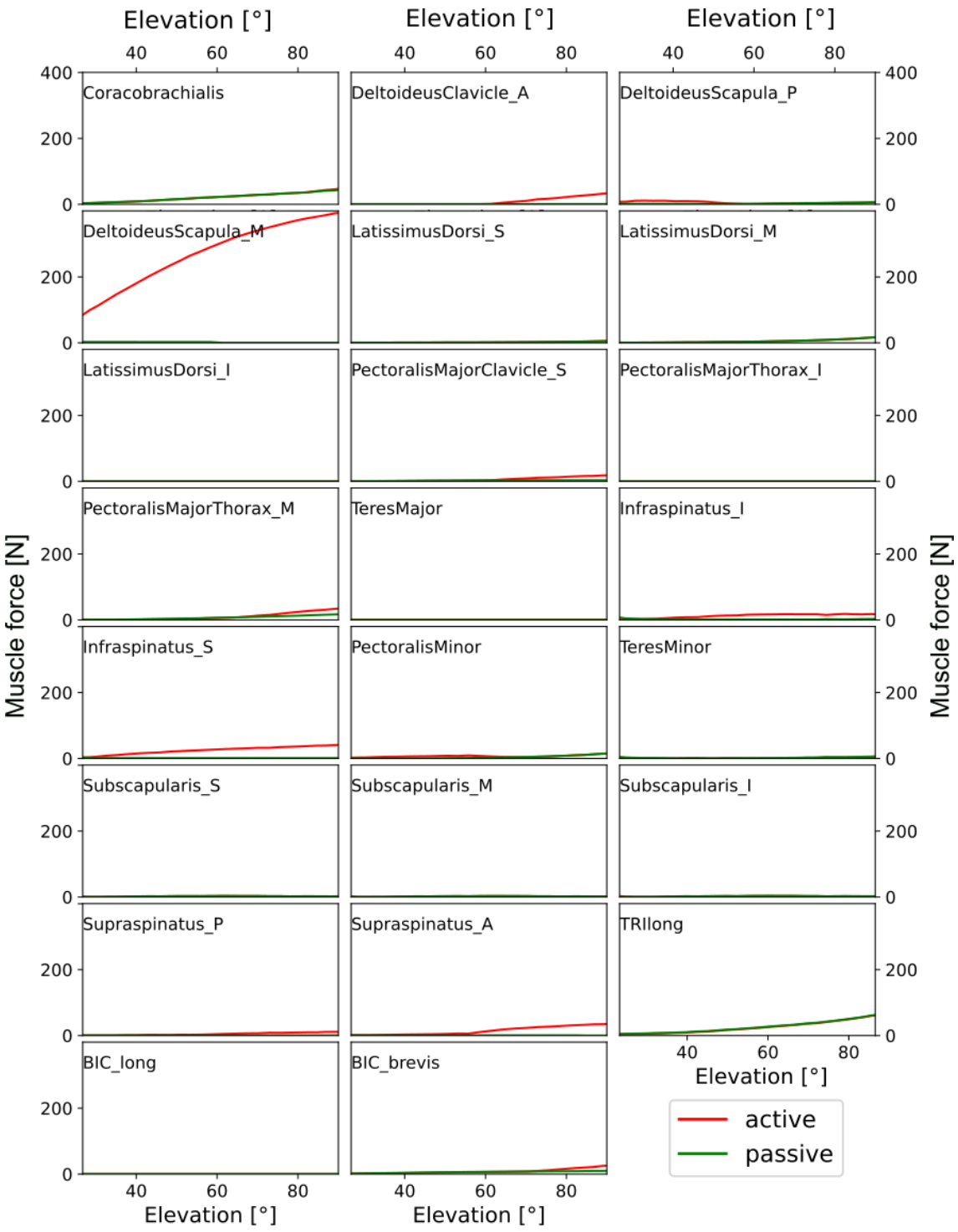

Fig. 85 Muscle forces in each muscle during active and passive abduction in anatomical position [X].

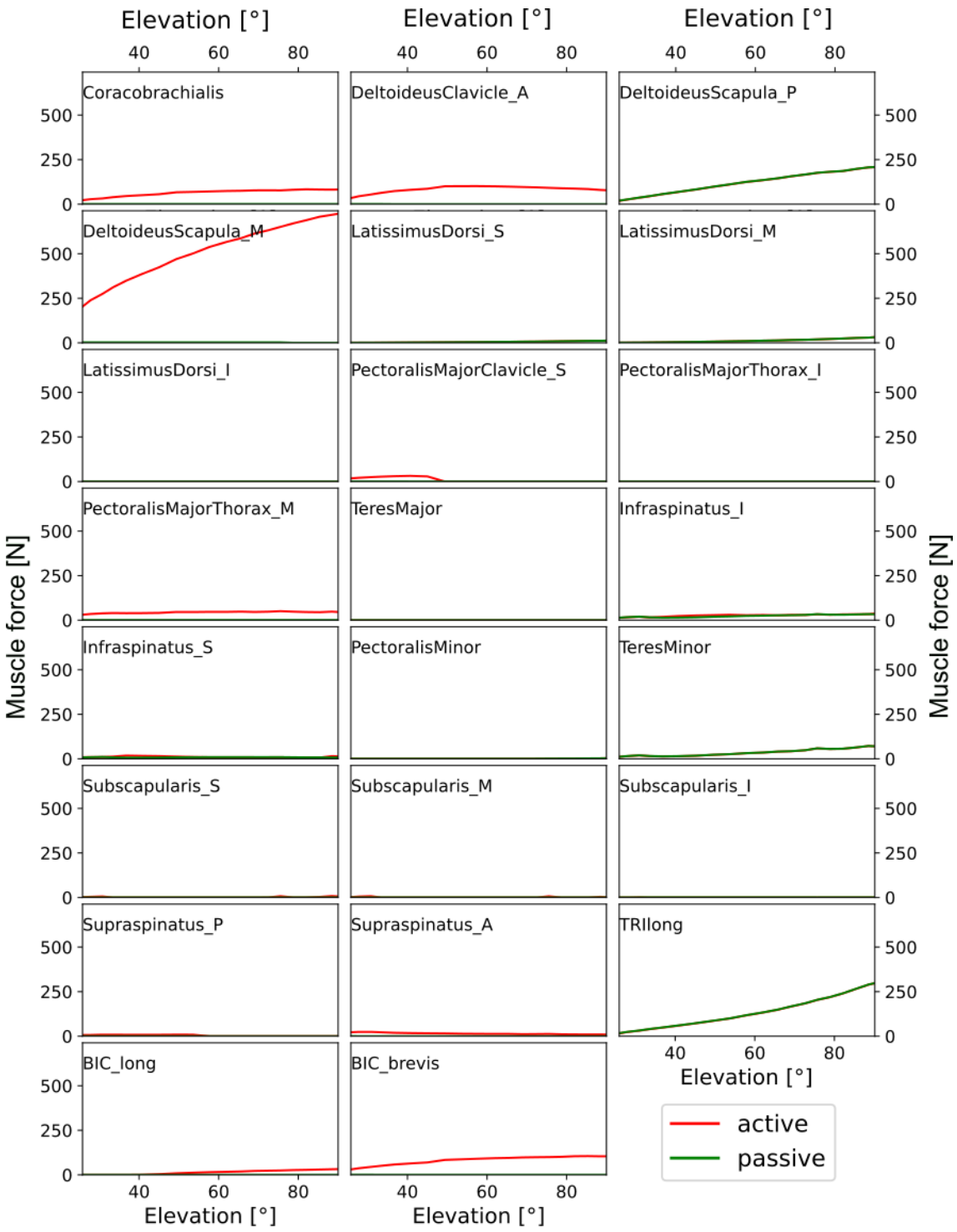

Fig. 86 Muscle forces in each muscle during active and passive forward flexion in anatomical position [X].

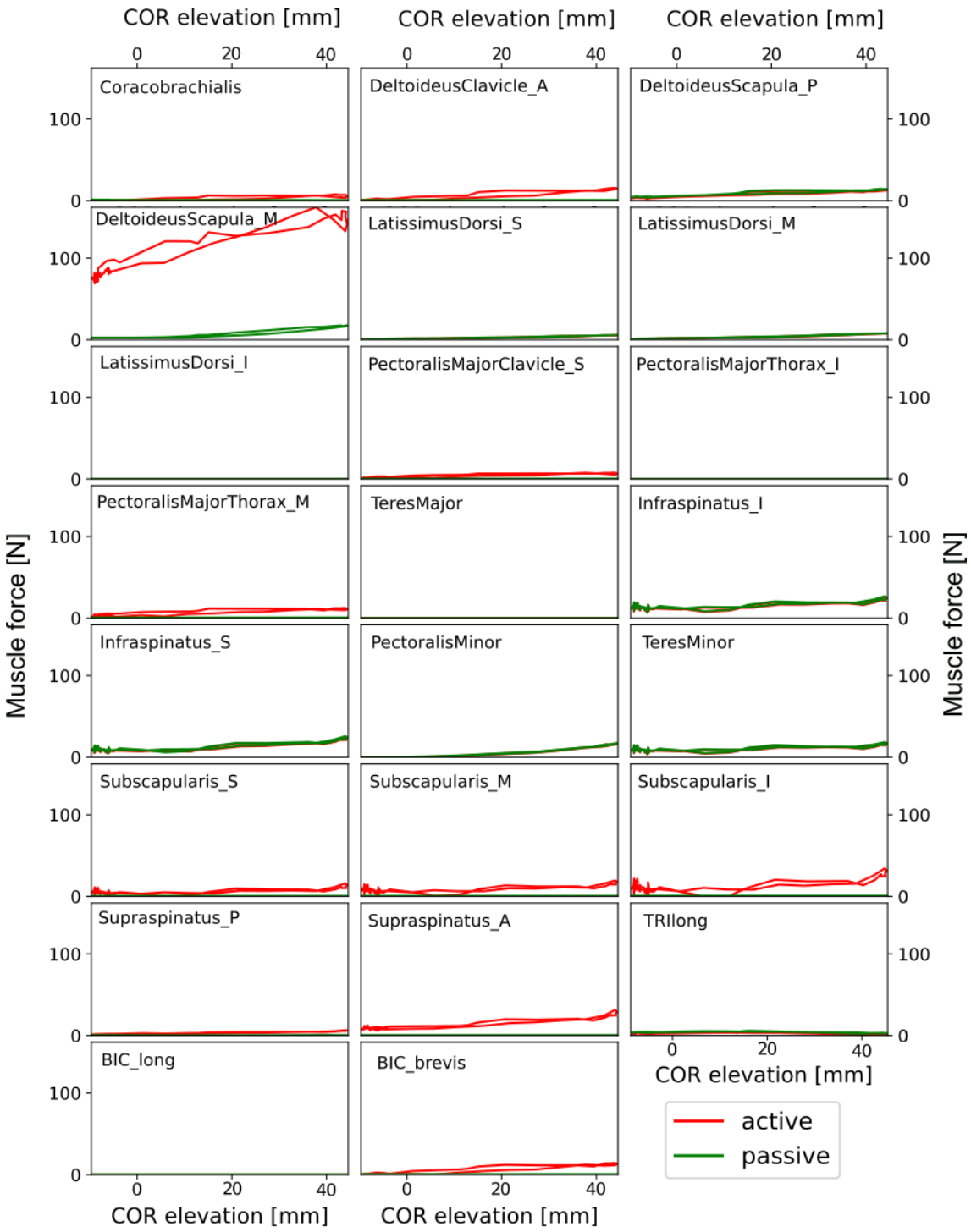

Fig. 87 Muscle forces in each muscle during active and passive shrugging in anatomical position [X].

5.4 Influence of Kinematics on Glenohumeral Joint Load

To evaluate the influence of kinematics on glenohumeral joint load, three distinct motions, each with three trials, were analysed with the glenohumeral joint in its anatomical position and with Thelen, 2003 [104] muscle model employed.

Across all three different motions, kinematics did not exert a significant impact on glenohumeral joint load. In abduction (Fig. 88), all three trials exhibited a similar trend at a very comparable level of load. The same pattern was observed in forward flexion (Fig. 89), where all three trials mirrored each other. In shrugging (Fig. 90), individual movements overlapped in terms of glenohumeral joint load. As was already mentioned in the previous chapter, the highest glenohumeral joint load was observed in forward flexion, reaching up to 1600 N, which is double that observed in abduction. In shrugging, only around 200 N of glenohumeral joint load was observed [IX].

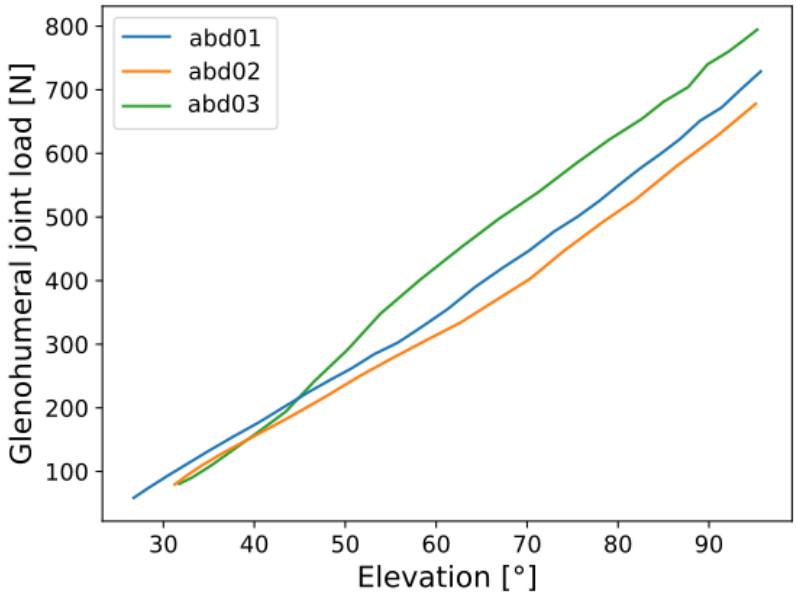

Fig. 88 The effect of independent trials on glenohumeral load in active abduction in anatomical position.

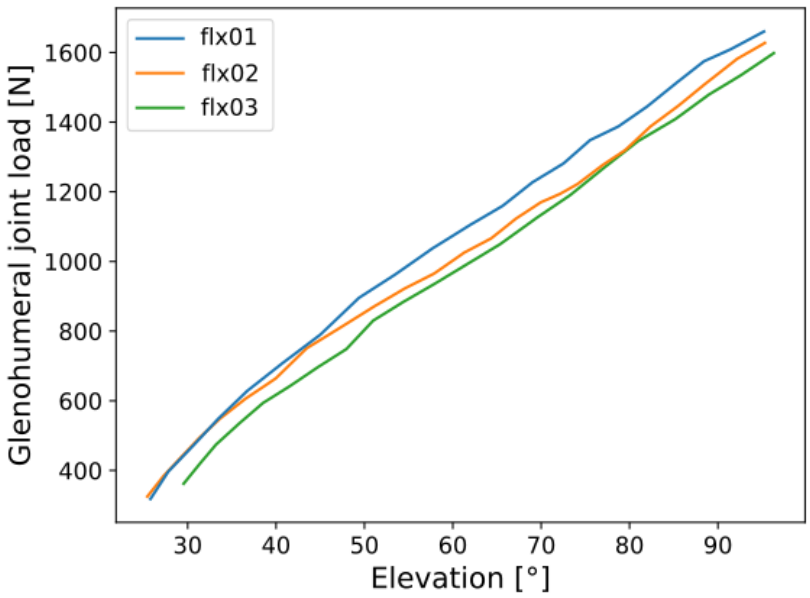

Fig. 89 The effect of independent trials on glenohumeral load in active forward flexion in anatomical position.

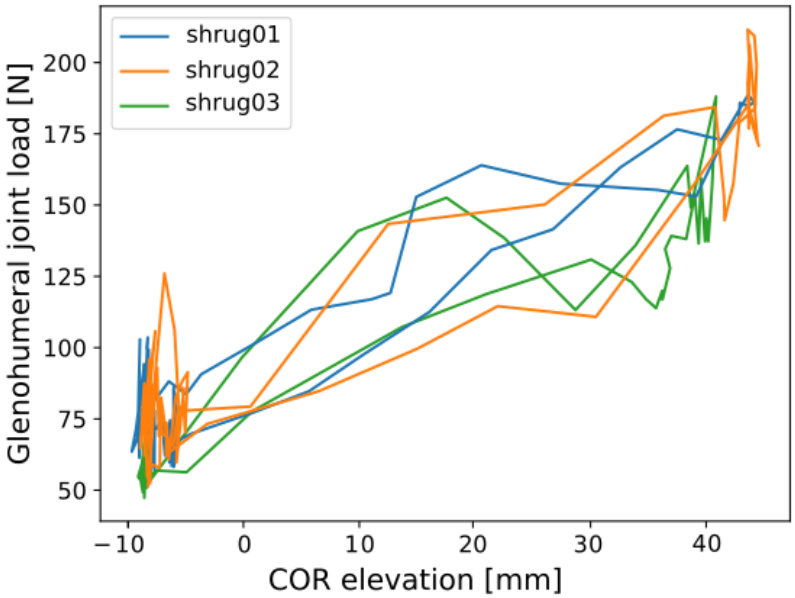

Fig. 90 The effect of independent trials on glenohumeral load in active shrugging in anatomical position.

5.5 Influence of RTSA on Glenohumeral Joint Load

Initially, we examined the impact of excluding three specific muscles in active motion after RTSA, with the glenohumeral joint in its anatomical position. Subscapularis, supraspinatus, and the long head of the biceps brachii are either non-functional for most RTSA indications or are severed during surgery and not

reconstructed into their anatomical position. In active abduction (Fig. 91) and active forward flexion (Fig. 92), the effect was negligible. However, in active shrugging (Fig. 93), there was a notable increase in glenohumeral joint load, nearly approaching that of abduction [IX].

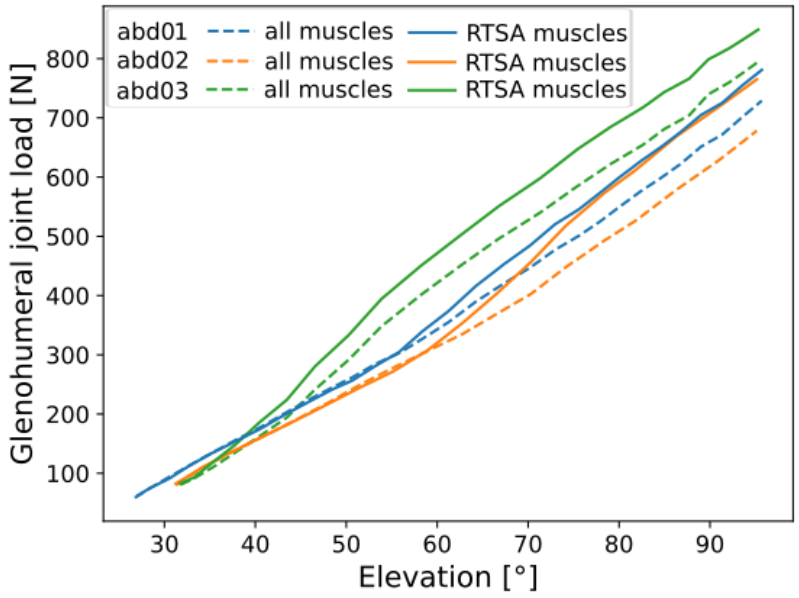

Fig. 91 The effect of modified musculoskeletal model on glenohumeral joint load in active abduction in anatomical position.

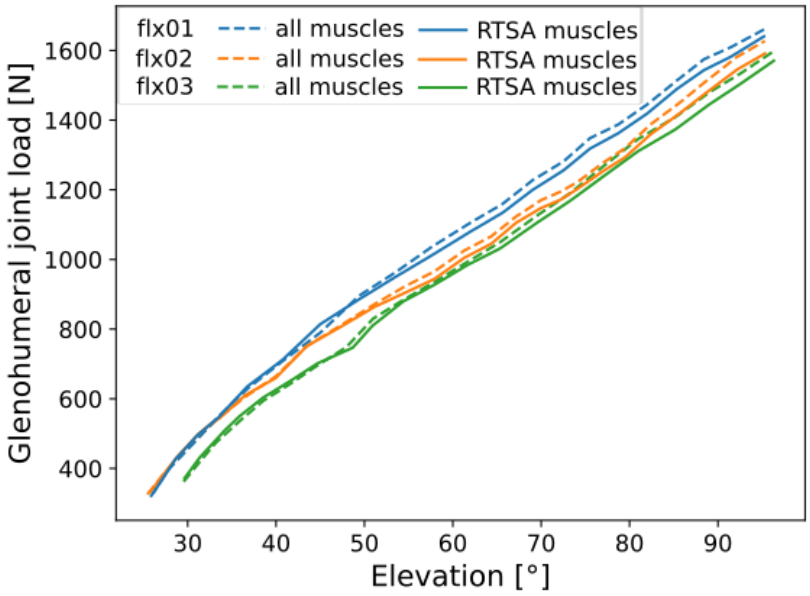

Fig. 92 The effect of modified musculoskeletal model on glenohumeral joint load in forward flexion in anatomical position.

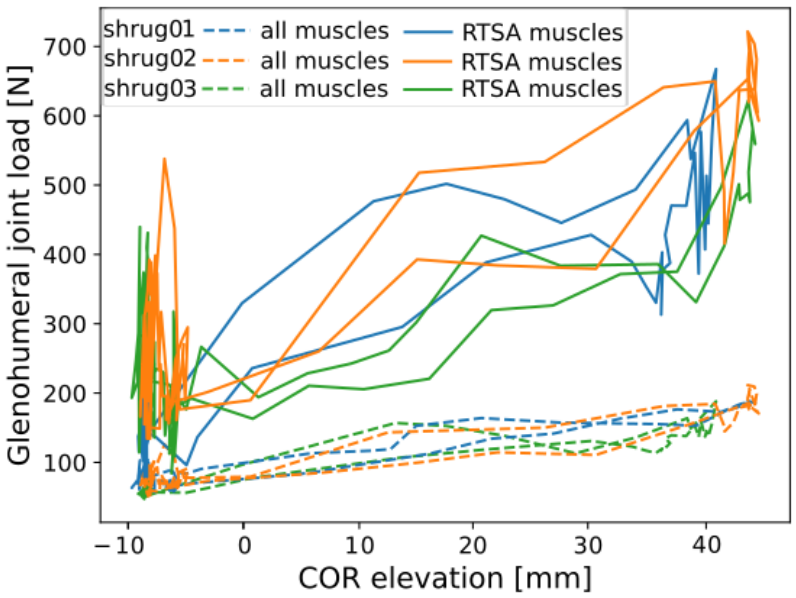

Fig. 93 The effect of modified musculoskeletal model on glenohumeral joint load in shrugging in anatomical position.

Subsequently, we assessed the influence of the actual surgery on glenohumeral joint load. To evaluate post-surgery data, a virtual surgery was performed using the average outcomes of a clinical study we conducted. This involved a medial shift of the COR by 19.9 mm and an inferior shift by 6.2 mm, along with humeral prolongation by 15.2 mm in the longitudinal axis direction and lateral shift by 11.8 mm perpendicular to the longitudinal axis [III]. Additionally, subscapularis, supraspinatus, and the long head of the biceps brachii were excluded. The data before surgery corresponds to the anatomical position of the glenohumeral joint with all muscles engaged.

The glenohumeral joint load slightly decreased in active abduction (Fig. 94) but significantly increased in active forward flexion (Fig. 95). In active shrugging (Fig. 96), there was a substantial increase in glenohumeral joint load, exceeding that of abduction in this case.

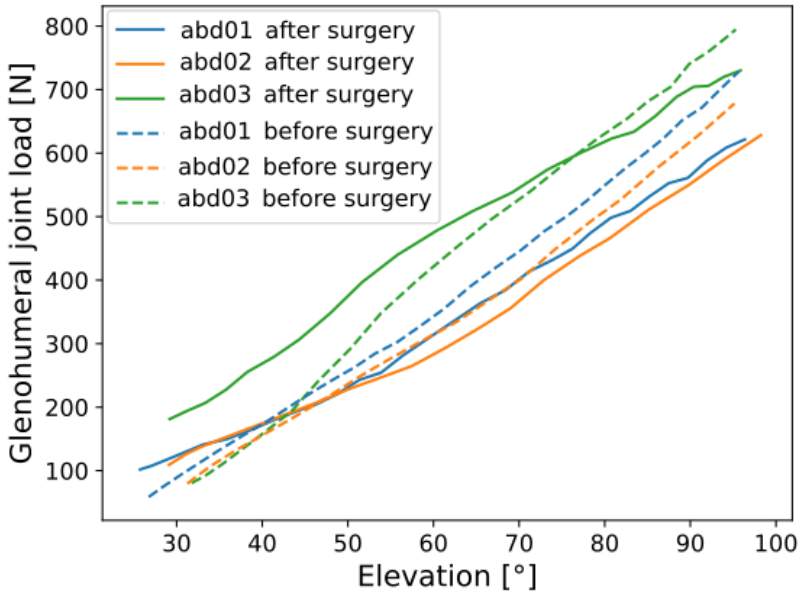

Fig. 94 The effect of RTSA on glenohumeral joint load in active abduction.

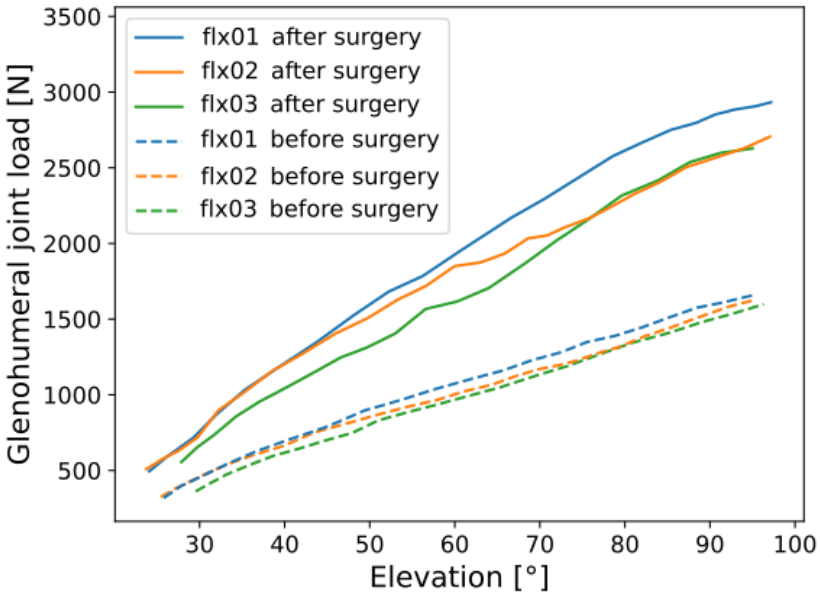

Fig. 95 The effect of RTSA on glenohumeral joint load in active forward flexion.

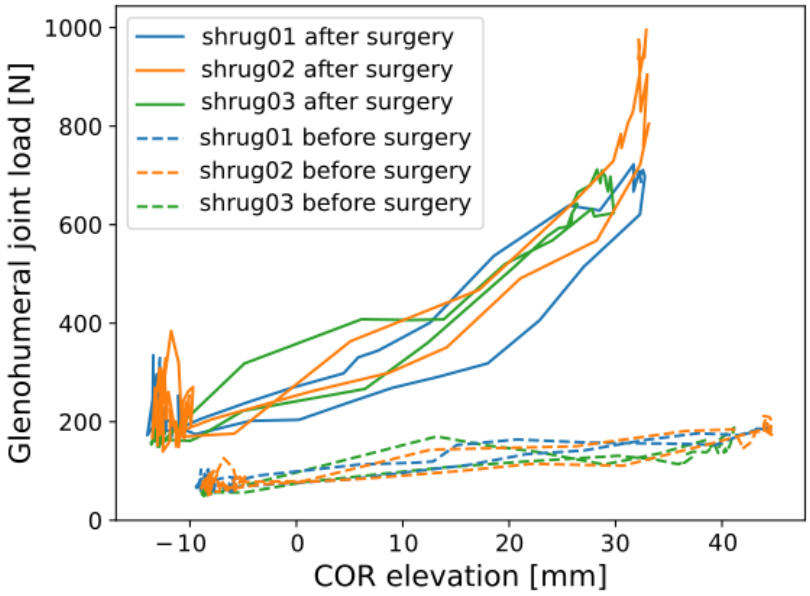

Fig. 96 The effect of RTSA on glenohumeral joint load in active shrugging.

The impact of RTSA was also assessed for each component of the glenohumeral joint reaction force in the sagittal and frontal planes. The R_x components represent the anterior-posterior direction, R_y represents the inferior-superior direction, and R_z represents the medial-lateral direction.

In active abduction (Fig. 97), the results post-surgery indicated that RTSA centers the glenohumeral joint load in the sagittal plane, specifically in the anterior-posterior direction, without a significant increase in the inferior-superior direction. However, the influence of RTSA on glenohumeral joint load in the frontal plane was minimal [IX].

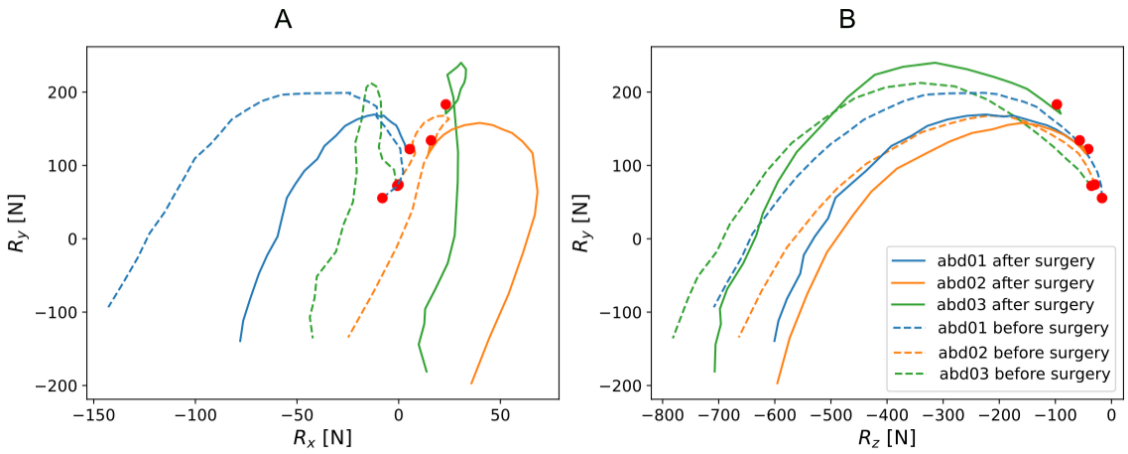

Fig. 97 The effect of RTSA on components of glenohumeral joint load in active abduction. In sagittal plane (A) and in frontal plane (B). Reaction force components R_x represent anterior-posterior direction, R_y represent inferior-superior direction,

and R_z represent medial-lateral direction. Red dot signifies beginning of the motion. The legend provided in the graph for the frontal plane is applicable to both graphs.

A substantial increase in glenohumeral joint load in all directions was observed in active forward flexion (Fig. 98). All components of the glenohumeral reaction force more than doubled, indicating that forward flexion poses a greater risk of glenohumeral joint dislocation than active abduction after RTSA [IX].

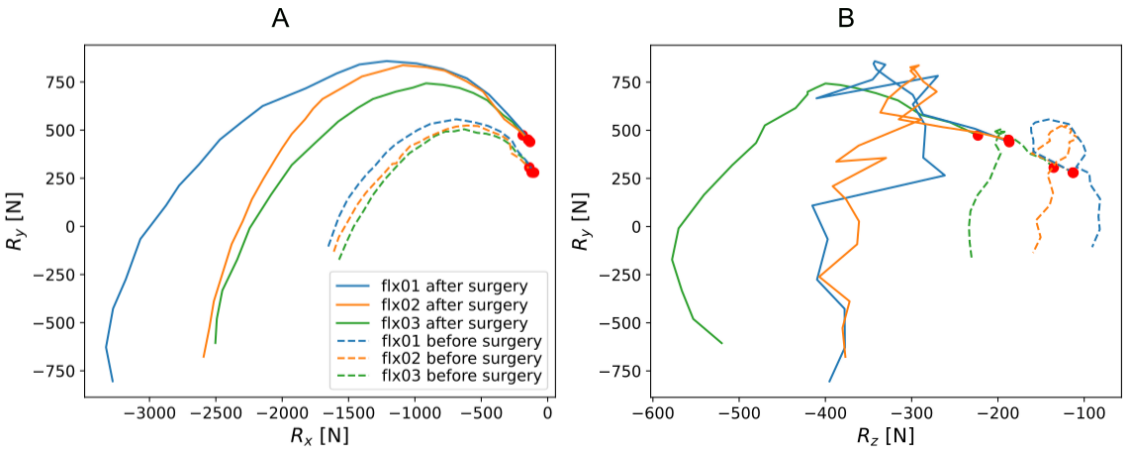

Fig. 98 The effect of RTSA on components of glenohumeral joint load in active forward flexion. In sagittal plane (A) and in frontal plane (B). Reaction force components R_x represent anterior-posterior direction, R_y represent inferior-superior direction, and R_z represent medial-lateral direction. Red dot signifies beginning of the motion. The legend provided in the graph for the sagittal plane is applicable to both graphs.

The most notable increase in the glenohumeral reaction force occurred during active shrugging after RTSA (Fig. 99). Particularly in the frontal plane, where the R_y and R_z components oscillate between 0 and 100 N in the anatomical glenohumeral joint, after RTSA, these values increased to up to 500 N in the medial direction and even up to 800 N in the superior direction. The impact of RTSA in the posterior direction was significantly lower than in the other two directions [IX].

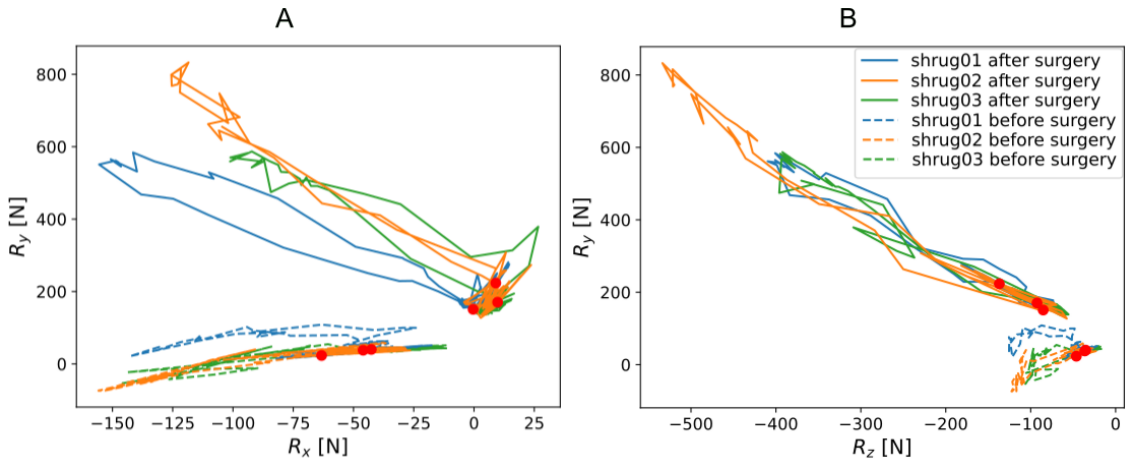

Fig. 99 The effect of RTSA on components of glenohumeral joint load in active shrugging. In sagittal plane (A) and in frontal plane (B). Reaction force components R_x represent anterior-posterior direction, R_y represent inferior-superior direction, and R_z represent medial-lateral direction. Red dot signifies beginning of the motion. The legend provided in the graph for the frontal plane is applicable to both graphs.

The impact of RTSA on muscle force in each muscle during active abduction, considered as a reference motion according to literature, was also assessed (Fig. 100). The most substantial impact of RTSA on muscle forces was observed in the middle deltoid, where the force was approximately halved compared to the anatomical shoulder. Conversely, the surgery had the opposite effect on the coracobrachialis, showing increased muscle force after RTSA, but the absolute difference was significantly lower than the decrease in muscle force observed in the middle deltoid. In the long head of the triceps brachii, it could be observed that RTSA initially prolonged the muscle at the beginning of abduction, but at 90 degrees of abduction, the muscle force mirrored that of the anatomical shoulder. The effect of RTSA on the other muscles was not significant [IX].

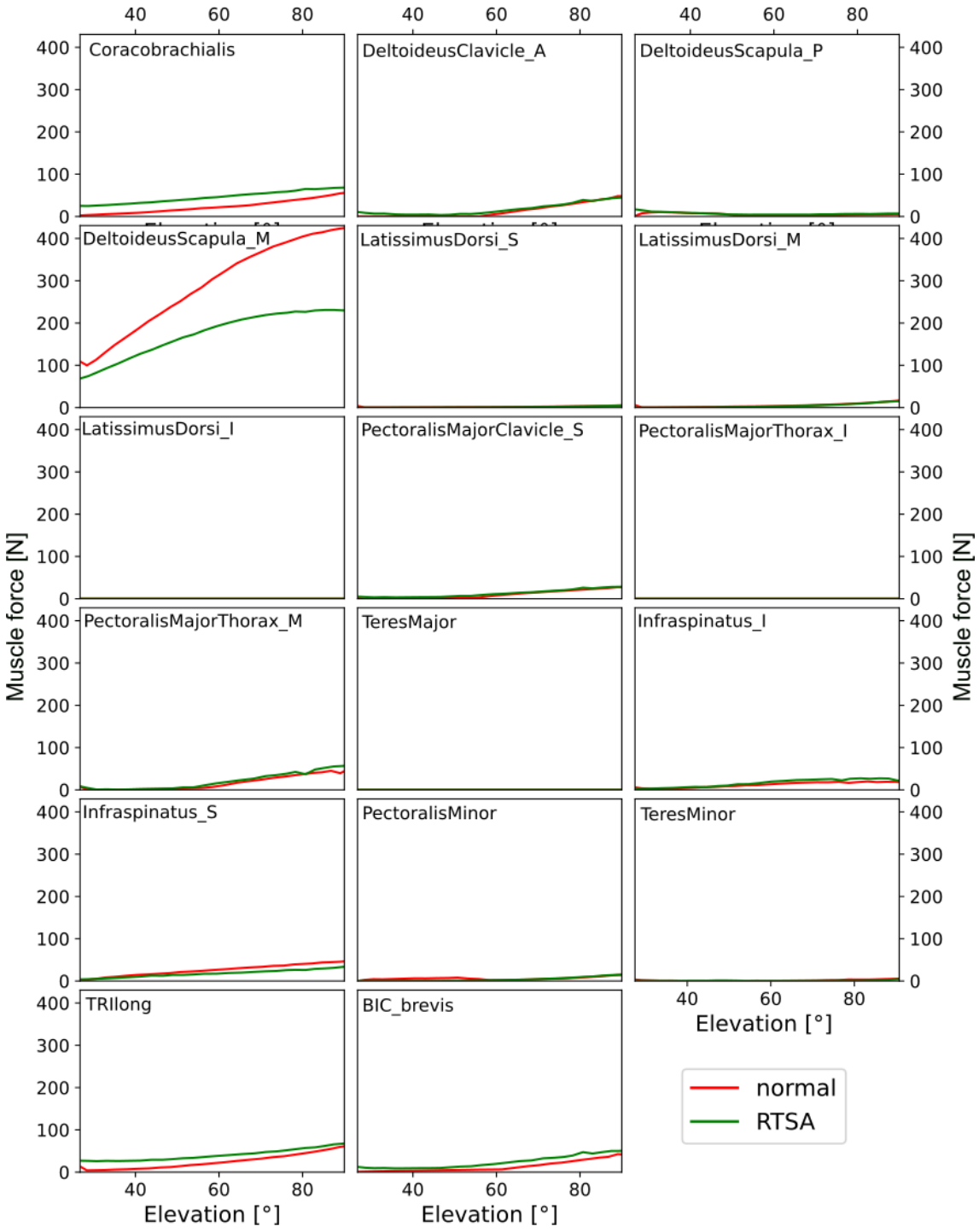

Fig. 100 Effect of RTSA on muscle force in each muscle during active abduction [IX].

5.6 Influence of RTSA Humerus Prolongation on Glenohumeral Joint Load

The effect of change of position of humerus after RTSA was assessed according to its prolongation and lateralization on glenohumeral joint load. The results were calculated with COR of glenohumeral joint in shifted position as was evaluated from our clinical study of RTSA patients, indicating a medial shift of 19.9 mm and an inferior shift of 6.2 mm [I, V]. Both active and passive motions were assessed at 30°, 60°, and 90° for abduction and forward flexion. A safe zone for humerus prolongation during RTSA was determined to prevent overloading the glenohumeral joint during these motions. The negative value in the meaning of x-axis stands for medialization and positive for lateralization in Figs 102–107. In the meaning in y-axis, the negative values mean shortening of humerus and positive stand for prolongation.

In 30 degrees of abduction (Fig. 101) the highest glenohumeral joint loads could be observed compared to 60 and 90 degrees of abduction. Based on the glenohumeral joint load in anatomical shoulder during abduction (around 800 N), counting this value as a margin of safe zone, a prolongation of around 25 mm with lateral or medial shift around 20 mm is possible. Lateralization was observed as more favourable than medialisation [III].

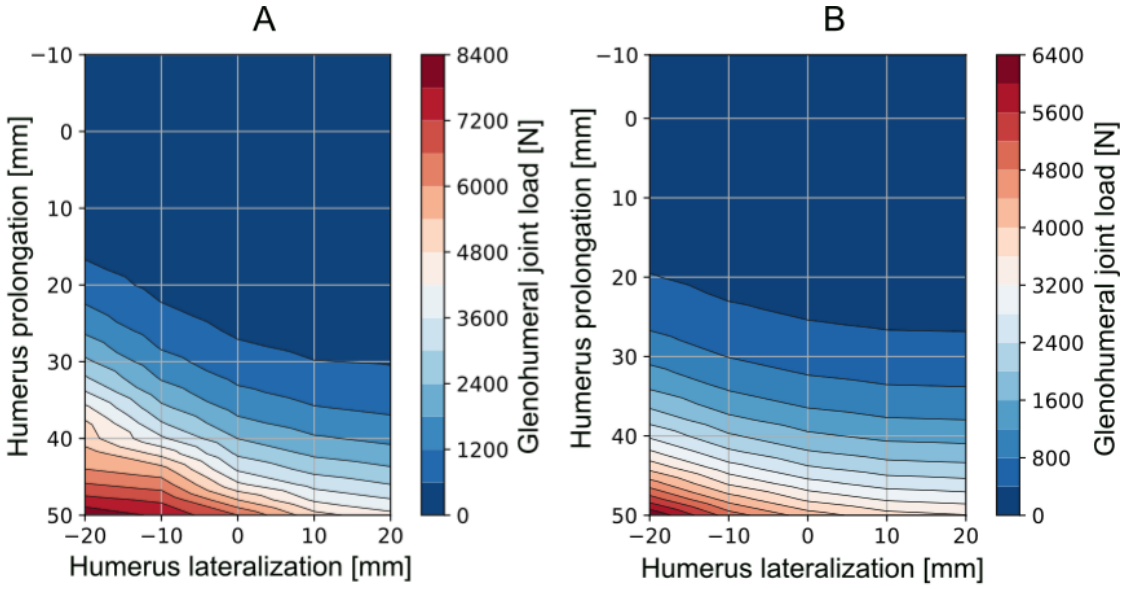

Fig. 101 Determination of the safe zone based on humerus prolongation and lateralization in RTSA. Shown in 30 degrees of active abduction (A) and passive abduction (B) [III].

In 60 degrees of abduction (Fig. 102), the estimated safe zone was nearly 35 mm for humerus prolongation, with minimal impact from lateralization or medialization within the evaluated range of -20–20 mm [III].

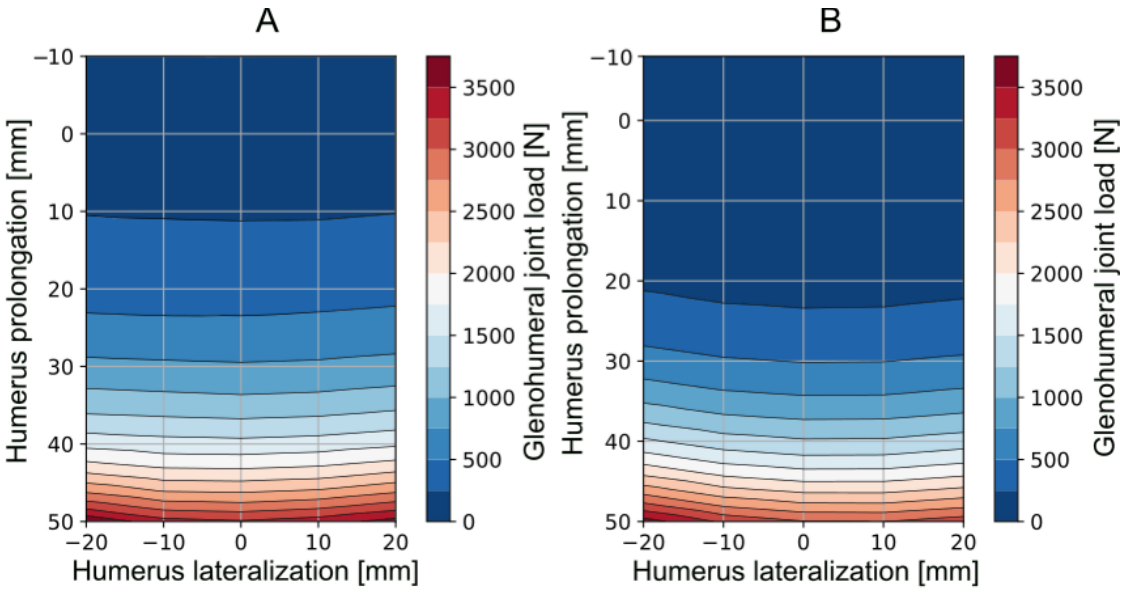

Fig. 102 Determination of the safe zone based on humerus prolongation and lateralization in RTSA. Shown in 60 degrees of active abduction (A) and passive abduction (B) [III].

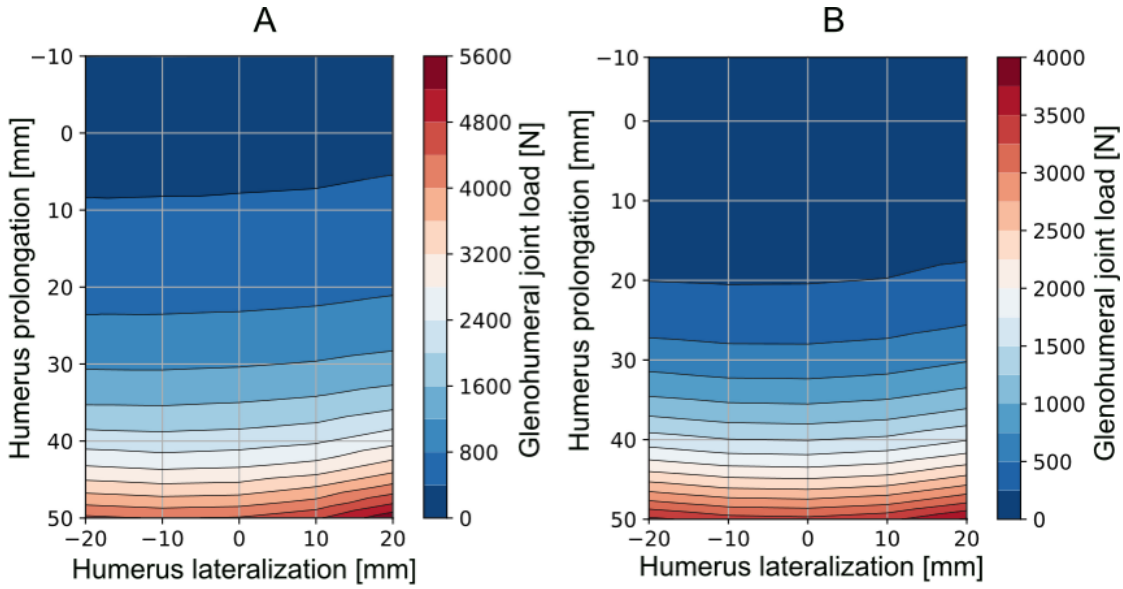

Fig. 103 Determination of the safe zone based on humerus prolongation and lateralization in RTSA. Shown in 90 degrees of active abduction (A) and passive abduction (B) [III].

In 90 degrees of abduction (Fig. 103) the observed safe zone for humerus prolongation was similar to that at 30 degrees (around 25 mm). In the sagittal plane, the shift showed opposite behaviour compared to 30 degrees, with medialization being slightly more favourable than lateralization [III].

The glenohumeral joint load during forward flexion is significantly higher compared to abduction. Unlike abduction, the glenohumeral joint load increases with the angle of forward flexion. At 30 degrees of forward flexion (Fig. 104), the glenohumeral joint load remains comparable to the anatomical state until 30 mm of humerus prolongation. The shift in frontal plane decreases the load in glenohumeral joint.

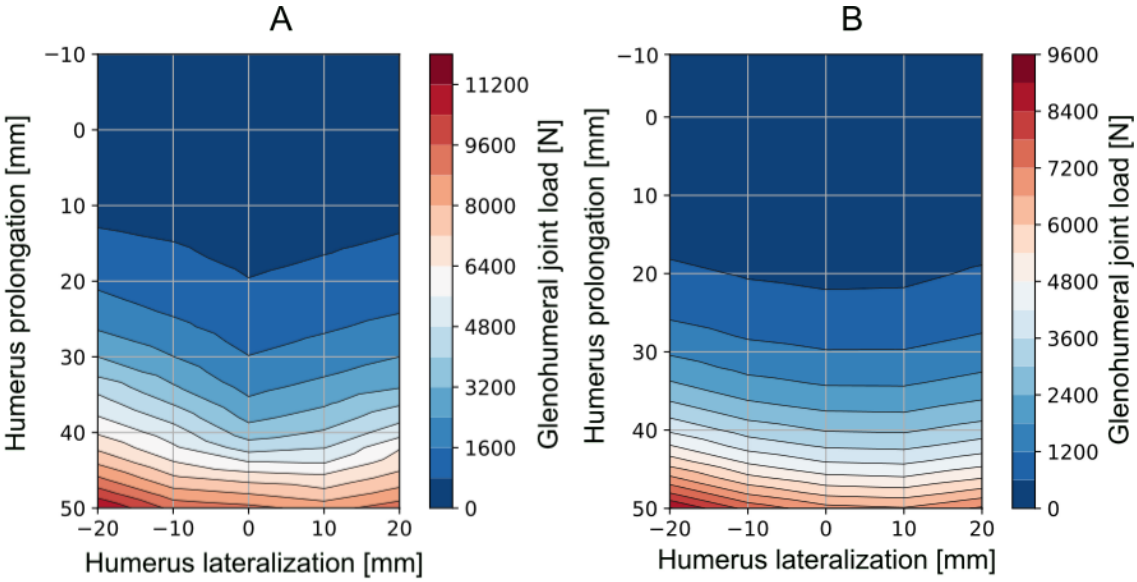

Fig. 104 Determination of the safe zone based on humerus prolongation and lateralization in RTSA. Shown in 30 degrees of active forward flexion (A) and passive forward flexion (B).

A significant increase in glenohumeral joint load is observed at 60 degrees of forward flexion (Fig. 105) compared to 30 degrees. The safe zone shrinks to 10 mm of humeral prolongation, with a small effect of lateralization, which is more favourable than medialization in this context.

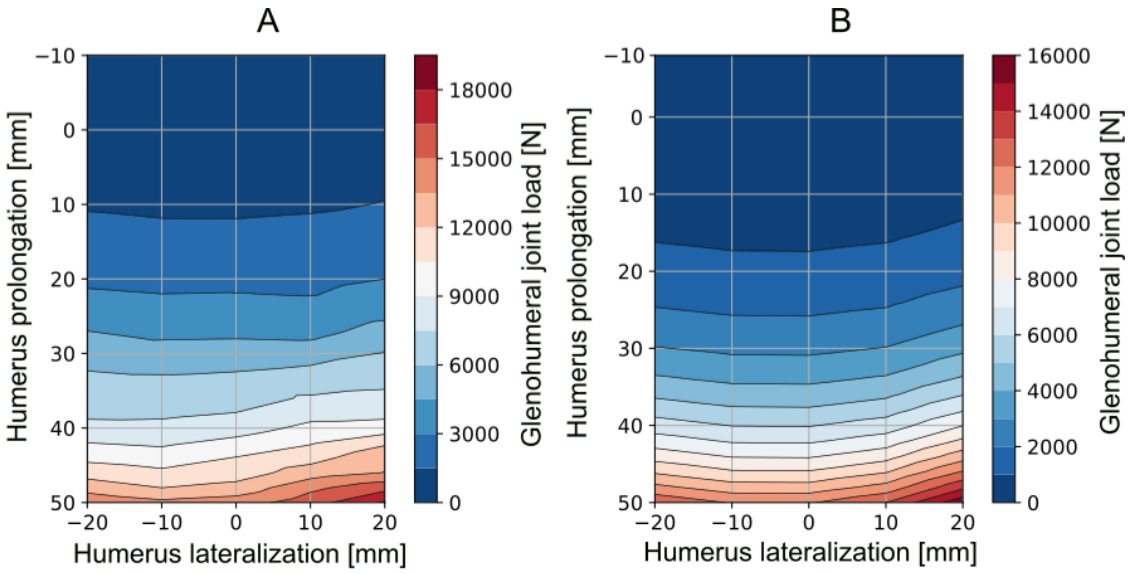

Fig. 105 Determination of the safe zone based on humerus prolongation and lateralization in RTSA. Shown in 60 degrees of active forward flexion (A) and passive forward flexion (B).

In 90 degrees of forward flexion (Fig. 106), the values of glenohumeral joint load indicate signs of overloading across the evaluated range, with values approaching 2000 N in 10 mm of humerus prolongation during active motion.

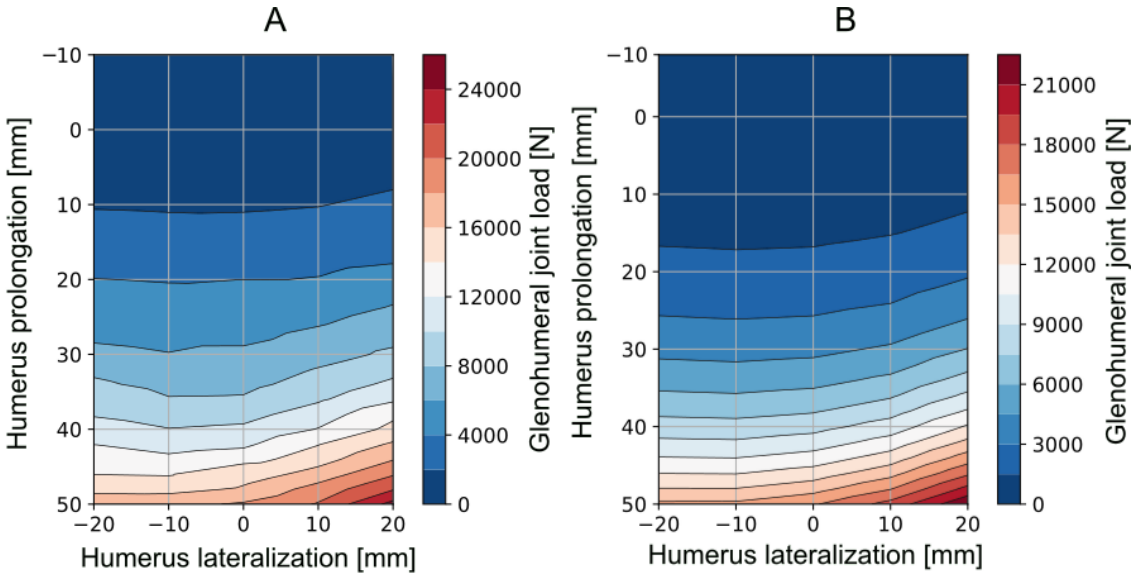

Fig. 106 Determination of the safe zone based on humerus prolongation and lateralization in RTSA. Shown in 90 degrees of active forward flexion (A) and passive forward flexion (B).

The impact of humerus prolongation on each muscle force is illustrated in Fig. 107. Humerus prolongation resulted in the pre-stressing of shoulder muscles, generating a load that participates on stabilizing the joint. The muscles most

affected include the deltoid, particularly its middle part, coracobrachialis, pectoralis major, long head of triceps brachii, and short head of biceps brachii.

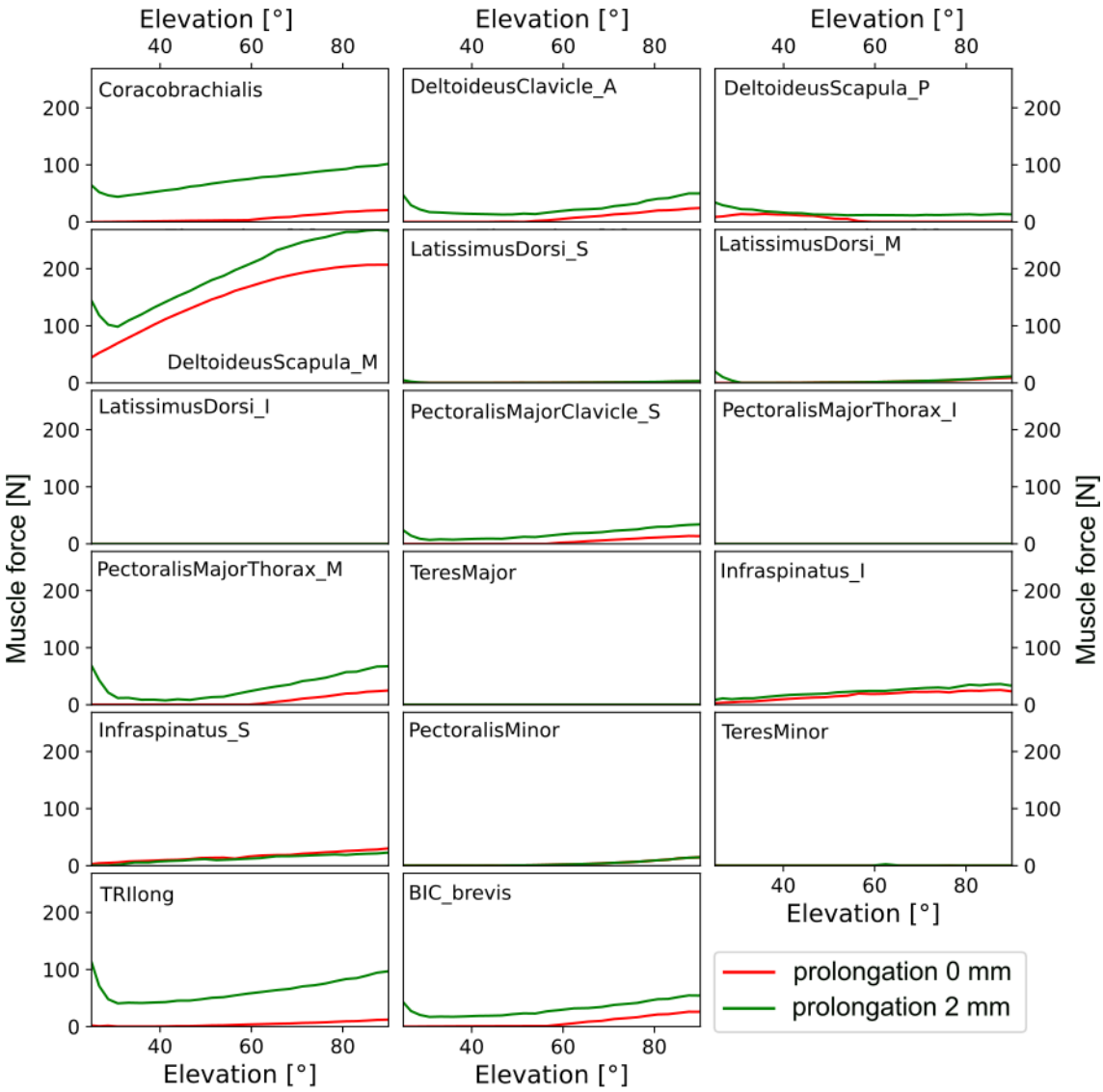

Fig. 107 Muscle forces in each muscle during active abduction, with 0 and 2 mm of humerus prolongation [III].

6 Discussion

To improve the outcomes of the RTSA, an in-depth knowledge of its biomechanics is necessary. For this purpose, the aim of this thesis was to evaluate the effect of changes in glenohumeral geometry in RTSA based on the clinically available data. The special focus was on humeral prolongation, which is neglected by most of the recent studies, but it is crucial in the terms of RTSA outcome.

One of the objectives was to assess the radiographic magnification of the glenohumeral region on plain X-rays to enhance the accuracy of the results derived from them. The commonly assumed standard magnification for shoulder radiographs is 5% [61]. However, our study revealed that this value is underestimated, and the radiographic magnification of the glenohumeral region can reach as high as 20% in certain patients [I, V]. In the majority of patients, the radiographic magnification exceeded 10% and exhibited substantial variation among individuals (Fig. 71) [I, V].

Previous studies have established a correlation between radiographic magnification in preoperative planning for hip arthroplasty and patient factors such as sex, age, weight, or body mass index [114; 115]. In our study, the only statistically significant factor was patient weight, as higher weight correlated with larger radiographic magnification (Fig. 72). The slightly higher magnification observed in male patients (Fig. 71) can be attributed to the observation of higher weight in males compared to females (Fig. 72). However, due to the significant inter-individual differences, this correlation (Fig. 72) is not applicable for clinically practical correction [I].

A limitation of this study is its reliance primarily on data obtained from a single clinical workplace and a single X-ray machine. The estimated magnification value may depend on the specific radiographic setup at the authors' workplace. Hornova et al., 2017 [116] demonstrated considerable variations in radiographic magnification between different clinical workplaces. It should also be noted that the radiographic device used in this study performed an intrinsic magnification correction of 5.2% according to DICOM image headers, where the imager pixel spacing of 0.143 mm appeared as a radiographic image with a pixel spacing of 0.136 mm.

3D planning techniques using CT imaging have been proposed to enhance precision in preoperative planning [117; 118]. However, recent investigations have indicated minor discrepancies between 3D planning and traditional 2D methods [119]. Additionally, careful consideration must be given to the potential risks associated with increased radiation exposure, as higher effective doses during CT shoulder examinations may increase the risk of developing cancer [120]. Nevertheless, one advantage of CT scans is the absence of a need for external calibration markers. Moreover, CT scans are typically readily available, and the radiation dosage from modern CT machines continues to decrease.

Plain radiographs serve as the initial assessment method for evaluating the glenohumeral joint [121]. It has been shown that the use of external markers can enhance the accuracy of preoperative templating. A spherical external calibration marker should be positioned at the anticipated joint height above the detector [122]. Therefore, we recommend employing an external calibration marker placed in the frontal plane crossing the acromion process when utilizing plain radiographs for shoulder arthroplasty templating. In cases where a calibration marker is not accessible, our findings suggest that relying on a fixed 5% magnification could introduce a systematic bias in preoperative planning.

Another objective was to assess the alterations in musculoskeletal geometry of the glenohumeral region after RTSA [VI, VIII]. We divided the task into two parts: evaluating the change in the COR and assessing the subsequent prolongation of the humerus. To ensure objectivity of the results, we included patients with various indications operated on by different surgeons.

While our approach for evaluating the change in the COR is simpler compared to other publications on the same topic, we obtained consistent results, particularly regarding the medialization of the COR. Our clinical study showed shift of COR of 19.9 ± 7.9 mm medially and 6.2 ± 7.4 mm inferiorly with 31 patients (32 shoulders) involved in the study [IV].

Rettig et al., 2013 [123] used an optical system for evaluating the COR displacement during postoperative examinations of RTSA patients. This caused a significant deviation from other studies as they evaluated the medialization of COR as 8.3 ± 4.3 mm, and they were unable to determine the inferior shift.

In contrast, studies like ours evaluated the displacement using X-ray images, showing good agreement, especially in terms of evaluating medialization. Chay-You et al., 2014 [124] used preoperative and postoperative X-rays for evaluation of COR shift. They measured distance from the most lateral point of acromion to the center of circle which they fitted to humeral head on the preoperative X-ray image and to the glenosphere on the postoperative X-ray image. The reported mean medialization was 20.2 mm which is in excellent agreement with our results of medialization [124] did not observed a significant change in inferior shift. This method is permissible only for replacements where the glenosphere is made of metal, which would be inapplicable in our study, where the glenosphere in made of radiolucent polyethylene.

Other studies also used X-rays to evaluate the shift of COR after RTSA. Boileau et al., 2005 [11] reported medialization of 19 ± 9.9 mm and inferior shift of 3.7 ± 9.2 mm with study involved 45 patients. Their results are in the best overall agreement with our study despite that they evaluated patients with Delta III prothesis (DePuy International Limited, Leeds, England) and our study involved patients with SMR Reverse Shoulder System (Lima Corporate, San Daniele del Friuli, Italy).

Saltzman et al., 2010 [125] involved 63 patients (68 shoulders) in their radiographical study. They reported slightly higher medialization (27 ± 4 mm) compared to our study. Reported inferior shift was 12 ± 3 mm. Ackland et al., 2019 [126] used 8 cadaveric upper extremities from six males and two females with mean age of 68 years to which they implanted reverse shoulder replacement. They reported medial shift of COR by 25.8 ± 6.3 mm and inferior shift by 16.4 ± 3.9 mm.

Inferior displacement, evaluated by Saltzman et al., 2010 [125] and Ackland et al., 2019 [126] did not align well with our study. This discrepancy is mainly because we assessed the shift concerning the preoperative condition rather than the anatomical position of the shoulder [VI, VIII]. Boileau et al., 2005 [11] utilized the preoperative state as a reference, mirroring our approach, aligning well with our findings. Different indications for RTSA are associated with varying pathological conditions of the shoulder and the preoperative displacement of the humeral head [127]. Consequently, our evaluation of the shift of the COR in the sagittal plane exhibits considerable variance superiorly and inferiorly, rather than in frontal plane, where the position of humeral head is rarely shifted medially or laterally before the surgery.

Potential limitation of our method for assessment of the alterations in COR after RTSA is the fact that, during X-rays, the glenohumeral joint is not always directly under the X-ray source, causing distortion in the dimensions of individual components.

Limited literature sources are available for assessing humeral displacement or arm extension after RTSA. Boileau et al., 2005 [11] employed a specialized device to measure the distance between the acromion and the olecranon in 45 patients, comparing these distances in the operated and opposite arm of the patients. They reported arm lengthening of 15 ± 11 mm, ranging from -5 to 40 mm. Lädermann et al., 2009 [71] and Lädermann et al., 2012 [72] conducted radiographical study to evaluate arm lengthening. Lädermann et al., 2009 [71] reported arm lengthening of 23 ± 12 mm, ranging from 1 to 47 mm involved 45 patients (47 shoulders). Lädermann et al., 2012 [72] reported arm lengthening of 16 ± 19 mm, ranging from -51 to 54 mm. Arm lengthening correlates with our inferior part of total change in musculoskeletal geometry which we got 17.2 ± 9.8 mm, ranging from 6.4 to 37.9 mm in 31 patients (32 shoulders) [III] showing a good agreement with previously reported results.

To precisely quantify humeral prolongation, we employed a distinctive method that initially assessed the shift of the COR. Subsequently, we determined the humeral shift from this adjusted COR (Fig. 49), believing it best simulated the actual alterations following RTSA. Evaluating only the COR shift omits shoulder prestressing, and considering only arm lengthening without accounting for COR shift fails to align with the authentic state of RTSA [III, VIII].

Our study reports a humeral prolongation of 15.2 ± 6.2 mm along the longitudinal axis of the humerus, ranging from 1.8 to 30.6 mm, accompanied by a lateral shift (perpendicular to the humerus's longitudinal axis) of 11.8 ± 4.5 mm, ranging from 1.3 to 17.9 mm [III]. According to our knowledge, these values are unprecedented in existing literature, as our study is the first to undertake such an evaluation.

A potential limitation of our method lies in using the humerus model to simulate the reverse replacement, introducing the possibility of errors in wrapping surfaces that may differ when the reverse replacement is actually implanted. This discrepancy could lead to variations in muscle moment arms. However, we contend

that these potential deviations are likely lower than the errors associated with using a generic model instead of a patient-specific model [II].

The choice of muscle model can significantly impact the outcomes of glenohumeral joint load, particularly evident in abduction (Fig. 82) [XI]. This influence stems not only from the formulation of the Hill-type muscle model but also from the muscle constants, which profoundly shape the muscle's characteristics. In their work, Haeufle et al., 2014 [102] utilized these constants derived from a cat's soleus muscle. Consequently, these constants influenced the stiffness of both parallel and serial elastic elements, rendering them stiffer compared to other muscle models. This adjustment resulted in significantly higher passive forces.

Romero et al., 2016 [128] explored comparable muscle models to ours and observed only minor distinctions among their findings. This disparity is likely due to differences in the focus of investigation between the two studies. Specifically, their investigation focused solely on one muscle, the biceps femoris, during flexion, where passive forces have a negligible impact. In contrast, our study delved into the examination of 23 muscles or their segments across three distinct motions in shoulder, all of which are significantly influenced by passive forces [XI].

The assessment of various muscle models on glenohumeral joint load revealed that all models (Haeufle et al., 2014 [102], Geyer et al., 2010 [107], McLean et al., 2003 [106], and Thelen, 2003 [104]) did not exhibit qualitative differences but rather quantitative distinctions [XI]. Bergmann et al., 2007 [85] in in vivo experiments, observed glenohumeral joint loads at 90 degrees of abduction ranging between 500 and 900 N based on patient weight. This range is comparable to the 800 N estimated using the Thelen, 2003 [104] muscle model. Conversely, McLean et al., 2003 [106] muscle model showed glenohumeral joint load of nearly 2 000 N in 90 degrees of abduction, Geyer et al., 2010 [107] muscle model showed over 2 000 N, and Haeufle et al., 2014 [102] even showed values up to 6 000 N [XI].

Considering these findings, we opted to utilize the Thelen, 2003 [104] muscle model for further investigation. This choice was influenced by its prevalence among the compared models (412 citations according to Web of Science) and, importantly, its close alignment with in vivo experimental values for glenohumeral joint load. Also, Also, Romero et al., 2016 [128], similarly emphasized the capability of Thelen's

muscle model to effectively control physiological parameters for simulations conducted in a reasonable timeframe.

We noted that the glenohumeral joint load values were highest in forward flexion, although abduction is the commonly employed reference movement in studies. However, Bergmann et al., 2011 [87] reported glenohumeral joint loads in forward flexion comparable to those in abduction. Our findings may stem from the musculoskeletal model settings, specifically configured for abduction, aligning the results with in vivo experiments. For instance, the muscle moment arms and wrapping points were calibrated to measured values derived from cadaver experiments conducted in abduction [98].

The assessment of the influence of modifying the musculoskeletal model by excluding three specific muscles (supraspinatus, subscapularis, and long head of biceps brachii) revealed only a limited impact on glenohumeral joint load. A slight increase in glenohumeral load was observed during abduction (Fig. 91). Conversely, in forward flexion (Fig. 92), the impact was reversed but still negligible, as the glenohumeral joint load slightly decreased. The excluded muscles exhibited a relatively higher impact during shrugging (Fig. 93); however, it's worth noting that the glenohumeral joint load during shrugging is considerably lower than in abduction and forward flexion. This observation supports a clinical finding that alterations to these muscles in RTSA do not significantly affect the joint's ability to perform motion [III].

In active abduction (Fig. 97), the post-surgery results indicated that RTSA centers the glenohumeral load in the sagittal plane, specifically in the anterior-posterior direction, without a significant increase in load in the inferior-superior direction. This positive effect of RTSA contributes to stabilizing the replaced joint [VII]. Through the assessment of muscle forces post-RTSA, we validated that the muscle force in the middle deltoid is reduced during active abduction, aligning with previous reports by Walker et al., 2011 [129] and others.

Based on the evaluated data on the influence of humerus prolongation on glenohumeral joint load, we identified a safe zone for changes in humerus shift during surgery to prevent overloading the glenohumeral joint. During active abduction, we observed a safe zone of approximately 25 mm of humerus prolongation, maintaining glenohumeral joint load within comparable values to the anatomical state, specifically up to 1,000 N. In terms of lateralization and

medialization, medialization appears more favorable in the early stage of abduction. However, as abduction reaches 90 degrees, the trend reverses, and lateralization becomes more favorable [IX].

The model for assessment of glenohumeral joint load presented in this thesis relies on a previously published musculoskeletal model derived from cadaveric measurements of a single patient. The variability in muscle attachment points, coupled with the unknown specific characteristics of muscles, such as maximum isometric force, muscle fiber pennation angle, or tendon characteristics, can introduce additional sources of variation in estimating muscle forces [130; 131] and glenohumeral joint load. Consequently, the results presented in this thesis should be regarded as qualitative findings with potential variations when extrapolated to a specific patient.

The current modelling approach provides a framework for assessing the impact of various pathological conditions and their corresponding surgical treatments on joint biomechanics. In future analyses, it would be beneficial to estimate the effects of patient-specific changes in the glenoid and its shape on glenohumeral joint load [132], as well as to evaluate the impact of muscle strengthening on joint stability. Additionally, refining the model to precisely describe flexion by incorporating muscle units responsible for sagittal plane flexion could enhance its accuracy. The proposed biomechanical analysis could also be integrated in the future with patient-specific estimations of muscle parameters, employing bone morphing methods [133] or the application of artificial intelligence [134].

7 Conclusions

The shoulder joint, responsible for numerous activities in daily living, stands out as the most mobile joint within the human body. Utilizing a biomechanical approach can provide insights into the roles of individual anatomical structures in a healthy shoulder and offer suitable treatment options for pathological conditions. In this thesis, our focus lies on the clinical analysis of reverse total shoulder arthroplasty.

The accuracy of biomechanical model depends on the accuracy of the input data [II]. As most of the data is obtained from plain radiographs, we have studied the range of radiographic magnification and its variability among patients. In a clinical study of 94 patients, the real magnification measured from plain radiographs taking joint replacement as a marker, was approximately 12% (ranging from 5% to 20%) [I, V]. This value considerably differs from value of 5% proposed by replacement producer and implemented in the surgery planning software [I, V].

The knowledge of actual magnification played a crucial role in a subsequent study of humerus prolongation, employing a novel algorithm that integrates data from plain radiographs and CT scans. [VI, VIII]. This approach not only reduced radiological exposure of a patient in a prospective study but also enabled the utilization of archived data in a retrospective study involving 32 shoulders. Our findings revealed an average humerus prolongation of 15.2 mm (ranging from 1.8 mm to 30.6 mm), a dimension not previously reported [III].

The effect of humerus prolongation was studied in a comprehensive shoulder model [X, XI]. Exploring the impact of humerus prolongation, we employed a comprehensive shoulder model. Our research demonstrated that RTSA contributes to lower muscle force in the middle deltoid, a primary abductor, and glenohumeral joint load. [IV, VII]. However, extensive humerus prolongation (greater than 3 cm) could increase glenohumeral joint load more than three times [III, IX]. Consequently, we defined a safe zone for humerus prolongation in RTSA that should be considered during surgical procedures. [III].

8 References

[1] BRUIJN, S. M.; MEIJER, O. G.; BEEK, P. J. and VAN DIEËN, J. H. The effects of arm swing on human gait stability. online. *Journal of Experimental Biology*. 2010, ed. 213, iss. 23, p. 3945-3952. ISSN 1477-9145. Available from: https://doi.org/10.1242/jeb.045112.

[2] EATHER, N.; WADE, L.; PANKOWIAK, A. and EIME, R. The impact of sports participation on mental health and social outcomes in adults: a systematic review and the 'Mental Health through Sport' conceptual model. online. *Systematic Reviews*. 2023, ed. 12, iss. 1. ISSN 2046-4053. Available from: https://doi.org/10.1186/s13643-023-02264-8.

[3] SHEEAN, A. J; DE BEER, J. F; DI GIACOMO, G.; ITOI, E. and BURKHART, S. S. Shoulder instability: State of the Art. online. *Journal of ISAKOS*. 2016, ed. 1, iss. 6, p. 347-357. ISSN 20597754. Available from: https://doi.org/10.1136/jisakos-2016-000070.

[4] BURNER, T.; ABBOTT, D.; HUBER, K.; STOUT, M.; FLEMING, R. et al. Shoulder Symptoms and Function in Geriatric Patients. online. *Journal of Geriatric Physical Therapy*. 2014, ed. 37, iss. 4, p. 154-158. ISSN 1539-8412. Available from: https://doi.org/10.1519/JPT.0b013e3182abe7d6.

[5] CRIMMINS, E. M. Lifespan and Healthspan: Past, Present, and Promise. online. *The Gerontologist*. 2015, ed. 55, iss. 6, p. 901-911. ISSN 0016-9013. Available from: https://doi.org/10.1093/geront/gnv130.

[6] SAMOUEI, R. and KEYVANARA, M. Identifying strategies for dealing with the aging population from the perspective of health system experts: A qualitative study. online. *Journal of Education and Health Promotion*. 2022, ed. 11, iss. 1. ISSN 2277-9531. Available from: https://doi.org/10.4103/jehp.jehp__1213__21.

[7] GARVING, Ch.; JAKOB, S.; BAUER, I.; NADJAR, R. and BRUNNER, U. H. Impingement Syndrome of the Shoulder. online. *Deutsches Ärzteblatt international*. 2017. ISSN 1866-0452. Available from: https://doi.org/10.3238/arztebl.2017.0765.

[8] LIN, D. J.; WONG, T. T. and KAZAM, J. K. Shoulder Arthroplasty, from Indications to Complications: What the Radiologist Needs to Know. online. *RadioGraphics*. 2016, ed. 36, iss. 1, p. 192-208. ISSN 0271-5333. Available from: https://doi.org/10.1148/rg.2016150055.

[9] BEST, M. J.; AZIZ, K. T.; WILCKENS, J. H.; MCFARLAND, E. G. and SRIKUMARAN, U. Increasing incidence of primary reverse and anatomic total shoulder arthroplasty in the United States. online. *Journal of Shoulder and Elbow Surgery*. 2021, ed. 30, iss. 5, p. 1159-1166. ISSN 10582746. Available from: https://doi.org/10.1016/j.jse.2020.08.010.

[10] DRAKE, G. N.; O'CONNOR, D. P. and EDWARDS, B. T. Indications for Reverse Total Shoulder Arthroplasty in Rotator Cuff Disease. online. *Clinical Orthopaedics & Related Research*. 2010, ed. 468, iss. 6, p. 1526-1533. ISSN 0009-921X. Available from: https://doi.org/10.1007/s11999-009-1188-9.

[11] BOILEAU, P.; WATKINSON, D. J.; HATZIDAKIS, A. M. and BALG, F. Grammont reverse prosthesis: Design, rationale, and biomechanics. online. *Journal of Shoulder and Elbow Surgery*. 2005, ed. 14, iss. 1, p. 147-161. ISSN 10582746. Available from: https://doi.org/10.1016/j.jse.2004.10.006.

[12] GOMBERAWALLA, M. M. and SEKIYA, J. K. Rotator Cuff Tear and Glenohumeral Instability. online. *Clinical Orthopaedics & Related Research*. 2014, ed. 472, iss. 8, p. 2448-2456. ISSN 0009-921X. Available from: https://doi.org/10.1007/s11999-013-3290-2.

[13] SCHAIRER, W. W.; NWACHUKWU, B. U.; LYMAN, S.; CRAIG, E. V. and GULOTTA, L. V. National utilization of reverse total shoulder arthroplasty in the United States. online. *Journal of Shoulder and Elbow Surgery*. 2015, ed. 24, iss. 1, p. 91-97. ISSN 10582746. Available from: https://doi.org/10.1016/j.jse.2014.08.026.

[14] KIM, J. Y.; RHEE, Y. G. and RHEE, S.-M. Clinical Outcomes after Reverse Total Shoulder Arthroplasty According to Primary Diagnosis. online. *Clinics in Orthopedic Surgery*. 2020, ed. 12, iss. 4. ISSN 2005-291X. Available from: https://doi.org/10.4055/cios19164.

[15] HALL, S. J. *BASIC BIOMECHANICS*. SIXTH EDITION. McGraw-Hill, 2012. ISBN 978-0-07-337644-8.

[16] ČIHÁK, R. *Anatomie 1*. 2. pub. Praha: Grada Publishing, 2001. ISBN 80-7169-970-5.

[17] LEVANGIE, P. K. and NORKIN, C. C. *Joint Structure and Function: A Comprehensive Analysis*. Fourth Edition. F. A. Davis Company, 2005. ISBN 0–8036–1191–9.

[18] NEUMANN, D. A. *KINESIOLOGY OF THE MUSCULOSKELETAL SYSTEM: Foundations for Rehabilitation*. Second Edition. Mosby, Inc., 2010. ISBN 978-0-323-03989-5.

[19] SAHA, A. K. Dynamic Stability of the Glenohumeral Joint. online. *Acta Orthopaedica Scandinavica*. 2009, ed. 42, iss. 6, p. 491-505. ISSN 0001-6470. Available from: https://doi.org/10.3109/17453677108989066.

[20] SIMON, S. R. *Orthopaedic basic science*. [Rosemont, Ill.]: American Academy of Orthopaedic Surgeons, 1994. ISBN 0892030593.

[21] GOHLKE, F.; ESSIGKRUG, B. and SCHMITZ, F.. The pattern of the collagen fiber bundles of the capsule of the glenohumeral joint. online. *Journal of Shoulder and Elbow Surgery*. 1994, ed. 3, iss. 3, p. 111-128. ISSN 10582746. Available from: https://doi.org/10.1016/S1058-2746(09)80090-6.

[22] BOARDMAN, N. D.; DEBSKI, R. E.; WARNER, J.P.; TASKIRAN, E.; MADDOX, L. et al. Tensile properties of the superior glenohumeral and coracohumeral ligaments. online. *Journal of Shoulder and Elbow Surgery*. 1996, ed. 5, iss. 4, p. 249-254. ISSN 10582746. Available from: https://doi.org/10.1016/S1058-2746(96)80050-4.

[23] HOWELL, S. M. and GALINAT, B. J. The glenoid-labral socket. A constrained articular surface. online. *Clinical Orthopaedics and Related Research*. 1989, p. 122-5.

[24] BELTRAN, J.; BENCARDINO, J.; PADRON, M.; SHANKMAN, S.; BELTRAN, L. et al. The middle glenohumeral ligament: normal anatomy, variants and pathology. online. *Skeletal Radiology*. 2002, ed. 31, iss. 5, p. 253-262. ISSN 0364-2348. Available from: https://doi.org/10.1007/s00256-002-0492-1.

[25] GRIM, M. and NAŇKA, O. *Atlas anatomie člověka*. 1. pub. Ilust. HELEKAL, I. Praha: Grada, 2014. ISBN 978-80-247-4012-6.

[26] GILL, T. K.; SHANAHAN, E. M.; TUCKER, . R.; BUCHBINDER, R. and HILL, C. L. Shoulder range of movement in the general population: age and gender stratified normative data using a community-based cohort. online. *BMC Musculoskeletal Disorders*. 2020, ed. 21, iss. 1. ISSN 1471-2474. Available from: https://doi.org/10.1186/s12891-020-03665-9.

[27] LUDEWIG, P. M; PHADKE, V.; BRAMAN, J. P; HASSETT, D. R; CIEMINSKI, C. J et al. Motion of the Shoulder Complex During Multiplanar Humeral Elevation. online. *The Journal of Bone and Joint Surgery-American Volume*. 2009, ed. 91, iss. 2, p. 378-389. ISSN 0021-9355. Available from: https://doi.org/10.2106/JBJS.G.01483.

[28] BARNES, Ch. J.; VAN STEYN, S. J. and FISCHER, R. A. The effects of age, sex, and shoulder dominance on range of motion of the shoulder. online. *Journal of Shoulder and Elbow Surgery*. 2001, ed. 10, iss. 3, p. 242-246. ISSN 10582746. Available from: https://doi.org/10.1067/mse.2001.115270.

[29] INMAN, V. T.; SAUNDERS, J. B. dec M. and ABBOTT, L. C. Observations of the Function of the Shoulder Joint. online. *Clinical Orthopaedics and Related Research*. 1996, ed. 330, p. 3-12. ISSN 0009-921X. Available from: https://doi.org/10.1097/00003086-199609000-00002.

[30] DRAKE, R. L.; VOGL, A. W. and MITCHELL, A. W. M. *Gray's Basic Anatomy*. online. 2. Elsevier, 2017. ISBN 9780323508506.

[31] SINGLETON, M. C. and LEVEAU, B. F. The Hip Joint: Structure, Stability, and Stress. online. *Physical Therapy*. 1975, ed. 55, iss. 9, p. 957-973. ISSN 0031-9023. Available from: https://doi.org/10.1093/ptj/55.9.957.

[32] KAKARLAPUDI, T. K. Knee instability: isolated and complex. online. *Western Journal of Medicine*. ed. 174, iss. 4, p. 266-272. ISSN 00930415. Available from: https://doi.org/10.1136/ewjm.174.4.266.

[33] MATSEN, F. A. *Practical evaluation and management of the shoulder*. Philadelphia: Saunders, 1994. ISBN 0-7216-4819-3.

[34] LIPPITT, S. and MATSEN, F. Mechanisms of Gelnohumeral Joint Stability. *Clinical Orthopaedics and Related Research*. 1993, ed. 93, iss. 291, p. 20-28.

[35] ITOI, E.; MOTZKIN, N. E.; BROWNE, A. O.; HOFFMEYER, P.; MORREY, B. F. et al. Intraarticular pressure of the shoulder. online. *Arthroscopy: The Journal of Arthroscopic & Related Surgery*. 1993, ed. 9, iss. 4, p. 406-413. ISSN 07498063. Available from: https://doi.org/10.1016/S0749-8063(05)80314-7.

[36] VEEGER, H.E.J. and VAN DER HELM, F.C.T. Shoulder function: The perfect compromise between mobility and stability. online. *Journal of Biomechanics*. 2007, ed. 40, iss. 10, p. 2119-2129. ISSN 00219290. Available from: https://doi.org/10.1016/j.jbiomech.2006.10.016.

[37] LABRIOLA, J. E.; LEE, T. Q.; DEBSKI, R. E. and MCMAHON, P. J. Stability and instability of the glenohumeral joint: The role of shoulder muscles. online. *Journal of Shoulder and Elbow Surgery*. 2005, ed. 14, iss. 1, p. 32-38. ISSN 10582746. Available from: https://doi.org/10.1016/j.jse.2004.09.014.

[38] DESHMUKH, A. V.; KORIS, M.; ZURAKOWSKI, D. and THORNHILL, T. S. Total shoulder arthroplasty: Long-term survivorship, functional outcome, and quality of life. online. *Journal of Shoulder and Elbow Surgery*. 2005, ed. 14, iss. 5, p. 471-479. ISSN 10582746. Available from: https://doi.org/10.1016/j.jse.2005.02.009.

[39] CUFF, D.; PUPELLO, D.; VIRANI, N.; LEVY, J. and FRANKLE, M. Reverse Shoulder Arthroplasty for the Treatment of Rotator Cuff Deficiency. online. *The Journal of Bone & Joint Surgery*. 2008, ed. 90, iss. 6, p. 1244-1251. ISSN 0021-9355. Available from: https://doi.org/10.2106/JBJS.G.00775.

[40] CHALMERS, P. N.; SLIKKER, W.; MALL, N. A.; GUPTA, A. K.; RAHMAN, Z. et al. Reverse total shoulder arthroplasty for acute proximal humeral fracture: comparison to open reduction–internal fixation and hemiarthroplasty. online. *Journal of Shoulder and Elbow Surgery*. 2014, ed. 23, iss. 2, p. 197-204. ISSN 10582746. Available from: https://doi.org/10.1016/j.jse.2013.07.044.

[41] MIZUNO, N.; DENARD, P. J; RAISS, P. and WALCH, G. Reverse Total Shoulder Arthroplasty for Primary Glenohumeral Osteoarthritis in Patients with a Biconcave Glenoid. online. *The Journal of Bone and Joint Surgery-American Volume*. 2013, ed. 95, iss. 14, p. 1297-1304. ISSN 0021-9355. Available from: https://doi.org/10.2106/JBJS.L.00820.

[42] BANKES, M. J. K. and EMERY, R. J. H. Pioneers of shoulder replacement: Themistocles Gluck and Jules Emile Péan. online. *Journal of Shoulder and Elbow Surgery*. 1995, ed. 4, iss. 4, p. 259-262. ISSN 10582746. Available from: https://doi.org/10.1016/S1058-2746(05)80018-7.

[43] JAAP WILLEMS, W. History of shoulder arthroplasty. online. *Journal of Arthroscopy and Joint Surgery*. 2021, ed. 8, iss. 1, p. 2-6. ISSN 22149635. Available from: https://doi.org/10.1016/j.jajs.2020.12.001.

[44] NEER, C. S. The Classic: Articular Replacement for the Humeral Head. online. *Clinical Orthopaedics & Related Research*. 2011, ed. 469, iss. 9, p. 2409-2421. ISSN 0009-921X. Available from: https://doi.org/10.1007/s11999-011-1944-5.

[45] KENMORE, P. I.; MACCARTEE, C. and VITEK, B. A simple shoulder replacement. online. *Journal of Biomedical Materials Research*. 1974, ed. 8, iss. 4, p. 329-330. ISSN 0021-9304. Available from: https://doi.org/10.1002/jbm.820080412.

[46] FAMA, G. and POZZUOLI, A. History of Reverse Shoulder Arthroplasty. online. In: GUMINA, S.; GRASSI, F. A. and PALADINI, P. (ed.). *Reverse Shoulder Arthroplasty*. Cham: Springer International Publishing, 2019, p. 3-23. ISBN 978-3-319-97742-3. Available from: https://doi.org/10.1007/978-3-319-97743-0_1.

[47] NEER, C. S.; WATSON, K. C. and STANTON, F. J. Recent experience in total shoulder replacement. online. *The Journal of Bone & Joint Surgery*. 1982, ed. 64, iss. 3, p. 319-337. ISSN 0021-9355. Available from: https://doi.org/10.2106/00004623-198264030-00001.

[48] REEVES, B.; JOBBINS, B.; FLOWERS, F.; DOWSON, D. and WRIGHT, V. Some problems in the development of a total shoulder endo-prosthesis. online. *Annals of the Rheumatic Diseases*. 1972, ed. 31, iss. 5, p. 425-426. ISSN 0003-4967. Available from: https://doi.org/10.1136/ard.31.5.425-b.

[49] KÖLBEL, R. and FRIEDEBOLD, G. Möglichkeiten der Alloarthroplastik an der Schulter. online. *Archiv für Orthopädische und Unfall-Chirurgie*. 1973, ed. 76, iss. 1, p. 31-39. ISSN 0003-9330. Available from: https://doi.org/10.1007/BF00416651.

[50] KESSEL, L. and BAYLEY, I. Prosthetic Replacement of Shoulder Joint: Preliminary Communication. online. *Journal of the Royal Society of Medicine*. 1979, ed. 72, iss. 10, p. 748-752. ISSN 0141-0768. Available from: https://doi.org/10.1177/014107687907201010.

[51] FENLIN, J. M. Total glenohumeral joint replacement. *Orthopedic Clinics of North America*. 1975, ed. 6, iss. 2, p. 565-583.

[52] BUECHEL, F. F.; PAPPAS, M. J. and DEPALMA, A. F. "Floating-socket" total shoulder replacement: Anatomical, biomechanical, and surgical rationale. online. *Journal of Biomedical Materials Research*. 1978, ed. 12, iss. 1, p. 89-114. ISSN 0021-9304. Available from: https://doi.org/10.1002/jbm.820120109.

[53] BAULOT, E.; SIRVEAUX, F. and BOILEAU, P. Grammont's Idea: The Story of Paul Grammont's Functional Surgery Concept and the Development of the Reverse Principle. online. *Clinical Orthopaedics & Related Research*. 2011, ed. 469, iss. 9, p. 2425-2431. ISSN 0009-921X. Available from: https://doi.org/10.1007/s11999-010-1757-y.

[54] GRAMMONT, P. M. and BAULOT, E. DELTA SHOULDER PROSTHESIS FOR ROTATOR CUFF RUPTURE. online. *Orthopedics*. 1993, ed. 16, iss. 1, p. 65-68. ISSN 0147-7447. Available from: https://doi.org/10.3928/0147-7447-19930101-11.

[55] O'TOOLE, G.; COGSWELL, L.; SAUZIERES, P.; VALENTI, P. and KATZ, D. A history of the reverse shoulder prosthesis. online. *International Journal of Shoulder Surgery*. 2007, ed. 1, iss. 4. ISSN 0973-6042. Available from: https://doi.org/10.4103/0973-6042.37113.

[56] LÉVIGNE, Ch.; BOILEAU, P.; FAVARD, L.; GARAUD, P.; MOLÉ, D. et al. Scapular notching in reverse shoulder arthroplasty. online. *Journal of Shoulder and Elbow Surgery*. 2008, ed. 17, iss. 6, p. 925-935. ISSN 10582746. Available from: https://doi.org/10.1016/j.jse.2008.02.010.

[57] NYFFELER, R. W.; WERNER, C. M. L.; SIMMEN, B. R. and GERBER, C. Analysis of a retrieved Delta III total shoulder prosthesis. online. *The Journal of Bone and Joint Surgery. British volume*. 2004, ed. 86-, iss. 8, p. 1187-1191. ISSN 0301-620X. Available from: https://doi.org/10.1302/0301-620X.86B8.15228.

[58] MOLÉ, D. and FAVARD, L. Omarthrose ecentrée. online. *Revue de Chirurgie Orthopédique et Réparatrice de l'Appareil Moteur*. 2007, ed. 93, iss. 6, p. 37-39. ISSN 00351040. Available from: https://doi.org/10.1016/S0035-1040(07)92708-7.

[59] FRANKLE, M. The Reverse Shoulder Prosthesis for glenohumeral arthritis associated with severe rotator cuff deficiency. A minimum two-year follow-up study of sixty patients. online. *The Journal of Bone and Joint Surgery (American)*. 2005, ed. 87, iss. 8. ISSN 0021-9355. Available from: https://doi.org/10.2106/JBJS.D.02813.

[60] TROUILLOUD, P.; GONZALVEZ, M.; MARTZ, P.; CHARLES, H.; HANDELBERG, F. et al. Duocentric® reversed shoulder prosthesis and Personal Fit® templates: innovative strategies to optimize prosthesis positioning and prevent scapular notching. online. *European Journal of Orthopaedic Surgery & Traumatology*. 2014, ed. 24, iss. 4, p. 483-495. ISSN 1633-8065. Available from: https://doi.org/10.1007/s00590-013-1213-2.

[61] BLOCH, H.-R. The SMR® Shoulder System of Lima Corporate. online. In: FRANKLE, Mark; MARBERRY, Scott a PUPELLO, Derek (ed.). *Reverse Shoulder Arthroplasty*. Cham: Springer International Publishing, 2016, p. 417-424. ISBN 978-3-319-20839-8. Available from: https://doi.org/10.1007/978-3-319-20840-4__41.

[62] CASTAGNA, A.; DELCOGLIANO, M.; DE CARO, F.; ZIVERI, G.; BORRONI, M. et al. Conversion of shoulder arthroplasty to reverse implants: clinical and radiological results using a modular system. online. *International Orthopaedics*. 2013, ed. 37, iss. 7, p 1297-1305. ISSN 0341-2695. Available from: https://doi.org/10.1007/s00264-013-1907-4.

[63] BRADLEY EDWARDS, T.; MORRIS, B. J. and HODOREK, B. Tornier Aequalis Ascend™ Flex Convertible Shoulder System. online. In: FRANKLE, M.; MARBERRY, S. a PUPELLO, D. (ed.). *Reverse Shoulder Arthroplasty*. Cham: Springer International Publishing, 2016, p. 441-447. ISBN 978-3-319-20839-8. Available from: https://doi.org/10.1007/978-3-319-20840-4__44.

[64] KONTAXIS, A. and JOHNSON, G.R. The biomechanics of reverse anatomy shoulder replacement – A modelling study. online. *Clinical Biomechanics*. 2009, ed. 24, iss. 3, p. 254-260. ISSN 02680033. Available from: https://doi.org/10.1016/j.clinbiomech.2008.12.004.

[65] DE WILDE, L. F.; AUDENAERT, E. A. and BERGHS, B. M. Shoulder prostheses treating cuff tear arthropathy: A comparative biomechanical study. online. *Journal of Orthopaedic Research*. 2004, ed. 22, iss. 6, p. 1222-1230. ISSN 0736-0266. Available from: https://doi.org/10.1016/j.orthres.2004.03.010.

[66] SIMOVITCH, R. W.; HELMY, N.; ZUMSTEIN, M. A. and GERBER, Ch. Impact of Fatty Infiltration of the Teres Minor Muscle on the Outcome of Reverse Total Shoulder Arthroplasty. online. *The Journal of Bone & Joint Surgery*. 2007, ed. 89, iss. 5, p. 934-939. ISSN 0021-9355. Available from: https://doi.org/10.2106/JBJS.F.01075.

[67] HERRMANN, S.; KÖNIG, Ch.; HELLER, M.; PERKA, C. and GREINER, S. Reverse shoulder arthroplasty leads to significant biomechanical changes in the remaining rotator cuff. online. *Journal of Orthopaedic Surgery and Research*. 2011, ed. 6, iss. 1. ISSN 1749-799X. Available from: https://doi.org/10.1186/1749-799X-6-42.

[68] GREINER, S.; SCHMIDT, Ch.; KÖNIG, Ch.; PERKA, C. and HERRMANN, S. Lateralized Reverse Shoulder Arthroplasty Maintains Rotational Function of the Remaining Rotator Cuff. online. *Clinical Orthopaedics & Related Research*. 2013, ed. 471, iss. 3, p. 940-946. ISSN 0009-921X. Available from: https://doi.org/10.1007/s11999-012-2692-x.

[69] GERBER, C.; PENNINGTON, S. D. and NYFFELER, R. W. Reverse Total Shoulder Arthroplasty. online. *Journal of the American Academy of Orthopaedic Surgeons*. 2009, ed. 17, iss. 5, p. 284-295. ISSN 1067-151X. Available from: https://doi.org/10.5435/00124635-200905000-00003.

[70] GUTIÉRREZ, S.; LUO, Z.-P.; LEVY, J. and FRANKLE, M. A. Arc of motion and socket depth in reverse shoulder implants. online. *Clinical Biomechanics*. 2009, ed. 24, iss. 6, p. 473-479. ISSN 02680033. Available from: https://doi.org/10.1016/j.clinbiomech.2009.02.008.

[71] LÄDERMANN, A.; WILLIAMS, M. D.; MELIS, B.; HOFFMEYER, P. and WALCH, G. Objective evaluation of lengthening in reverse shoulder arthroplasty. online. *Journal of Shoulder and Elbow Surgery*. 2009, ed. 18, iss. 4, p. 588-595. ISSN 10582746. Available from: https://doi.org/10.1016/j.jse.2009.03.012.

[72] LÄDERMANN, A.; WALCH, G.; LUBBEKE, A.; DRAKE, G. N.; MELIS, B. et al. Influence of arm lengthening in reverse shoulder arthroplasty. online. *Journal of Shoulder and Elbow Surgery*. 2012, ed. 21, iss. 3, p. 336-341. ISSN 10582746. Available from: https://doi.org/10.1016/j.jse.2011.04.020.

[73] ROSSY, W. H. and KWON, Y. W. Biomechanics of the Reverse Shoulder Arthroplasty. online. In: FRANKLE, M.; MARBERRY, S. a PUPELLO, D. (ed.). *Reverse Shoulder Arthroplasty*. Cham: Springer International Publishing, 2016, p. 31-37. ISBN 978-3-319-20839-8. Available from: https://doi.org/10.1007/978-3-319-20840-4__3.

[74] POPPEN, N. K. and WALKER, P. S. Forces at the glenohumeral joint in abduction. *Clinical Orthopaedics and Related Research*. 1978, ed. 1978, iss. 135, p. 165-170.

[75] VAN DER HELM, F. C. T. A finite element musculoskeletal model of the shoulder mechanism. online. *Journal of Biomechanics*. 1994, ed. 27, iss. 5, p. 551-569. ISSN 00219290. Available from: https://doi.org/10.1016/0021-9290(94)90065-5.

[76] VAN DER HELM, F. C. T. and VEENBAAS, R. Modelling the mechanical effect of muscles with large attachment sites: Application to the shoulder mechanism. online. *Journal of Biomechanics*. 1991, ed. 24, iss. 12, p. 1151-1163. ISSN 00219290. Available from: https://doi.org/10.1016/0021-9290(91)90007-A.

[77] VAN DER HELM, F. C. T.; VEEGER, H. E. J.; PRONK, G. M.; VAN DER WOUDE, L. H. V. and ROZENDAL, R. H. Geometry parameters for musculoskeletal modelling of the shoulder system. online. *Journal of Biomechanics*. 1992, ed. 25, iss. 2, p. 129-144. ISSN 00219290. Available from: https://doi.org/10.1016/0021-9290(92)90270-B.

[78] VEEGER, H. E. J.; VAN DER HELM, F. C. T.; VAN DER WOUDE, L. H. V.; PRONK, G. M. and ROZENDAL, R. H. Inertia and muscle contraction parameters for musculoskeletal modelling of the shoulder mechanism. online. *Journal of Biomechanics*. 1991, ed. 24, iss. 7, p. 615-629. ISSN 00219290. Available from: https://doi.org/10.1016/0021-9290(91)90294-W.

[79] TERRIER, A.; VOGEL, A.; CAPEZZALI, M. and FARRON, A. An algorithm to allow humerus translation in the indeterminate problem of shoulder abduction. online. *Medical Engineering & Physics*. 2008, ed. 30, iss. 6, p. 710-716. ISSN 13504533. Available from: https://doi.org/10.1016/j.medengphy.2007.07.011.

[80] VEEGER, H. E. J.; YU, B.; AN, K.-N. and ROZENDAL, R. H. Parameters for modeling the upper extremity. online. *Journal of Biomechanics*. 1997, ed. 30, iss. 6, p. 647-652. ISSN 00219290. Available from: https://doi.org/10.1016/S0021-9290(97)00011-0.

[81] SINS, L.; TÉTREAULT, P.; HAGEMEISTER, N. and NUñO, N. Adaptation of the AnyBody™ Musculoskeletal Shoulder Model to the Nonconforming Total Shoulder Arthroplasty Context. online. *Journal of Biomechanical Engineering*. 2015, ed. 137, iss. 10. ISSN 0148-0731. Available from: https://doi.org/10.1115/1.4031330.

[82] LEMIEUX, P. O.; HAGEMEISTER, N.; TÉTREAULT, P. and NUñO, N. Influence of the medial offset of the proximal humerus on the glenohumeral destabilising forces during arm elevation: a numerical sensitivity study. online. *Computer Methods in Biomechanics and Biomedical Engineering*. 2013, ed. 16, iss. 1, p. 103-111. ISSN 1025-5842. Available from: https://doi.org/10.1080/10255842.2011.607813.

[83] LEMIEUX, P.-O.; NUñO, N.; HAGEMEISTER, N. and TÉTREAULT, P. Mechanical analysis of cuff tear arthropathy during multiplanar elevation with the AnyBody shoulder model. online. *Clinical Biomechanics*. 2012, ed. 27, iss. 8, p. 801-806. ISSN 02680033. Available from: https://doi.org/10.1016/j.clinbiomech.2012.04.008.

[84] FAVRE, P.; SNEDEKER, J. G. and GERBER, Ch. Numerical modelling of the shoulder for clinical applications. online. *Philosophical Transactions of the Royal Society A: Mathematical, Physical and Engineering Sciences*. 2009, ed. 367, iss. 1895, p. 2095-2118. ISSN 1364-503X. Available from: https://doi.org/10.1098/rsta.2008.0282.

[85] BERGMANN, G.; GRAICHEN, F.; BENDER, A.; KÄÄB, M.; ROHLMANN, A. et al. In vivo glenohumeral contact forces—Measurements in the first patient 7 months postoperatively. online. *Journal of Biomechanics*. 2007, ed. 40, iss. 10, p. 2139-2149. ISSN 00219290. Available from: https://doi.org/10.1016/j.jbiomech.2006.10.037.

[86] DAMM, P. and BENDER, A. (ed.). *Orthoload*. online. 2023. Available from: https://orthoload.com/.

[87] BERGMANN, G.; GRAICHEN, F.; BENDER, A.; ROHLMANN, A.; HALDER, A. et al. In vivo gleno-humeral joint loads during forward flexion and abduction. online. *Journal of Biomechanics*. 2011, ed. 44, iss. 8, p. 1543-1552. ISSN 00219290. Available from: https://doi.org/10.1016/j.jbiomech.2011.02.142.

[88] SCHINDELIN, J.; ARGANDA-CARRERAS, I.; FRISE, E.; KAYNIG, V.; LONGAIR, M. et al. Fiji: an open-source platform for biological-image analysis. online. *Nature Methods*. 2012, ed. 9, iss. 7, p. 676-682. ISSN 1548-7091. Available from: https://doi.org/10.1038/nmeth.2019.

[89] FEDOROV, A.; BEICHEL, R.; KALPATHY-CRAMER, J.; FINET, J.; FILLION-ROBIN, J.-Ch. et al. 3D Slicer as an image computing platform for the Quantitative Imaging Network. online. *Magnetic Resonance Imaging*. 2012, ed. 30, iss. 9, p. 1323-1341. ISSN 0730725X. Available from: https://doi.org/10.1016/j.mri.2012.05.001.

[90] GARLAND, M. and HECKBERT, P. S. Surface simplification using quadric error metrics. online. In: *Proceedings of the 24th annual conference on Computer graphics and interactive techniques - SIGGRAPH '97*. New York, New York, USA: ACM Press, 1997, p. 209-216. ISBN 0897918967. Available from: https://doi.org/10.1145/258734.258849.

[91] CIGNONI, P.; CALLIERI, M.; CORSINI, M.; DELLEPIANE, M.; GANOVELLI, F. et al. MeshLab: an Open-Source Mesh Processing Tool. In: SCARANO, V.; DE CHIARA, R. and ERRA, U. *Eurographics Italian Chapter Conference*. The Eurographics Association, 2008, p. 129-136. ISBN 978-3-905673-68-5. Available from: https://doi.org/10.2312/LocalChapterEvents/ItalChap/ItalianChapConf2008/129-136.

[92] *Least Squares Sphere Fit.* online. In: JEKEL, Ch. Charles Jekel. 2015. Available from: https://jekel.me/2015/Least-Squares-Sphere-Fit/.

[93] GAO, F. and HAN, L. Implementing the Nelder-Mead simplex algorithm with adaptive parameters. online. *Computational Optimization and Applications*. 2012, ed. 51, iss. 1, p. 259-277. ISSN 0926-6003. Available from: https://doi.org/10.1007/s10589-010-9329-3.

[94] SETH, A.; DONG, M.; MATIAS, R. and DELP, S. L. Muscle Contributions to Upper-Extremity Movement and Work From a Musculoskeletal Model of the Human Shoulder. online. *Frontiers in Neurorobotics*. 2019, ed. 13. ISSN 1662-5218. Available from: https://doi.org/10.3389/fnbot.2019.00090.

[95] DELP, S. L.; ANDERSON, F. C.; ARNOLD, A. S.; LOAN, P.; HABIB, A. et al. OpenSim: Open-Source Software to Create and Analyze Dynamic Simulations of Movement. online. *IEEE Transactions on Biomedical Engineering*. 2007, ed. 54, iss. 11, p. 1940-1950. ISSN 0018-9294. Available from: https://doi.org/10.1109/TBME.2007.901024.

[96] SETH, A.; MATIAS, R.; VELOSO, A. P.; DELP, S. L. and REN, L. A Biomechanical Model of the Scapulothoracic Joint to Accurately Capture Scapular Kinematics during Shoulder Movements. online. *PLOS ONE*. 2016, ed. 11, iss. 1. ISSN 1932-6203. Available from: https://doi.org/10.1371/journal.pone.0141028.

[97] KLEIN BRETELER, M. D.; SPOOR, C. W. and VAN DER HELM, F. C. T. Measuring muscle and joint geometry parameters of a shoulder for modeling purposes. online. *Journal of Biomechanics*. 1999, ed. 32, iss. 11, p. 1191-1197. ISSN 00219290. Available from: https://doi.org/10.1016/S0021-9290(99)00122-0.

[98] ACKLAND, D. C.; PAK, P.; RICHARDSON, M. and PANDY, M. G. Moment arms of the muscles crossing the anatomical shoulder. online. *Journal of Anatomy*. 2008, ed. 213, iss. 4, p. 383-390. ISSN 0021-8782. Available from: https://doi.org/10.1111/j.1469-7580.2008.00965.x.

[99] EDWARDS, T. B.; WILLIAMS, M. D.; LABRIOLA, J. E.; ELKOUSY, H. A.; GARTSMAN, G. M. et al. Subscapularis insufficiency and the risk of shoulder dislocation after reverse shoulder arthroplasty. online. *Journal of Shoulder and Elbow Surgery*. 2009, ed. 18, iss. 6, p. 892-896. ISSN 10582746. Available from: https://doi.org/10.1016/j.jse.2008.12.013.

[100] SELIM, N. M. and BADAWY, E. R. Consider Long Head of Biceps Tendon for Reconstruction of Massive, Irreparable Rotator Cuff Tear. Online. Arthroscopy Techniques. 2021, ed. 10, iss. 2, p. 457-467. ISSN 22126287. Available from: https://doi.org/10.1016/j.eats.2020.10.024.

[101] WU, G.; VAN DER HELM, F. C. T.; VEEGER, H. E. J.; MAKHSOUS, M.; VAN ROY, P. et al. ISB recommendation on definitions of joint coordinate systems of various joints for the reporting of human joint motion—Part II: shoulder, elbow, wrist and hand. online. *Journal of Biomechanics*. 2005, ed. 38, iss. 5, p. 981-992. ISSN 00219290. Available from: https://doi.org/10.1016/j.jbiomech.2004.05.042.

[102] HAEUFLE, D. F. B.; GÜNTHER, M.; BAYER, A. and SCHMITT, S. Hill-type muscle model with serial damping and eccentric force–velocity relation. online. *Journal of Biomechanics*. 2014, ed. 47, iss. 6, p. 1531-1536. ISSN 00219290. Available from: https://doi.org/10.1016/j.jbiomech.2014.02.009.

[103] GÜNTHER, M.; SCHMITT, S. and WANK, V. High-frequency oscillations as a consequence of neglected serial damping in Hill-type muscle models. online. *Biological Cybernetics*. 2007, ed. 97, iss. 1, p. 63-79. ISSN 0340-1200. Available from: https://doi.org/10.1007/s00422-007-0160-6.

[104] THELEN, D. G. Adjustment of Muscle Mechanics Model Parameters to Simulate Dynamic Contractions in Older Adults. online. *Journal of Biomechanical Engineering*. 2003, ed. 125, iss. 1, p. 70-77. ISSN 0148-0731. Available from: https://doi.org/10.1115/1.1531112.

[105] GORDON, A. M.; HUXLEY, A. F. and JULIAN, F. J. The variation in isometric tension with sarcomere length in vertebrate muscle fibres. online. *The Journal of Physiology*. 1966, ed. 184, iss. 1, p. 170-192. ISSN 0022-3751. Available from: https://doi.org/10.1113/jphysiol.1966.sp007909.

[106] MCLEAN, S. G.; SU, A. and VAN DEN BOGERT, A. J. Development and Validation of a 3-D Model to Predict Knende Joint Loading During Dynamic Movement. online. *Journal of Biomechanical Engineering*. 2003, ed. 125, iss. 6, p. 864-874. ISSN 0148-0731. Available from: https://doi.org/10.1115/1.1634282.

[107] GEYER, H. and HERR, H. A Muscle-Reflex Model That Encodes Principles of Legged Mechanics Produces Human Walking Dynamics and Muscle Activities. online. *IEEE Transactions on Neural Systems and Rehabilitation Engineering*. 2010, ed. 18, iss. 3, p. 263-273. ISSN 1534-4320. Available from: https://doi.org/10.1109/TNSRE.2010.2047592.

[108] GEYER, H.; SEYFARTH, A. and BLICKHAN, R. Positive force feedback in bouncing gaits?. online. *Proceedings of the Royal Society of London. Series B: Biological Sciences*. 2003, ed. 270, iss. 1529, p. 2173-2183. ISSN 0962-8452. Available from: https://doi.org/10.1098/rspb.2003.2454.

[109] VAN ARKEL, R. J.; MODENESE, L.; PHILLIPS, A. T. M. and JEFFERS, J. R. T. Hip abduction can prevent posterior edge loading of hip replacements. online. *Journal of Orthopaedic Research*. 2013, ed. 31, iss. 8, p. 1172-1179. ISSN 0736-0266. Available from: https://doi.org/10.1002/jor.22364.

[110] WU, W.; LEE, P. V. S.; BRYANT, A. L.; GALEA, M. and ACKLAND, D. C. Subject-specific musculoskeletal modeling in the evaluation of shoulder muscle and joint function. online. *Journal of Biomechanics*. 2016, ed. 49, iss. 15, p. 3626-3634. ISSN 00219290. Available from: https://doi.org/10.1016/j.jbiomech.2016.09.025.

[111] VAN VEEN, B.; MONTEFIORI, E.; MODENESE, L.; MAZZà, C. and VICECONTI, M. Muscle recruitment strategies can reduce joint loading during level walking. online. *Journal of Biomechanics*. 2019, ed. 97. ISSN 00219290. Available from: https://doi.org/10.1016/j.jbiomech.2019.109368.

[112] SHROUT, P. E. and FLEISS, J. L. Intraclass correlations: Uses in assessing rater reliability. online. *Psychological Bulletin*. 1979, ed. 86, iss. 2, p. 420-428. ISSN 0033-2909. Available from: https://doi.org/10.1037//0033-2909.86.2.420.

[113] FOX, J. *Applied Regression Analysis and Generalized Linear Models*. Third Edition. SAGE Publications, Inc, 2015. ISBN 9781452205663.

[114] JAHNKE, A.; ENGL, S.; SEEGER, J. B.; BASAD, E.; RICKERT, M. et al. Influences of fit and fill following hip arthroplasty using a cementless short-stem prosthesis. online. *Archives of Orthopaedic and Trauma Surgery*. 2015, ed. 135, iss. 11, p. 1609-1614. ISSN 0936-8051. Available from: https://doi.org/10.1007/s00402-015-2302-y.

[115] POURMOGHADDAM, A.; DETTMER, M.; FREEDHAND, A. M.; DOMINGUES, B. C. and KREUZER, S. W. A Patient-Specific Predictive Model Increases Preoperative Templating Accuracy in Hip Arthroplasty. online. *The Journal of Arthroplasty*. 2015, ed. 30, iss. 4, p. 622-626. ISSN 08835403. Available from: https://doi.org/10.1016/j.arth.2014.11.021.

[116] HORNOVÁ, J.; RŮŽIČKA, P.; HRUBINA, M.; ŠŤASTNÝ, E.; KOŠKOVÁ, A. et al. Magnification of digital hip radiographs differs between clinical workplaces. online. *PLOS ONE*. 2017, ed. 12, iss. 11. ISSN 1932-6203. Available from: https://doi.org/10.1371/journal.pone.0188743.

[117] CHO, S.-H. and JEONG, J. Radiologic Results of Three-Dimensional Templating for Total Shoulder Arthroplasty. online. *Clinics in Orthopedic Surgery*. 2020, ed. 12, iss. 2. ISSN 2005-291X. Available from: https://doi.org/10.4055/cios19100.

[118] MIN, K. S.; FOX, H. M.; BEDI, A.; WALCH, G. and WARNER, J. J. P. Patient-specific planning in shoulder arthroplasty. online. *The Bone & Joint Journal*. 2020, ed. 102-, iss. 3, p. 365-370. ISSN 2049-4394. Available from: https://doi.org/10.1302/0301-620X.102B3.BJJ-2019-1153.R1.

[119] OLAIYA, O. R; NADEEM, I.; HORNER, N. S; BEDI, A.; LEROUX, T. et al. Templating in shoulder arthroplasty – A comparison of 2D CT to 3D CT planning software: A systematic review. online. *Shoulder & Elbow*. 2020, ed. 12, iss. 5, p. 303-314. ISSN 1758-5732. Available from: https://doi.org/10.1177/1758573219888780.

[120] IORDACHE, S. D.; GOLDBERG, N.; PAZ, L.; PEYLAN, J.; HUR, R. B. et al. Radiation Exposure From Computed Tomography Of The Upper Limbs. online. *Acta Orthopaedica Belgica*. 2017, ed. 83, iss. 4, p. 581-588.

[121] GATES, S.; SAGER, B. and KHAZZAM, M. Preoperative glenoid considerations for shoulder arthroplasty: a review. online. *EFORT Open Reviews*. 2020, ed. 5, iss. 3, p. 126-137. ISSN 2396-7544. Available from: https://doi.org/10.1302/2058-5241.5.190011.

[122] ARCHIBECK, M. J.; CUMMINS, T.; TRIPURANENI, K. R.; CAROTHERS, J. T.; MURRAY-KREZAN, C. et al. Inaccuracies in the Use of Magnification Markers in Digital Hip Radiographs. online. *Clinical Orthopaedics & Related Research*. 2016, ed. 474, iss. 8, p. 1812-1817. ISSN 0009-921X. Available from: https://doi.org/10.1007/s11999-016-4704-8.

[123] RETTIG, O.; MAIER, M. W.; GANTZ, S.; RAISS, P.; ZEIFANG, F. et al. Does the reverse shoulder prosthesis medialize the center of rotation in the glenohumeral joint?. online. *Gait & Posture*. 2013, ed. 37, iss. 1, p. 29-31. ISSN 09666362. Available from: https://doi.org/10.1016/j.gaitpost.2012.04.019.

[124] ANG, Ch.-Y.; LAI, K.-W.; TJIAUW TJOEN, D. L. and CHANG CHEE CHENG, P. Reverse shoulder arthroplasty: The Singapore General Hospital experience and a simple method of measuring change in the center-of-rotation. online. *Journal of Orthopaedics*. 2015, ed. 12, iss. 2, p. 97-101. ISSN 0972978X. Available from: https://doi.org/10.1016/j.jor.2014.04.019.

[125] SALTZMAN, M. D.; MERCER, D. M.; WARME, W. J.; BERTELSEN, A. L. and MATSEN, F. A. A method for documenting the change in center of rotation with reverse total shoulder arthroplasty and its application to a consecutive series of 68 shoulders having reconstruction with one of two different reverse prostheses. online. *Journal of Shoulder and Elbow Surgery*. 2010, ed. 19, iss. 7, p. 1028-1033. ISSN 10582746. Available from: https://doi.org/10.1016/j.jse.2010.01.021.

[126] ACKLAND, D. C.; WU, W.; THOMAS, R.; PATEL, M.; PAGE, R. et al. Muscle and Joint Function After Anatomic and Reverse Total Shoulder Arthroplasty Using a Modular Shoulder Prosthesis. online. *Journal of Orthopaedic Research*. 2019, ed. 37, iss. 9, p. 1988-2003. ISSN 0736-0266. Available from: https://doi.org/10.1002/jor.24335.

[127] LINAKER, C. H. and WALKER-BONE, K. Shoulder disorders and occupation. online. *Best Practice & Research Clinical Rheumatology*. 2015, ed. 29, iss. 3, p. 405-423. ISSN 15216942. Available from: https://doi.org/10.1016/j.berh.2015.04.001.

[128] ROMERO, F. and ALONSO, F. J. A comparison among different Hill-type contraction dynamics formulations for muscle force estimation. online. *Mechanical Sciences*. 2016, ed. 7, iss. 1, p. 19-29. ISSN 2191-916X. Available from: https://doi.org/10.5194/ms-7-19-2016.

[129] WALKER, M.; BROOKS, J.; WILLIS, M. and FRANKLE, M.. How Reverse Shoulder Arthroplasty Works. online. *Clinical Orthopaedics & Related Research*. 2011, ed. 469, iss. 9, p. 2440-2451. ISSN 0009-921X. Available from: https://doi.org/10.1007/s11999-011-1892-0.

[130] TAKAHASHI, K.; SHIOTANI, H.; EVANGELIDIS, P. E.; SADO, N. and KAWAKAMI, Y. Three-dimensional architecture of human medial gastrocnemius fascicles in vivo: Regional variation and its dependence on muscle size. online. *Journal of Anatomy*. 2022, ed. 241, iss. 6, p. 1324-1335. ISSN 0021-8782. Available from: https://doi.org/10.1111/joa.13750.

[131] CHARLES, J. P.; GRANT, B.; D'AOûT, K. and BATES, K. T. Subject-specific muscle properties from diffusion tensor imaging significantly improve the accuracy of musculoskeletal models. online. *Journal of Anatomy*. 2020, ed. 237, iss. 5, p. 941-959. ISSN 0021-8782. Available from: https://doi.org/10.1111/joa.13261.

[132] FULIN, P.; KYSILKO, M.; POKORNY, D.; PADR, R.; KASPRIKOVA, N. et al. Study of the variability of scapular inclination and the glenoid version - considerations for preoperative planning: clinical-radiological study. online. *BMC Musculoskeletal Disorders*. 2017, ed. 18, iss. 1. ISSN 1471-2474. Available from: https://doi.org/10.1186/s12891-016-1381-4.

[133] MODENESE, L. and KOHOUT, J. Automated Generation of Three-Dimensional Complex Muscle Geometries for Use in Personalised Musculoskeletal Models. online. *Annals of Biomedical Engineering*. 2020, ed. 48, iss. 6, p. 1793-1804. ISSN 0090-6964. Available from: https://doi.org/10.1007/s10439-020-02490-4.

[134] DAVID, S.; BAČIć, B.; RICHTER, C. and MUNDT, M. Editorial: Artificial intelligence to enhance biomechanical modelling. online. *Frontiers in Sports and Active Living*. 2023, ed. 5. ISSN 2624-9367. Available from: https://doi.org/10.3389/fspor.2023.1188035.

List of publications related to the dissertation

Articles

[I] Kratochvíl, A.; Daniel, M.; Fulín, P., Pokorný D. Radiographical magnification of the shoulder region. Online. *Obere Extremität*. 2024. doi: 10.1007/s11678-024-00802-x (IF 0.4)

[II] Votava J., Kratochvíl A., Daniel M. Intra and inter-rater variability in the construction of patient-specific musculoskeletal model. Online. *Gait & Posture*. 2023. doi: 10.1016/j.gaitpost.2023.12.001. (IF 2.4)

[III] Kratochvíl, A.; Daniel, M.; Fulín, P., Walder J. The influence of humeral lengthening in reverse total shoulder arthroplasty on glenohumeral biomechanics. 2024. Submitted to The Journal of Bone and Joint Surgery.

Conference proceedings

[IV] Kratochvíl, A.; Daniel, M.; Fulín, P. ANALYSIS OF DISPLACEMENT OF CENTER OF ROTATION DURING REVERSE SHOULDER ARTHROPLASTY. In: 28th WORKSHOP OF APPLIED MECHANICS BOOK OF PAPERS. Praha: Czech Technical University in Prague, 2020. p. 42-44. ISBN 978-80-01-06791-8.

[V] Kratochvíl, A.; Daniel, M.; Fulín, P.; Pokorný, D. X-RAY MAGNIFICATION OF THE SHOULDER JOINT. In: 29th WORKSHOP OF APPLIED MECHANICS BOOK OF PAPERS. Praha: CTU FME. Department of Mechanics, Biomechanics and Mechatronics, 2021. p. 30-33. ISBN 978-80-01-06909-7.

[VI] Kratochvíl, A.; Daniel, M. Fitting postoperative 2D X-ray to preoperative 3D CT scan in patients with total shoulder arthroplasty. [Invited unpublished scientific lecture] 2022-11-11.

[VII] Kratochvíl, A.; Daniel, M.; Votava, J.; Pokorný, D.; Fulín, P. MECHANICS OF STABILIZATION IN REVERSE SHOULDER ARTHROPLASTY. In: 24th International Scientific Conference APPLIED MECHANICS 2023 BOOK OF ABSTRACTS. Bratislava: Strojnícka fakulta STU v Bratislave, 2023. ISBN 978-80-227-5294-7.

[VIII] Kratochvíl, A.; Daniel, M.; Fulín, P.; Walder, J. Metoda stanovení změn ve svalově-kosterní geometrii u pacientů s reverzní náhradou ramenního kloubu. In: XIV.

mezinárodní konference BIOIMPLANTOLOGIE. Praha: Národní knihovna ČR, 2023. ISBN 978-80-11-03134-3.

[IX] Kratochvíl, A.; Daniel, M. Biomechanika reverzní náhrady ramenního kloubu. In: Human Biomechanics 2023 – Sborník. Praha: České vysoké učení technické v Praze, Fakulta strojní, 2023. ISBN 978-80-01-07179-3.

[X] Kratochvíl, A.; Daniel, M.; Fulín, P.; Walder, J. Pasivní odezva svalové tkáně u pacientů s reverzní náhradou glenohumerálního kloubu. In: Biomateriály a jejich povrchy XVI.. Praha: České vysoké učení technické v Praze, Fakulta strojní, 2023. 1.. ISBN 978-80-01-07212-7.

[XI] Kratochvíl, A.; Daniel, M. The Impact Of Varied Hill-Type Muscle Model Formulations On Glenohumeral Joint Loading. In: 25th International Scientific Conference APPLIED MECHANICS 2024 BOOK OF ARTICLES. Žilina: Faculty of Mechanical Engineering University of Žilina, 2024.

List of publications not related to the dissertation

Articles

Drátovská, V.; Sedláček, R.; Padovec, Z.; Růžička, P.; Kratochvíl, A. The Mechanical Properties and Fatigue Prediction of a New Generation of Osteosynthetis Devices. Strojnícky časopis. 2021, 71(2), 101-108. ISSN 2450-5471. (Scopus Cite Score 1.7)

Bodnárová, J.; Kratochvíl, A.; Daniel, M. Development and Mechanical Testing of Implant for Cranial Reconstruction After Burr Hole Trepanation. Journal of Medical Devices. 2023, 17(3), ISSN 1932-619X. (IF 0.9)

Conference proceedings

Kratochvíl, A.; Daniel, M. SYSTEM FOR DETERMINATION OF SHOULDER JOINT MOTION ACTIVITY. In: 21st Workshop of Applied Mechanics - Proceedings. Praha: České vysoké učení technické v Praze, Fakulta strojní, 2016. pp. 25-28. ISBN 978-80-01-06085-8.

Kratochvíl, A.; Daniel, M. Monitoring of shoulder joint motion activity. In: Studentská tvůrčí činnost 2017. Praha: ČVUT v Praze - Fakulta strojní, 2017. ISBN 978-80-01-06143-5.

Kratochvíl, A.; Daniel, M. THE BENEFIT OF EMG IN DETERMINATION OF SHOULDER JOINT MOVEMENT PATTERNS. In: Proceedings of the 23rd Congress of the European Society of Biomechanics. ESCUELA TÉCNICA SUPERIOR DE INGENIERÍA Universidad de Sevilla, 2017.

Kratochvíl, A. Measuring by QCM. In: 23rd Workshop of Applied Mechanics - Proceedings. Praha: České vysoké učení technické v Praze, Fakulta strojní, 2017. p. 9-11. ISBN 978-80-01-06372-9.

Kratochvíl, A. Optimization of Motion Analysis System for Using in Daily Living. In: Studentská tvůrčí činnost 2019. Praha: České vysoké učení technické v Praze, Fakulta strojní, 2019. ISBN 978-80-01-06564-8.

Kratochvíl, A.; Daniel, M. WEARABLE DEVICE FOR MEASURING ACCELERATIONS AND VELOCITY. In: Book of abstracts of the 4th International Conference on Movement Analysis. Kladno: České vysoké učení technické v Praze, Fakulta biomedicínského inženýrství, 2019. p. 20-21. ISBN 978-80-01-06587-7.

Kratochvíl, A.; Daniel, M. SYSTEM FOR DIRECT VELOCITY MEASURING. In: 26th Workshop of Applied Mechanics. Praha: ČVUT v Praze, Fakulta strojní, Ústav mechaniky, biomechaniky a mechatroniky, 2019. ISBN 978-80-01-06604-1.

Kratochvíl, A.; Daniel, M. SYSTEM FOR LONG-TERM MONITORING OF PATIENTS WITH SHOULDER DISEASE. In: Proceedings of the 25th Congress of the European Society of Biomechanics. Wien: TU Wien, 2019. p. 601. ISBN 978-3-903024-96-0.

Kratochvíl, A.; Votava, J. Biomechanika (v) pohybu [Invited unpublished scientific lecture] Rektorát ČVUT: 2019-10-31.

Drátovská, V.; Sedláček, R.; Padovec, Z.; Růžička, P.; Kratochvíl, A. Fatigue Life Prediction and FEM Simulation of Mechanical Response of the Distal Fibular Bone Plates. In: 23rd International Scientific Conference Applied Mechanics 2022 Book of Abstracts. Praha: CTU FME. Department of Mechanics, Biomechanics and Mechatronics, 2022. p. 29-32. ISBN 978-80-01-06974-5.

Kratochvíl, A.; Sedláček, R.; Kubášová, K.; Losertová, M. Effect of Aging on Mechanical Properties of NiTi. In: 23rd International Scientific Conference Applied Mechanics 2022 Book of Abstracts. Praha: CTU FME. Department of Mechanics, Biomechanics and Mechatronics, 2022. ISBN 978-80-01-06974-5.

Říha, M.; Kratochvíl, A.; Sedláček, R. The Mechanical Properties of Titanium Bone Plates Produced by Additive Technology. In: 23rd International Scientific Conference Applied Mechanics 2022 Book of Abstracts. Praha: CTU FME. Department of Mechanics, Biomechanics and Mechatronics, 2022. ISBN 978-80-01-06974-5.

Drátovská, V.; Sedláček, R.; Padovec, Z.; Růžička, P.; Kratochvíl, A. The Analysis of Fatigue Life Prediction of the Metallic Bone Plates for Osteosynthesis. In: 60th annual international conference on Experimental Stress Analysis - Book of Extended Abstracts. Praha: CTU FME. Department of Mechanics, Biomechanics and Mechatronics, 2022. p. 24-25. ISBN 978-80-01-07010-9.

Říha, M.; Kratochvíl, A.; Sedláček, R. Stanovení mechanických vlastností titanových dlah vyrobených aditivní technologií. In: Sborník abstraktů Konference studentské tvůrčí činnosti STČ 2022. Praha: CTU. Faculty of Mechanical Engineering, 2022.

Kratochvíl, A.; Sedláček, R.; Růžička, P.; Drátovská, V. Vliv pasivace povrchu 3D tištěných dlah na únavovou životnost. In: Biomateriály a jejich povrchy XV.. Praha: CTU. Faculty of Mechanical Engineering, 2022. ISBN 978-80-01-07023-9.

Bodnárová, J.; Kratochvíl, A.; Daniel, M. Vývoj kraniotomických implantátů s využitím metody aditivní výroby. In: Human Biomechanics 2023 – Sborník. Praha: České vysoké učení technické v Praze, Fakulta strojní, 2023. ISBN 978-80-01-07179-3.

Drátovská, V.; Kratochvíl, A.; Sedláček, R.; Padovec, Z.; Konvičková, S. Exploring The Impact Of Printing Position On Mechanical Properties Of Additively Manufactured Ti6Al4V. In: 25th International Scientific Conference APPLIED MECHANICS 2024 BOOK OF ARTICLES. Žilina: Faculty of Mechanical Engineering University of Žilina, 2024.

Kubášová, K.; Kratochvíl, A.; Losertová, M.; Kopelent, M.; Sedláček, R. Effect Of Heat Treatment On The Super Elastic Properties Of NiTi Wires. In: 25th International Scientific Conference APPLIED MECHANICS 2024 BOOK OF ARTICLES. Žilina: Faculty of Mechanical Engineering University of Žilina, 2024.

Research reports

Vondrová, J.; Kratochvíl, A.; Sedláček, R. Porovnání mechanických vlastností čistého titanu (Ti Grade 4) a slitiny titanu Ti-6Al-4V (Ti Grade 5). [Research Report] Praha: ČVUT v Praze, Fakulta strojní, Ústav mechaniky, biomechaniky a mechatroniky, 2018. Report no. 12105/18/16.

Kratochvíl, A.; Padovec, Z.; Sedláček, R. Konstrukce a analýza přípravku pro čtyřbodový ohyb. [Research Report] Praha: ČVUT v Praze, Fakulta strojní, Ústav mechaniky, biomechaniky a mechatroniky, 2018. Report no. 12105/18/23.

Horný, L.; Sedláček, R.; Vodička, J.; Kubášová, K.; Hrdinová, H.; Petřivý, Z.; Říhová, J.; Kratochvíl, A. et al. Výroční zpráva o výzkumných a vývojových činnostech konaných v rámci projektu Vývoj nové generace hřebů pro osteosyntézu dlouhých kostí dolní končetiny (FV30348). [Research Report] Praha: ČVUT v Praze, Fakulta strojní, Ústav mechaniky, biomechaniky a mechatroniky, 2018. Report no. 12105/18/26.

Růžička, P.; Kratochvíl, A.; Kronek, J.; Sedláček, R.; Zach, L. Mechanické zkoušky a konstitutivní modely 3D tištěného polymer. [Research Report] Praha: České vysoké učení technické v Praze, Fakulta strojní, 2018. Report no. 12105/18/36.

Sedláček, R.; Kratochvíl, A.; Vondrová, J.; Padovec, Z. METODIKA TESTOVÁNÍ PROSTŘEDKŮ PRO DLAHOVOU OSTEOSYSTÉZU A JEJÍ AKREDITACE. [Research Report] Praha: ČVUT v Praze, Fakulta strojní, Ústav mechaniky, biomechaniky a mechatroniky, 2019. Report no. 12105/19/13.

Sedláček, R.; Kratochvíl, A.; Padovec, Z.; Růžička, P. STATICKÉ A ÚNAVOVÉ OHYBOVÉ ZKOUŠKY DLAH. [Research Report] Praha: ČVUT v Praze, Fakulta strojní, Ústav mechaniky, biomechaniky a mechatroniky, 2019. Report no. 12105/19/14.

Suchý, T.; Sedláček, R.; Kratochvíl, A. DEGRADAČNÍ CHOVÁNÍ HOŘČÍKOVÝCH SLITIN V SIMULOVANÝCH TĚLNÍCH PODMÍNKÁCH. [Research Report] Praha: ČVUT v Praze, Fakulta strojní, Ústav mechaniky, biomechaniky a mechatroniky, 2019. Report no. 12105/19/18.

Kratochvíl, A.; Růžička, P. Zatížení patní kosti. [Research Report] Praha: ČVUT v Praze, Fakulta strojní, Ústav mechaniky, biomechaniky a mechatroniky, 2019. Report no. 12105/19/35.

Růžička, P.; Kratochvíl, A.; Králík, V.; Kronek, J.; Chlup, H.; Pich, P.; Šepitka, J.; Vondrová, J. et al. Numerické a experimentální ověření pevnosti konstrukce vybraného implantátu. [Technical Report] Praha: České vysoké učení technické v Praze, Fakulta strojní, 2019. Report no. 12105/19/37.

Sedláček, R.; Kratochvíl, A.; Padovec, Z.; Růžička, P.; Drátovská, V. Ohybové zkoušky dlah – statika, únava, predikce životnosti. [Research Report] Praha: CTU FME. Department of Mechanics, Biomechanics and Mechatronics, 2020. Report no. 12105/20/17.

Růžička, P.; Kratochvíl, A.; Kronek, J.; Pich, P.; Zach, L.; Králík, V.; Vondrová, J.; Kubášová, K. Numerické a experimentální ověření pevnosti konstrukce finálních implantátů. [Technical Report] Praha: České vysoké učení technické v Praze, Fakulta strojní, 2020. Report no. 12105/20/45.

Sedláček, R.; Kratochvíl, A.; Padovec, Z.; Růžička, P.; Drátovská, V. Ohybové zkoušky fibulární distální dlahy – statika, únava, predikce životnosti. [Research Report] Praha: CTU FME. Department of Mechanics, Biomechanics and Mechatronics, 2021. Report no. 12105/21/16.

Sedláček, R.; Kratochvíl, A.; Padovec, Z.; Drátovská, V.; Růžička, P. Ohybové zkoušky humerální proximální dlahy – statika, únava, predikce životnosti. [Research Report] Praha: CTU FME. Department of Mechanics, Biomechanics and Mechatronics, 2021. Report no. 12105/21/17.

Sedláček, R.; Kratochvíl, A.; Padovec, Z.; Růžička, P.; Drátovská, V. Ohybové zkoušky tibiální distální mediální dlahy – statika, únava, predikce životnosti. [Research

Report] Praha: CTU FME. Department of Mechanics, Biomechanics and Mechatronics, 2021. Report no. 12105/21/18.

Kratochvíl, A.; Růžička, P.; Sedláček, R. Ohybové zkoušky radiální distální volární dlahy – statika. [Research Report] Praha: CTU FME. Department of Mechanics, Biomechanics and Mechatronics, 2021. Report no. 12105/21/24.

Růžička, P.; Kratochvíl, A.; Sedláček, R.; Drátovská, V. Ohybové zkoušky radiální distální volární dlahy – statika, únava. [Research Report] Praha: CTU FME. Department of Mechanics, Biomechanics and Mechatronics, 2022. Report no. 12105/22/15.

Chlup, H.; Sedláček, R.; Kratochvíl, A.; Goldmann, T.; Růžička, P. Experimentální zkoušky a numerické simulace spoje kostních šroubu s kostí. [Research Report] 2022. Report no. 12105/22/19.

Conference hosting

Kubášová, K.; Kratochvíl, A.; Mendová, K. Human Biomechanics 2023. [Conference Hosting] 2023.

Annex A

FN MOTOL

ETICKÁ KOMISE FAKULTNÍ NEMOCNICE V MOTOLE
V Úvalu 84, 150 06 Praha 5 , telefon 224 431 195, fax 224 431 196
e-mail:etickakomise@fnmotol.cz, www.fnmotol.cz

STANOVISKO ETICKÉ KOMISE K VÝZKUMNÉMU PROJEKTU
OPINION OF THE ETHICS COMMITTEE ON RESEARCH PROJECT

Název výzkumného projektu / *The title of the research project:*

Monitorace hybnosti ramenního kloubu a délky paže před a po implantaci endoprotézy ramenního kloubu

Navrhovatel / *Applicant*: **MUDr. Petr Fulín, Ph.D., I. ortopediská klinika 1.LF a FN v Motole 2.LF UK FN Motol, V Úvalu 84, 150 06 Praha 5**

EK vydává /*EC issues* **souhlasné stanovisko / *favourable opinion***

Etická komise prohlašuje, že byla ustavena a pracuje podle jednacího řádu v souladu se správnou klinickou praxí (GCP) a platnými předpisy / *The Ethics committee hereby declares that it was established and operates in accordance with its Rules of Procedure in compliance with Good Clinical Practice and valid legal regulations.*

Datum přijetí / *Date of Submission*: **8. 10. 2018** Jednací č. / *Reference No.*: **EK-1204/18**
Datum jednání EK / *Date of EC Session:* **10. 10. 2018**

10. 10. 2018	**MUDr. Vratsilav Šmelhaus**	
.....	.....	.....
Datum / Date	předseda/ *Chairman*	podpis předsedy EK / *Signature of Chairman*

Seznam členů Etické komise / *List of the IEC members*

Jméno a příjmení *Name and Surname*	Muž / Žena *Male / Female*	Odbornost *Occupation*	Závislost *Liability*	Hlasoval *Voted*
MUDr. Vratislav Šmelhaus	M	M.D.	☒	☒
Bc. Eva Sarah Al Jamal	F	Officer	☒	☐
Anna Dobešová	F	Pensioner	☐	☒
Doc. MUDr. Jiří Dušek, CSc.	M	M.D.	☒	☒
PharmDr. Petr Horák	M	Pharmacist	☒	☐
Prof. MUDr. Jakub Hort, Ph.D.	M	M.D.	☒	☐
Prof. MUDr. Michal Hrdlička, CSc.	M	M.D.	☒	☐
Prof. MUDr. Václav Chaloupecký, CSc.	M	M.D.	☒	☐
Prof. MUDr. Jiří Charvát, CSc.	M	M.D.	☒	☐
Mgr. Zuzana Eva Švihelová	M	Lawyer	☒	☒
JUDr. Kateřina Královcová	F	Lawyer	☐	☒
Prim. MUDr. Zdeněk Linke	M	M.D.	☒	☒
Prof. MUDr. Lidka Lisá, DrSc.	F	M.D.	☒	☐
Doc. MUDr. Jitka Zelenková, CSc.	F	M.D.	☒	☐
Doc. MUDr. Jan Zuna, Ph.D.	M	M.D.	☒	☒